Technische Universität Dortmund

Fakultät für Chemie und Chemische Biologie

Dissertation

zur Erlangung des akademischen Grades eines Doktors der Naturwissenschaften (Dr. rer. nat.)

Regulation of EGF Receptor Activation by Phosphohistidine Phosphatase PHPT1

Julia Wernicke

31. Mai 2017

Diese Arbeit wurde angefertigt am
Max-Planck-Institut für molekulare Physiologie in Dortmund

1. Gutachter: Prof. Dr. Philippe I.H. Bastiaens
2. Gutachter: Prof. Dr. Christian Hedberg

Eidesstattliche Versicherung (Affidavit)

_____ _____

Name, Vorname
(Surname, first name)

Matrikel-Nr.
(Enrolment number)

Belehrung:

Wer vorsätzlich gegen eine die Täuschung über Prüfungsleistungen betreffende Regelung einer Hochschulprüfungsordnung verstößt, handelt ordnungswidrig. Die Ordnungswidrigkeit kann mit einer Geldbuße von bis zu 50.000,00 € geahndet werden. Zuständige Verwaltungsbehörde für die Verfolgung und Ahndung von Ordnungswidrigkeiten ist der Kanzler/die Kanzlerin der Technischen Universität Dortmund. Im Falle eines mehrfachen oder sonstigen schwerwiegenden Täuschungsversuches kann der Prüfling zudem exmatrikuliert werden, § 63 Abs. 5 Hochschulgesetz NRW.

Die Abgabe einer falschen Versicherung an Eides statt ist strafbar.

Wer vorsätzlich eine falsche Versicherung an Eides statt abgibt, kann mit einer Freiheitsstrafe bis zu drei Jahren oder mit Geldstrafe bestraft werden, § 156 StGB. Die fahrlässige Abgabe einer falschen Versicherung an Eides statt kann mit einer Freiheitsstrafe bis zu einem Jahr oder Geldstrafe bestraft werden, § 161 StGB.

Die oben stehende Belehrung habe ich zur Kenntnis genommen:

Official notification:

Any person who intentionally breaches any regulation of university examination regulations relating to deception in examination performance is acting improperly. This offence can be punished with a fine of up to EUR 50,000.00. The competent administrative authority for the pursuit and prosecution of offences of this type is the chancellor of the TU Dortmund University. In the case of multiple or other serious attempts at deception, the candidate can also be unenrolled, Section 63, paragraph 5 of the Universities Act of North Rhine-Westphalia.

The submission of a false affidavit is punishable.

Any person who intentionally submits a false affidavit can be punished with a prison sentence of up to three years or a fine, Section 156 of the Criminal Code. The negligent submission of a false affidavit can be punished with a prison sentence of up to one year or a fine, Section 161 of the Criminal Code.

I have taken note of the above official notification.

_____ _____

Ort, Datum
(Place, date)

Unterschrift
(Signature)

Titel der Dissertation:
(Title of the thesis):

_____

_____

_____

Ich versichere hiermit an Eides statt, dass ich die vorliegende Dissertation mit dem Titel selbstständig und ohne unzulässige fremde Hilfe angefertigt habe. Ich habe keine anderen als die angegebenen Quellen und Hilfsmittel benutzt sowie wörtliche und sinngemäße Zitate kenntlich gemacht.
Die Arbeit hat in gegenwärtiger oder in einer anderen Fassung weder der TU Dortmund noch einer anderen Hochschule im Zusammenhang mit einer staatlichen oder akademischen Prüfung vorgelegen.

I hereby swear that I have completed the present dissertation independently and without inadmissible external support. I have not used any sources or tools other than those indicated and have identified literal and analogous quotations.

The thesis in its current version or another version has not been presented to the TU Dortmund University or another university in connection with a state or academic examination.*

*Please be aware that solely the German version of the affidavit ("Eidesstattliche Versicherung") for the PhD thesis is the official and legally binding version.

_____ _____

Ort, Datum
(Place, date)

Unterschrift
(Signature)

Contents

List of Figures

Abbreviations

2,3-DPG	2,3-diphosphoglycerate
ACL	Adenosine triphosphate citrate lyase
Ala	Alanine
APD	Avalanche photodiode
APS	Ammonium persulfate
Arg	Arginine
ATP	Adenosine triphosphate
BD	Binding domain
BSA	Bovine Serum Albumin
CaM	Calmodulin
CaM-BD	Calmodulin binding domain
CCV	Clathrin-coated vesicle
CME	Clathrin-mediated endocytosis
CRISPR	Clustered regulatory interspaced short palindromic repeats
Cys	Cysteine
ddNTP	2`,3`-dideoxy- nucleotide
Dil	1,1`-dioctadecyl-3,3,3`,3`-tetramethylindocarbocyanine perchlorate
DMEM	Dulbecco`s modified eagle`s medium
DNA	Deoxyribonucleic acid
DPSS	Diode pumped solid state
EDTA	Ethylenediaminetetraacetic acid
EE	Early endosomes
FLIM	Fluorescence lifetime imaging microscopy
FRET	Fluorescence resonance energy transfer
Gln	Glutamine
GPCR	G-Protein coupled receptor
GRB2	Growth factor receptor bound protein 2
His	Histidine
HPLC	High-Performance Liquid Chromatography
JM	Juxtamembrane
LB	Lysogeny Broth
LE	Late endosome
LSCM	Laser scanning confocal microscopy

MVB	Multi vesicular body
NADPH	Nicotinamide adenine dinucleotide phosphate
NDPK	Nucleoside diphosphate kinase
NOX	NADPH oxidase
OD	Optical density
PBS	Phosphate-buffered saline
PCR	Polymerase chain reaction
PHPT	Phosphohistidine phosphatase
PMSF	Phenylmethylsulfonyl fluoride
PtdIns	Phosphatidylinositol
PTP	Protein tyrosine phosphatase
PVDF	Polyvinylidene fluoride
RE	Recycling endosome
ROS	Reactive oxygen species
RT	Room temperature
SDS-PAGE	Sodium dodecyl sulfate-polyacrylamide gel electrophoresis
siRNA	Small interfering ribonucleic acid
TAE	Tris base, acetic acid, EDTA
TB	Terrific broth
TBS	Tris-buffered saline
TCR	T cell receptor
TEMED	N,N,N`,N`-tetramethylethylenediamine
Thr	Threonine
TM	Transmembrane
TRPV5	Transient receptor potential-vanilloid-5
Tyr	Tyrosine
WLL	White light laser
wt	Wild type

Abstract

Phosphorylation of polybasic stretches in membrane-associated proteins creates an electrostatic switch influencing their interactions with membrane lipids. Such modification affects their localization, conformational fluctuations and ultimately function. One example for this is the epidermal growth factor receptor (EGFR), which is involved in the pathogenesis of many cancers.

EGFR activation is coupled to a conformational change, where the intracellular domain is released from an autoinhibitory interaction with the plasma membrane after ligand induced calmodulin (CaM) binding. The CaM dependent receptor activation occurs in analogy to the ion channel KCa3.1, which is regulated via histidine phosphorylation. Histidine (His358) phosphorylation of the KCa3.1 channel by nucleoside diphosphate kinase B (NME2) induces binding of the active calcium-CaM complex and further activation, while dephosphorylation by phosphohistidine phosphatase 1 (PHPT1) results in an inactive conformation.

For EGFR, a single histidine residue (His648), located in the polybasic CaM binding domain (BD), may act as a possible regulatory site. This study demonstrates that the His648 residue is essential for intact ligand induced EGFR activation. For the first time, PHPT1 is identified as a new key player in regulating EGFR activation. Transient PHPT1 overexpression amplifies Tyr phosphorylation of spontaneously activated EGFR, whereas the ligand induced EGFR phosphorylation is reduced. The previously identified oncogenic propensities of PHPT1 could be explained by its enhancement of spontaneous EGFR activation. In addition, the phosphohistidine kinases NME1 and NME2 show the opposite effect in regulating EGFR activation, indicative for a regulation of EGFR activation by the phosphohistidine phosphatase/kinase system in vertebrates. Furthermore, the results suggest that PHPT1 modulates receptor activation in absence and presence of ligand in two independent mechanisms.

Zusammenfassung

Die Phosphorylierung von Membranproteinen, speziell in dessen polybasischen Segmenten, kann als elektrostatischer Schalter fungieren. Dieser reguliert die Interaktion mit Membranlipiden und folglich die Lokalisierung, Konformationsänderung bis hin zur Funktion der Proteine. Ein Beispiel für ein Membranprotein, dessen Konformation durch elektrostatische Interaktionen mit der Plasmamembran bestimmt ist, ist der EGF-Rezeptor (engl. epidermal growth factor). Dieser ist in der Pathogenese verschiedenster Krebsarten involviert.

Die EGFR Aktivierung geht mit einer Konformationsänderung einher, in der nach Ligandenstimulation die intrazelluläre Domäne des Rezeptors das regulatorische Protein Calmodulin (CaM) bindet und somit die autoinhibitorische Interaktion zwischen Plasmamembran und Rezeptor C-terminus aufgehoben wird. Die CaM abhängige Rezeptoraktivierung verläuft in Analogie zu einem weiteren Membranprotein, dem Ionenkanal KCa3.1, dessen Aktivität mittels Histidinphosphorylierung reguliert wird. Während dieses Regulationsprozesses wird der Ionenkanal von der Nukleosid Diphosphat Kinase B (NME2) phosphoryliert (H358), woraufhin der Calcium-CaM Komplex gebunden und der aktive Konformationszustand eingeleitet wird. Die Dephosphorylierung durch die Phosphohistidin Phosphatase 1 (PHPT1) führt hingegen zur Inaktivierung.

Ein allein stehendes Histidin (His648), lokalisiert in der CaM Bindedomäne des EGFRs, dient demnach womöglich als regulatorische Phosphorylierungsstelle. In dieser Arbeit wird gezeigt, dass das Histidin (His648) essenziell für eine intakte ligandenabhängige Rezeptoraktivierung ist. Des Weiteren führt die transiente Überexpression der Phosphatase PHPT1 zu einer amplifizierten Tyr Phosphorylierung von spontan aktivierten Rezeptormolekülen, wohingegen die ligandenabhängige Phosphorylierung reduziert wird. Somit wird PHPT1 erstmals als neue Schlüsselkomponente in der Regulierung der EGFR Aktivierung identifiziert sowie die möglichen Ursachen ihres onkogenen Potentials, basierend auf einer amplifizierten spontanen Aktivierung des EGFRs. Neben der Regulation durch PHPT1 wurden die Phosphohistidin Kinasen NME1 und NME2 näher untersucht. Diese weisen den entgegengesetzten Effekt zu PHPT1 auf und bekräftigen somit, dass die EGFR Aktivierung nicht nur von PHPT1, sondern zudem von dem kompletten Phosphohistidin Phosphatase/Kinase System reguliert wird. Darüber hinaus

wird gezeigt, dass die spontane sowie die ligandenabhängige Aktivierung durch zwei voneinander unabhängigen Mechanismen moduliert wird.

1 Introduction

1.1 Charged protein-lipid interaction at the plasma membrane

In the cascade of gene-RNA-protein networks, much work has been done to investigate the role of proteins in regulating gene expression, metabolism and apoptosis. All these proteins, acting in a specific network topology, must be regulated spatiotemporally in a precise and dynamic manner. Protein regulatory networks have to be flexible enough to adapt to changes in the extracellular environment. As part of their localization, proteins located at the plasma membrane are the link between the extracellular environment and the inside of the cell and they therefore have to be able to recognize extracellular stimuli and propagate signals into the cell to translate it into specific cell fates[1].

There are several ways to regulate membrane-bound proteins, one of which is via charged protein-lipid interaction. In mammalian cells approximately 70 % of the total lipids consist of glycerophospholipids, while less then 20 % are represented by anionic phosphatidylinositol (PtdIns)[2]. PtdIns are involved in the regulation of signal transduction at the plasma membrane by stabilizing the active conformation of membrane bound proteins via electrostatic interaction through its negatively charged phosphate group. They are also involved in regulating membrane trafficking as well as transport functions of membranes[3]. At structural level, PtdIns consist of an inositol molecule linked to the hydrophobic tail via an anionic phosphate group (Figure 1A). The acidic phospholipid PtdIns are phosphorylated at the 3`, 4` and 5` positions to form PtdIns(4)P, PtdIns(3,4)P_2, PtdIns(4,5)P_2 and PtdIns(3,4,5)P_3, which are enriched in the inner leaflet of the plasma membrane to generate a net negative charge.

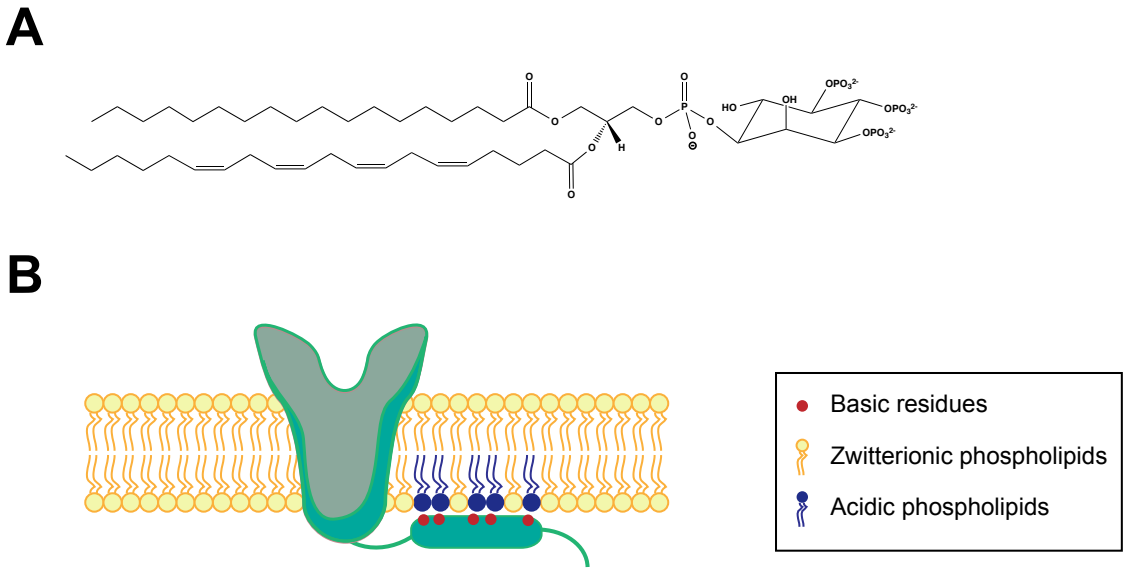

Figure 1: Charged protein-lipid interaction. (A) Structure of the acidic phospholipid PtdIns(3,4,5)P_3 as an example. **(B)** Typical charged protein-lipid interaction through electrostatic interactions between the acidic phospholipids in the inner leaflet of the plasma membrane and a polybasic sequence of a membrane-associated protein.

For an intact electrostatic protein-lipid interaction the protein requires a positively charged lipid-binding domain or a polybasic sequence directly located next to the transmembrane domain (Figure 1B). In addition, the interaction becomes stabilized by hydrophobic residues, interacting with the acyl chains of the bilayer made up by phospholipids[4]. These interactions are able to locate cytosolic proteins to the plasma membrane, thus enabling their biological activity[5,6]. Additionally, these anionic phospholipids facilitate the release of protein domains containing functional sites, which recruit effector proteins to enable transmembrane signal transduction[7,8]. Several membrane-bound proteins, like specific ion channels and transporters, require a conformational change to get activated. This change of conformation is regulated by several components, whereas the electrostatic interaction with PtdIns(4,5)P_2 represents one of them[9,10].

1.2 Regulation of charged protein-lipid interaction

The ionic protein-lipid interaction between phosphorylated PtdIns in the plasma membrane and polybasic protein sequences are regulated by different factors. One important second messenger is the calcium cation Ca^{2+}, which is able to neutralize negatively charged phospholipids, regulate PtdIns degradation and activate calmodulin

(CaM), which acts as a competitor to interrupt the protein-lipid interaction[11,12,13]. The role of the Ca^{2+}-binding molecule CaM is to transfer the Ca^{2+} signal by modulating the activity of downstream enzymes. It has no catalytic activity on its own, only consisting of a negatively charged surface to bind polybasic proteins interacting with the enriched anionic phospholipids in the plasma membrane. The additional negative charges induce an electrostatic repulsion causing an interruption of the protein-lipid interaction[14,15,4].

One membrane-associated protein, regulated through this mechanism, is the potassium channel KCa3.1. CaM is constitutively bound to its cytosolic C-terminal tail, where Ca^{2+} binding induces the open state of the channel[16]. The CaM binding domains (CaM-BD) include a series of basic and hydrophobic amino acid residues going from L344 to Q353 (L_{344}AAINAFRQ_{353}) and from K360 to K373 (K_{360}LREQVNSMVDISK_{373}) surrounding a single histidine (His) residue His358[17]. Activation of the ion channel KCa3.1 requires PtdIns(3)P and phosphorylation of His358, which is catalysed by nucleoside diphosphate kinase-B (NME2), while the dephosphorylation by phosphohistidine phosphatase 1 (PHPT1) inhibits the channel by forming the closed state[18,19,20]. The exact mechanism how His phosphorylation and CaM binding regulate KCa3.1 activation has so far not been fully elucidated. Not only ion channels are regulated by protein-lipid interaction[21,22], also G-protein coupled receptors (GPCR)[23], transporter proteins[24] or receptor tyrosine kinases like the epidermal growth factor receptor (EGFR)[25] reveal those regulation mechanisms. Additionally, EGFR is activated in a CaM dependent manner and reveals a single His residue located in the polybasic CaM binding domain such as the ion channel KCa3.1.

1.3 Epidermal Growth Factor Receptor

1.3.1 Clinical significance

The membrane-bound protein EGFR is a receptor tyrosine kinase belonging to the ErbB family. Due to its role as signal transducer, EGFR activation regulates various cellular processes including proliferation, differentiation and survival. The role of aberrant EGFR activity and expression level in oncogenesis has been extensively studied and shows a broad clinical significance[26,27,28]. Overexpression or mutations in ErbB family members are causing an amplified receptor activation, which leads to more than 30 % of breast cancers, 40 % of glioblastomas and 60 % of non-small-cell lung cancers[29,30,31].

Therefore, it is important to elucidate the exact mechanism of EGFR activation and to identify the involved key players in its regulation.

1.3.2 Structure and activation mechanism of EGFR

EGFR consists of an extracellular part, separated into domains I-IV, followed by a transmembrane (TM) helix and an intracellular part. The intracellular part contains a kinase domain and a flexible C-terminal tail, linked to TM helix by a juxtamembrane (JM) segment (Figure 2A)[32,33].

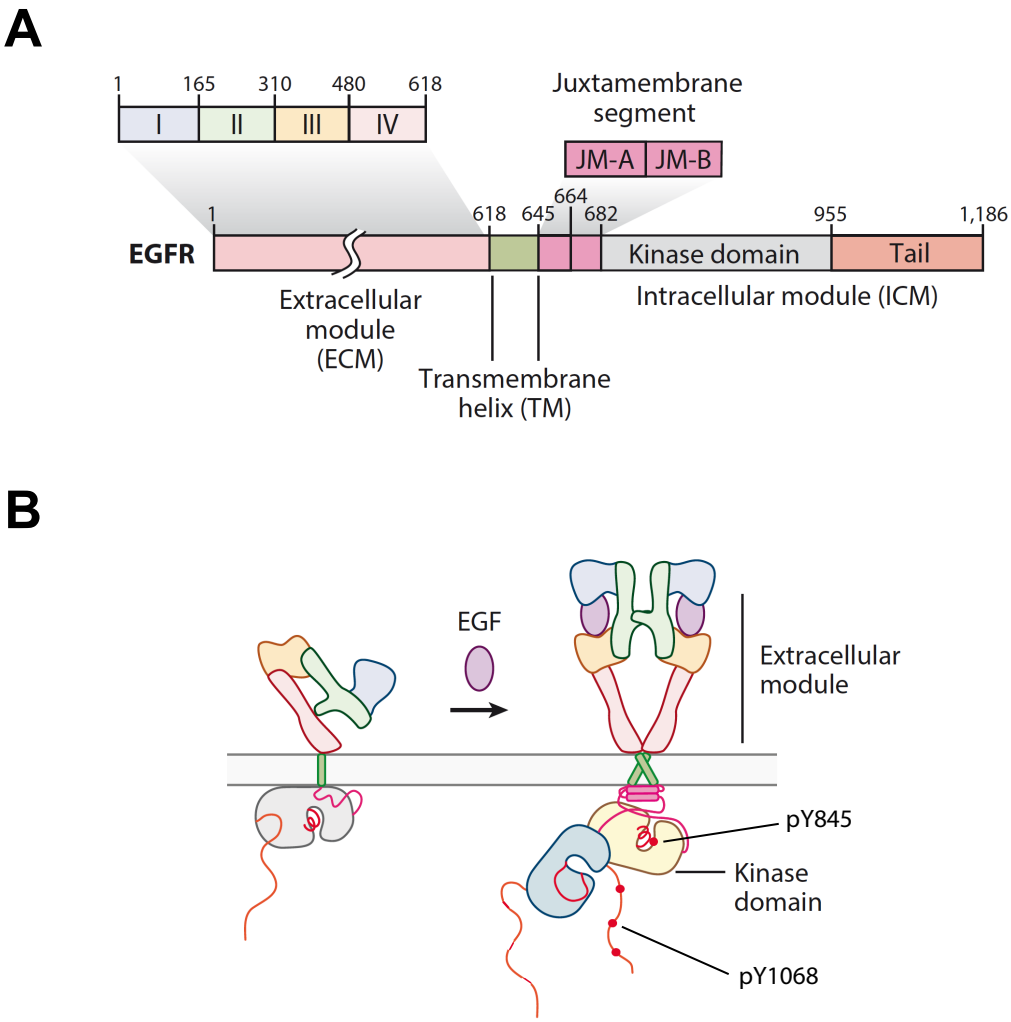

Figure 2: Architecture of EGFR. (A) Domain architecture of EGFR. **(B)** Ligand dependent activation of receptor forming an asymmetric active dimer conformation, which activates kinase activity and induces further auto-phosphorylation. **(**Figure adapted from Kovacs *et al*. 2015[34])

Ligand binding occurs via the extracellular part causing a conformational change, which forms an active asymmetric dimer conformation (Figure 2B). Therefore, the

extracellular domain switches between two states, the compact tethered and the extended form promoting dimerization[35]. The extended state facilitates the formation of a helical dimer between two TM α-helices associated through *N*-terminal GxxxG-like motifs[36]. This conformational change is required to form an antiparallel helical dimer between the JM segments of two receptor molecules, which stabilizes the asymmetric dimer conformation[37]. Finally, the asymmetric kinase dimer is formed, in which one kinase domain, the activator, switches on the receiver kinase[38]. The active kinase domain induces a *trans*-phosphorylation of tyrosine (Tyr) residues located in the catalytic loop and in the C-terminal tail, which are recognized by effector proteins to release downstream signalling cascades[34]. EGFR gets Tyr phosphorylated at different positions. Tyr845, located in the activation loop of the kinase domain, represents a phosphorylation site, which has a regulatory autocatalytic function by increasing EGFR activity[39]. Therefore, it regulates several cellular processes such as cell proliferation, metabolism as well as cell cycle control. The residue is not only auto-phosphorylated by EGFR, but additionally external-phosphorylated by Src kinase[40]. For receptor signal propagation, the effector protein growth factor receptor bound protein 2 (Grb2) has to bind phosphorylated Tyr1068 at the C-terminal tail of EGFR, thus resulting in Tyr1068 acting as a signalling site (Figure 2B)[41].

EGFR does not only form dimers, but also higher-order clusters have been observed after receptor activation[42]. The ligand dependent activation of EGFR is well studied, while the activation mechanism in absence of ligand has to be further elucidated. It has been shown that the spontaneous activation of the receptor occurs through short-lived dimers due to thermal fluctuations in the plasma membrane and only at high expression level[43,44,45]. There is evidence for distinct molecular states, where spontaneous EGFR activation takes place mainly in the monomeric state[46].

1.3.3 Regulation of EGFR activity by receptor internalization

EGFR activity is controlled by intracellular trafficking (endocytosis), which induces receptor recycling or degradation. This prevents a hyperactivation of the receptor on the plasma membrane, which would turn normal cells into malignant cells. Therefore, the majority of ligand bound EGFR is internalized via clathrin-mediated endocytosis (CME). The phosphorylation of Tyr1045 recruits c-Cbl, an E3 ligase, which ubiquitinates the receptor[47]. The polyubiquitinated receptor is recruited to clathrin-

coated pits and induces a unidirectional vesicular trafficking causing lysosomal degradation. First, the ligand-receptor complex located in clathrin-coated vesicles (CCVs) fuse to early endosomes (EE). These endosomes maturate to late endosomes (LE) and multi vesicular bodies (MVB) and fuse with lysosomes for final protein degradation[48,49]. In contrast to the lysosomal degradation of ligand bound EGFR, the spontaneous activated EGFR monomer induces a continuous recycling back to the plasma membrane through the recycling endosome (RE)[46]. Compared to the ligand bound mechanism, the receptor is not ubiquitinated, which is the signal for sorting into late endosomes and lysosomal degradation. In both cases, the signalling is terminated by dephosphorylation, catalysed by specific phosphatases in the perinuclear area.

1.3.4 JM-PM interaction as an autoinhibitory mechanism

There are several mechanisms regulating EGFR in terms of signalling onset and termination in the cell. In addition to the vesicular trafficking, the autoinhibitory mechanisms of EGFR create a highly energetic barrier, which has to be overcome to activate the receptor. Autoinhibition of EGFR occurs on many levels including the closed, tethered state of the extracellular domain[50], the disordered N lobe dimerization interface of the kinase domain[39] and the electrostatic interaction between the intracellular part and the plasma membrane[51], which stabilize the inactive conformational state. The JM segment, involved in the electrostatic interaction between receptor and plasma membrane, plays an important regulatory role for EGFR activation. Depletion of the JM region prevents the phosphorylation of the *C*-terminal tail, which normally transduces signalling[52]. In addition, oncogenic EGFR JM mutations (V665M and L679F), increasing receptor activation, thus revealing a clinical importance for this domain[29].

The JM region is divided into two segments, the *N*-terminal JM-A and *C*-terminal JM-B part. It contains abundant positively charged residues forming a polybasic sequence directly located next to the transmembrane domain. The active conformational state reveals an antiparallel helix dimer for JM-A, formed between two L_{655}RRLL_{659} motifs[25], whereas one JM-B segment of an acceptor kinase extensively interact with the kinase C-lobe of a donor kinase (Figure 3A)[53,54]. In contrast to this, it has been observed that JM-A is embedded in the plasma membrane when the inactive conformation is formed. Therefore, hydrophobic residues of this segment interact with the interior of the plasma

membrane bilayer and basic residues with the anionic head groups of PtdIns(4,5)P_2[51,55]. Not only the JM is involved in interacting with the plasma membrane, also the kinase domain contains hydrophobic and basic residues, which promote the embedded state[38,56]. Both conformational states, the inactive and active one, are stabilized by electrostatic interactions with the plasma membrane, whereas the inactive embedded state is favoured.

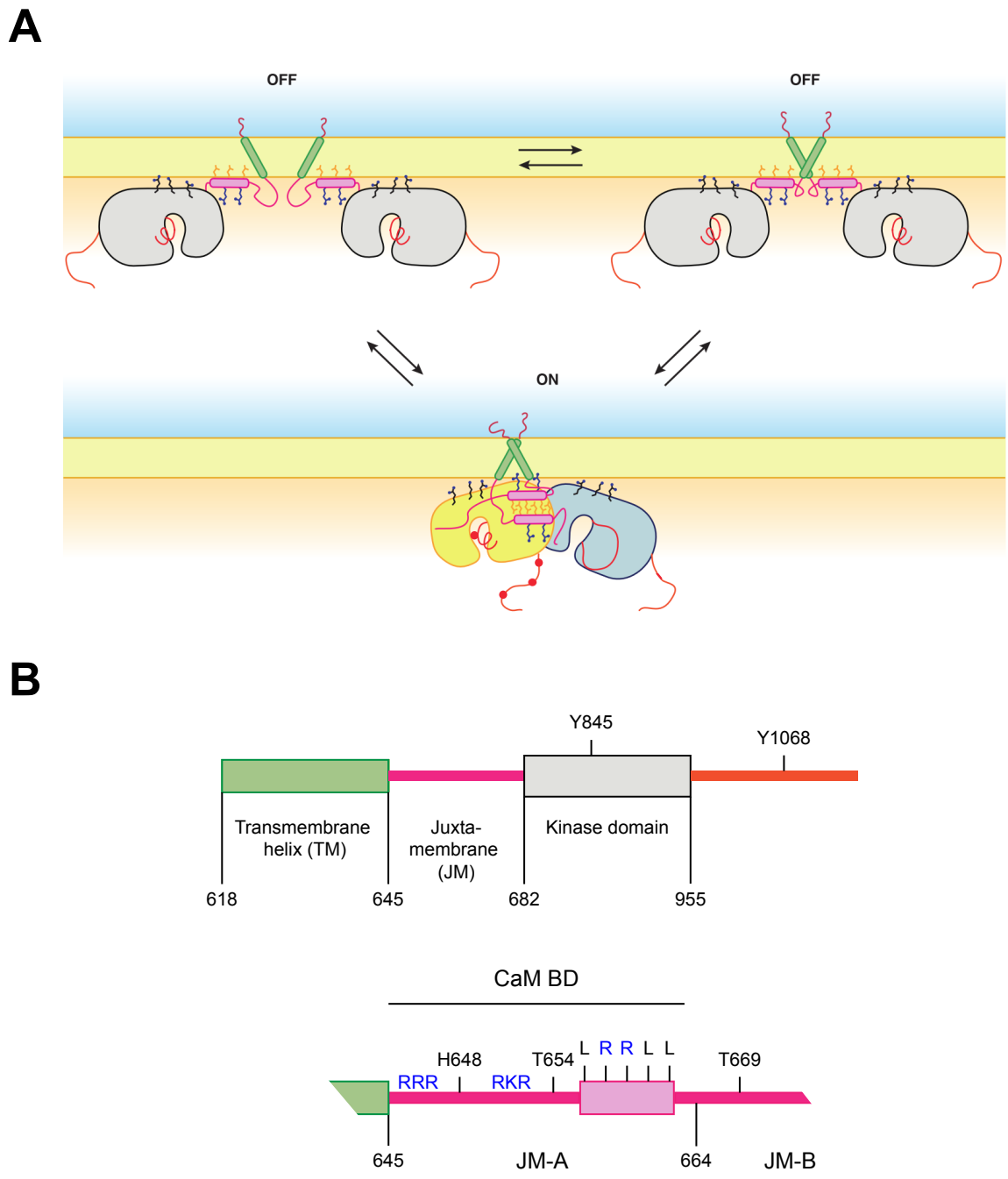

Figure 3: The JM conformation during EGFR activation. (A) EGFR interaction with the plasma membrane in the inactive (OFF) and active (ON) state. Extracellular part is excluded for simplification. **(B)** Sequence of the TM and intracellular part, especially of JM-A segment in detail. (Figure adapted from Endres *et al.* 2014[56])

Within the JM of EGFR, there are three clusters of positively charged residues ($R_{645}RR_{647}$, $R_{651}KR_{653}$ and $R_{656}R_{657}$) interacting with anionic lipids PtdIns(4,5)P_2, which are enriched in the cell membrane encompassing the receptor molecules (Figure 3B)[57]. The first positive cluster ($R_{645}RR_{647}$) is located directly next to the plasma membrane

and interacts with PtdIns(4,5)P_2 to stabilize the active anti-parallel helical dimer of two JM-A segments away from the membrane[25]. Within the JM there are two single threonine (Thr) residues Thr654 and Thr669, located in JM-A directly next to the LRRLL-motif and in JM-B. These sites are phosphorylated and act as regulatory sites[58,59]. In both cases phosphorylation lead to an impaired EGF-induced EGFR phosphorylation[52]. Furthermore, there is one single His residue (His648) located in the polybasic stretch of the JM-A segment, which has been overlooked by previous studies. Additionally, the JM-A segment contains a CaM-binding domain (CaM-BD) (R_{645}RRHIVRKRTLRRLLQ_{660})[60]. In recent studies it has been demonstrated that CaM binds EGFR and facilitates the ligand dependent activation, while the receptor activity is inhibited by mutating this region[61]. EGF stimulation increases the intracellular calcium ion concentration generating active Ca^{2+}-CaM complexes, which bind EGFR and release the intracellular part from the membrane surface by suppressing the inactive embedded state (Figure 4)[62,63,64]. Therefore, CaM facilitates the ligand activation of EGFR.

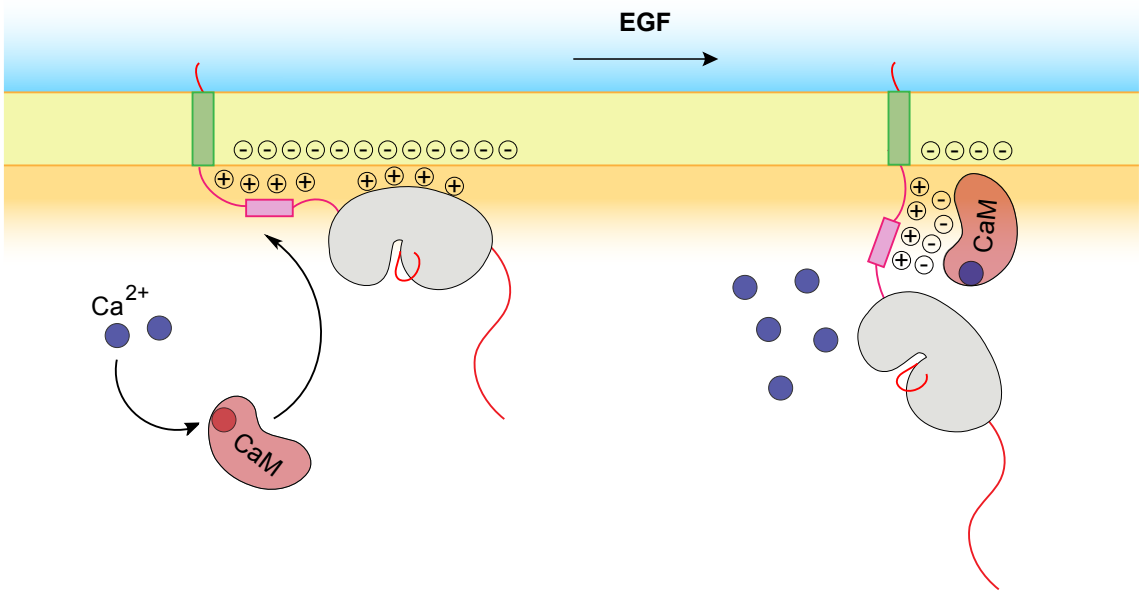

Figure 4: Suppression of the inactve embedded EGFR state by CaM. Release of the intracellular part of EGFR after EGF stimulation by CaM binding.

While Thr654 phosphorylation inhibits CaM binding and therefore reduces ligand-induced EGFR activation, Thr669 phosphorylation shows no effect[65]. The detailed regulatory mechanism based on how JM is affecting EGFR activation, has to be further elucidated.

1.4 Phosphohistidine phosphatases and kinases

1.4.1 Phosphohistidine as posttranslational modification

Posttranslational protein modification by phosphorylation is a key mechanism in the regulation of signalling cascades from cell surface receptors to the nucleus. A receptor molecule gets activated at the plasma membrane and binds other effector proteins in the cytoplasm and activates a signalling network. Finally, the signal is transmitted to the nucleus, where transcription factors regulate essential cell processes like proliferation or apoptosis[66]. While the *O*-phosphorylation of serine (Ser), Thr and Tyr residues has been extensively studied in signal transduction, *N*-phosphorylation of His residues remains poorly understood in mammalian cells[67,68,69]. His phosphorylation turns out to be challenging to detect due to its instability caused by the unstable phosphoramidate bond, which is generated by phosphorylating an imidazole ring (Figure 5). There exist two isoforms 1- and 3-phosphohistidine. Due to the highly energetic P-N bond, phosphohistidine represents a short-lived posttranslational modification, undergoing dephosphorylation even under acidic conditions and at elevated temperature[70]. Therefore, His phosphorylation represents a new overlooked posttranslational modification, which might be more essential for signal transduction in mammalian cells than what previous studies have shown.

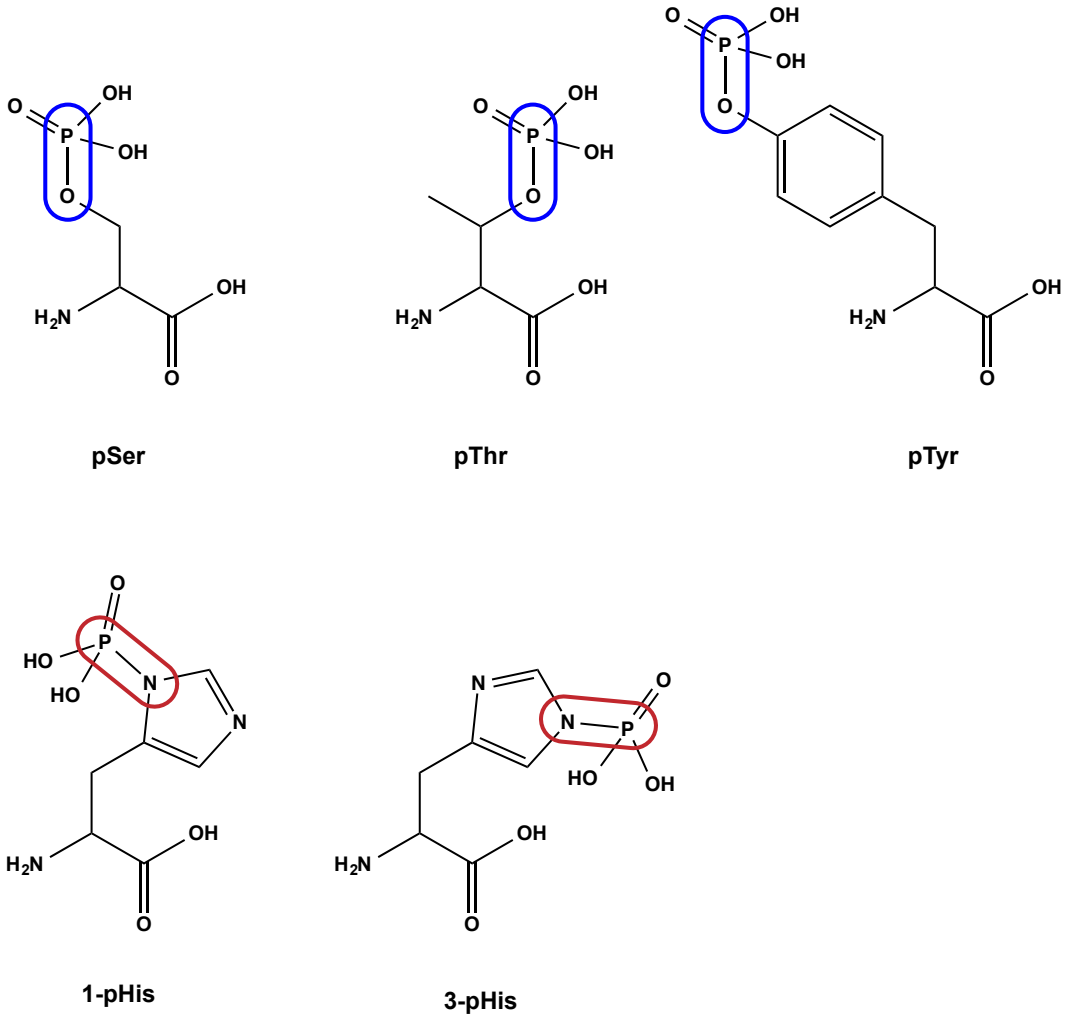

Figure 5: *O*- and *N*-phosphorylated amino acids. Stable phosphoester of *O*-phosphorylated amino acids pSer, pThr and pTyr (blue) and labile phosphoramidate of *N*-phosphorylated His, 1-pHis and 3-pHis (red).

1.4.2 PHPT1 and NDPK

There are phosphatases catalysing the dephosphorylation of phosphohistidine, like the phosphoserine and phosphothreonine phosphatases, PP1, PP2A, PP2C and PGAM5[71,72]. Besides the phosphatase LHPP, which is known to dephosphorylate His residues *in vitro*[73,74], only one specific phosphohistidine phosphatase (PHPT), PHPT1, has been identified in mammalians to date[75]. PHPT1 shows potential clinical relevance. It is involved in the tumour invasion and migration in lung cancer cell lines[76,77] and it also affects the cell proliferation and differentiation in glioblastoma cells and rapidly dividing epithelial human tissue[78]. Overexpression of PHPT1 induces cell damage in human umbilical-vein endothelial cells[79], an increased tumour size of clear-cell renal

carcinoma and therefore reduces patient survival[80]. Due to its carcinogenic potential, PHPT1 has been identified as an oncogene.

PHPT1 is a cytosolic enzyme consisting of 125 amino acids. The secondary structure is defined by six β-strands surrounded by two α–helices (Figure 6A). The active site is formed by a positively charged region including conserved residues, which binds phosphohistidine containing substrates (Figure 6B)[81]. Mutations in this area of two specific His residues (His53 and His102) to alanine (Ala) causes an attenuation of phosphatase activity[82]. Therefore, these specific residues play a crucial role for the catalytic activity.

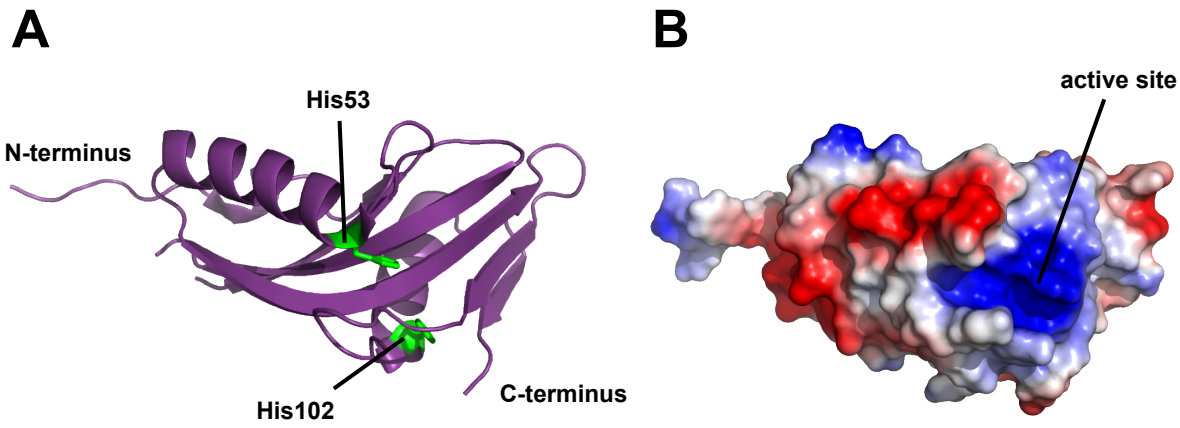

Figure 6: Crystal structure of PHPT1. (A) Cartoon representation of PHPT1. The residues His53 and His102 are highlighted in green. **(B)** The postivie (blue) and negative (red) electrostatic potential of PHPT1 as a solid surface represantion. (PDB ID: 2HW4)

In contrast to phosphotyrosine phosphatases, there is no catalytic cysteine (Cys) in the active site. Additionally, the *C*-terminus plays an important role for enzyme activity. A depletion of the last five residues leads to a loss of function. Moreover, the primary structure of the *C*-terminus contains highly conserved residues, indicating that the *C*-terminus is essential for catalytic activity[83]. PHPT1 shows a complete different structure compared to other phosphatases and no common substrate recognition sequence. Therefore, the exact mechanism for substrate recognition and catalysis remains to be elucidated in the future[81].

If His residues are dephosphorylated, it must exist a kinase catalysing the reverse reaction. A small kinase, nucleoside diphosphate kinase (NDPK), has been identified as

a His phosphorylating protein. There are two isoforms of NDPK, NME1 and NME2, acting as histidine kinases in mammals[84,85]. To become catalytically competent, the kinase has to oligomerize into a hexamer. NDPKs are involved in nucleotide metabolism by forming pHis-containing enzyme intermediates, which transfer the phosphate from a nucleoside triphosphate to a nucleoside diphosphate[86,87]. Furthermore, it has been shown that auto-phosphorylated NDPK transfers the highly energetic phosphoryl group to His containing substrate proteins[67]. Additionally, the auto-phosphorylated state increases the affinity to lipids causing a recruitment of cytosolic NDPKs to the membrane, where the enzyme phosphorylates several membrane proteins[88]. While PHPT1 acts as an oncogene, the kinases NME1 and NME2 have been identified as metastasis suppressor genes[89].

1.4.3 Common targets of PHPT1 and NDPK

PHPT1 and NDPK represent the phosphatase-kinase system for His phosphorylation in mammalian cells (Figure 7A). Several common targets of PHPT1 and NDPK have been identified, like adenosine triphosphate citrate lyase (ACL)[90], beta-subunit of G-proteins[91] and two ion channels, transient receptor potential-vanilloid-5 (TRPV5) and KCa3.1[20,92] (Figure 7B).

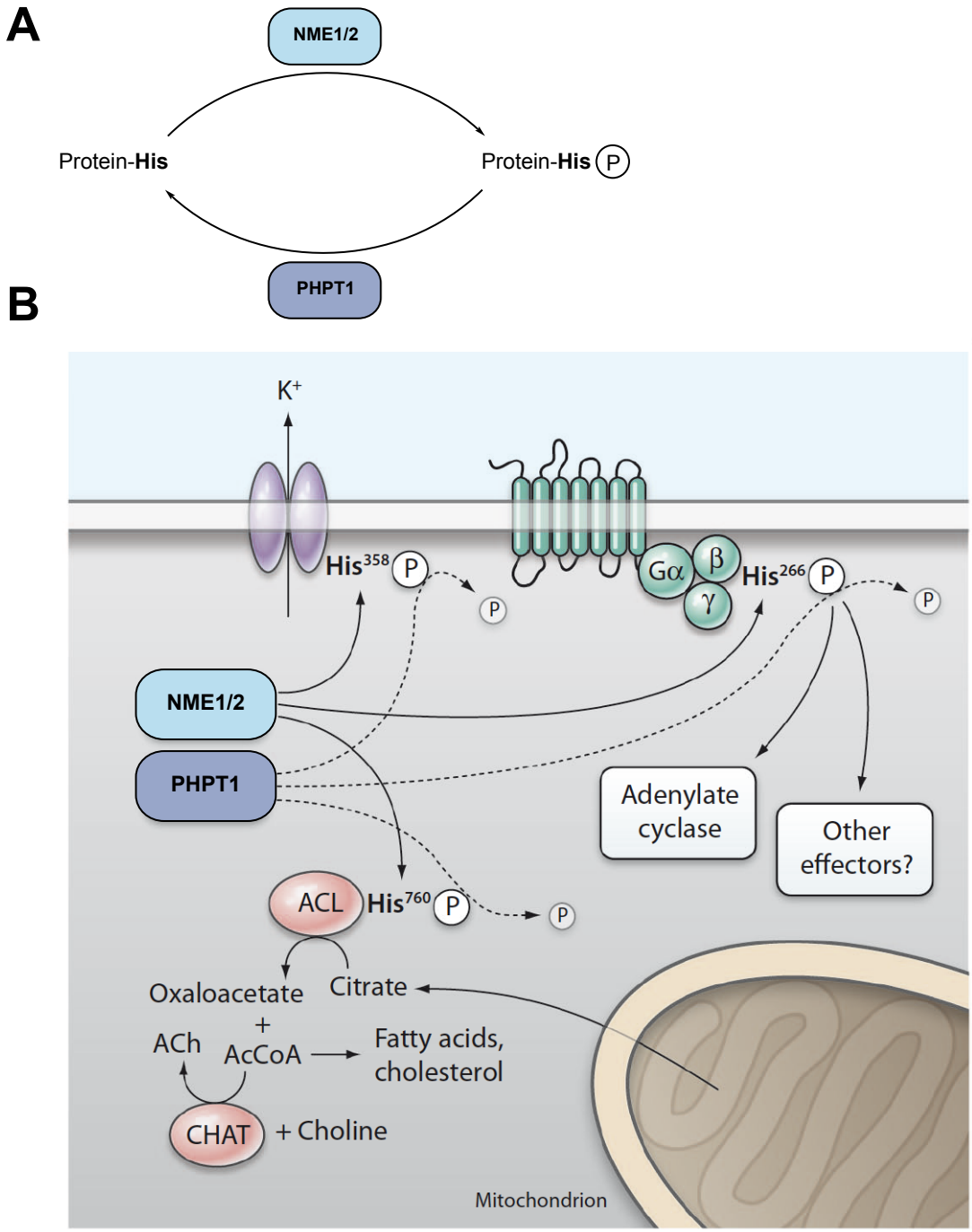

Figure 7: Reversible His phosphorylation in vertebrates. (A) General scheme of regulating His phosphorylation by the phosphohistidine kinases NME1 and NME2, and the phosphatase PHPT1. **(B)** Specific His phosphorylated targets regulated by NME1/2 and PHPT1. (Figure adapted from Klumpp *et al.* 2009[67])

ACL gets His phosphorylated by NME1[93], while an overexpression of PHPT1 causes a dephosphorylation leading to apoptosis of neuronal cells and a reduced cell viability[94,95]. It is reasonable to conclude that PHPT1 might be involved in neurodegenerative diseases[84]. A second target of PHPT1 is the β-subunit of G-proteins. An overexpression

of NME2, phosphorylating His266 of G-proteins, amplifies phosphorylation of G-proteins` β-subunit, thus increasing the activation of G-proteins[96,85]. Due to the G-protein mediated insulin secretion, an overexpression of PHPT1, results in dephosphorylation of pHis266[91], causes type 2 diabetes in the human insulin-producing β-cell line INS 832/13[97]. In addition to ACL and G-proteins, two specific ion channels have been observed to become His phosphorylated by NME2. One of these is the Ca^{2+}-permeable ion channel TRPV5, which plays a crucial role in Ca^{2+} homeostasis in the kidneys. By phosphorylating His711 located at the *C*-terminal tail of the channel, NME2 induces the active conformational state and Ca^{2+} flux in the cell. Subsequently, the dephosphorylation catalysed by PHPT1 inhibits the receptor activity[92]. The second ion channel is the Ca^{2+} activated potassium channel KCa3.1, which adopts its active conformation followed by His358 phosphorylation in the intracellular *C*-terminal tail. The phosphorylation is catalysed by NME2, whereas PHPT1 dephosphorylates the channel and induces the inactive conformation. A channel inhibition causes a decreased Ca^{2+} influx followed by a reduced proliferation in T-cells due to the Ca^{2+} dependent T cell receptor activation. Both ion channels, TRPV5 and KCa3.1, require the binding of active Ca^{2+}-CaM complexes for fully activation[20].

It has been shown that PHPT1 and NDPK affect signal transduction cascades like G-protein and Ca^{2+} signalling influencing crucial cellular processes, but more signalling cascades regulated by His phosphorylation might be identified in the future.

2 Objective

An aberrant EGFR activation plays a crucial role in the cancerogenesis of various types of cancers, thus showing a broad clinical significance[26,27,28]. The receptor gets activated in presence of ligand by forming an active asymmetric dimer, while the spontaneous activation in absence of ligand occurs mainly in the monomeric state, forming only short-lived transient dimers for activation. The ligand induced activation has been extensively studied, whereas the spontaneous activation has recently gained more attention[98].

The complete mechanism of EGFR activity regulation is not yet fully understood, not even all regulators are known. Although previous studies have identified certain regulators of EGFR activation such as PTPs, phosphohistidine phosphatases have so far not been considered. PHPT1, as the first specific phosphohistidine phosphatase identified in vertebrates, regulates the downstream signalling of membrane bound proteins like the calcium signalling via the ion channel KCa3.1 or GPCR. In analogous to KCa3.1, EGFR contains a CaM binding domain in its polybasic JM and in which a single His residue (His648) is located. While KCa3.1 requires His phosphorylation in this domain for binding the active calcium-CaM complex and further activation, the dephosphorylation by PHPT1 transfers the ion channel to an inactive conformational state. This raises the question whether PHPT1 regulates EGFR activation in a related mechanism.

To answer this question, we have to investigate the effect of PHPT1 on spontaneous and ligand induced EGFR activation as well as the role of the His648 residue and if it serves as a substrate site for PHPT1.

3 Material and Methods

3.1 Material

3.1.1 Chemicals

2`-deoxyadenosine-5`-triphosphate (dATP)	Invitrogen™ Life Technologies
2`-deoxycytidine-5`-triphosphate (dCTP)	Invitrogen™ Life Technologies
2`-deoxyguanosine-5`-triphosphate (dGTP)	Invitrogen™ Life Technologies
2`-deoxythymidine-5`-triphosphate (dTTP)	Invitrogen™ Life Technologies
Ammonium persulfate (APS)	SERVA Electrophoresis GmbH
Ampicillin sodium salt	SERVA Electrophoresis GmbH
Bromophenol blue	Sigma-Aldrich®
Complete Mini EDTA-free protease inhibitor tablets	Roche Applied Science
Dil staining	ThermoFisher Scientific
Dimehtyl sulfoxid (DMSO)	SERVA Electrophoresis GmbH
Ethanol	J.T.Baker
Ethylendiaminetetraacetic acid (EDTA)	Fluka® Analytical
Glycerol	GERBU Biotechnik GmbH
Hoechst® 33342	ThermoFisher Scientific
Kanamycin sulfate	GERBU Biotechnik GmbH
Magnesium chloride ($MgCl_2$)	Merck KG
Methanol	Sigma-Aldrich®
N,N,N`,N`-tetramethylethylenediamine (TEMED)	Sigma-Aldrich®
Phenylmethylsulfonyl fluoride (PMSF)	Sigma-Aldrich®
Phosphatase inhibitor cocktail 2	Sigma-Aldrich®
Phosphatase inhibitor cocktail 3	Sigma-Aldrich®
Poly-L-lysine	Sigma-Aldrich®
Roti®-Histofix 4%	Carl Roth GmbH
Sodium azide	Sigma-Aldrich®
Sodium chloride (NaCl)	Fluka® Analytical
Sodium dodecyl sulfate (SDS)	Carl Roth GmbH
Tris-base	Carl Roth GmbH

Tris-HCl	J.T.Baker
Triton X-100	SERVA Electrophoresis GmbH
Tween 20	SERVA Electrophoresis GmbH
UltraPure™ Agarose	Invitrogen™ Life Technologies

3.1.2 Enzymes, proteins and antibodies

α-Tubulin mouse (#T6074) (WB 1:2500)	Sigma Aldrich®
Accu Prime Pfx DNA Polymerase (#12344024)	Thermo Fisher Scientific
Alexa Fluor® 647 Donkey anit-Mouse IgG (#A-31571)	Thermo Fisher Scientific
Alexa Fluor® 647 Goat anti-Rabbit IgG (#A-21244)	Thermo Fisher Scientific
Anti-N1-pHis (1-pHis) Ab (#MABS1330) (WB 1:200)	Merck Millipore
Anti-N3-pHis (3-pHis) Ab (#MABS1351) (WB 1:200)	Merck Millipore
Anti-phospho tyrosine mouse Ab pY72 (p172.1)	InVivo Biotech Services
Bovine serum albumin (BSA) (#B9000S)	New England Biolabs
Chameleon® Duo Pre-stained Protein Ladder (#928-60000)	LI-COR® Biosciences
EGFR goat Ab (#AF231) (WB 1:500, IF 1:200)	R&D System®
EGFR pY1045 rabbit Ab (#2237) (WB 1:500)	Cell Signalling
EGFR pY1068 rabbit Ab (#2234) (WB 1:500, IF 1:200)	Cell Signalling
EGFR pY845 mouse Ab (#558381) (WB 1:500, IF 1:200)	BD Pharmingen™
EGFR total rabbit Ab (#4267) (WB 1:500)	Cell Signalling
Epidermal growth factor human (#E9644)	Sigma Aldrich®
IRDye® 680RD Donkey anti-Mouse IgG (#925-68072)	LI-COR® Biosciences
IRDye® 800CW Donkey anti-Goat IgG (#925-32214)	LI-COR® Biosciences
IRDye® 800CW Donkey anti-Rabbit IgG (#925-32213)	LI-COR® Biosciences
mCherry mouse Ab (#632543) (IP 1:100)	Living Colors®
mCitrine rabbit Ab (#632592) (IP 1:200)	Living Colors®
NME1	Provided by Stephen Fuhs

PfuTurbo DNA Polymerase (#600250)	Agilent Technologies
PGAM1	Provided by Stephen Fuhs
PHPT1 rabbit Ab (#H6790) (WB 1:1000)	Sigma Aldrich®
Protein-G-Sepharose®, Fast Flow (#P3296-5ML)	Sigma-Aldrich®
Restriction endonucleases	New England Biolabs Inc.
T4 DNA Ligase (#750589)	Thermo Fisher Scientific

3.1.3 Oligonucleotides

All oligonucleotides were purchased from Eurofins in HPLC purified form. All primer sequences are found in supplementary material.

3.1.4 Plasmids

EGFR-mCitrine (pmCitrine-N1)	Provided by Bastiaens lab
EGFR-mCitrine H648A (pmCitrine-N1)	Provided by Bastiaens lab
FLAG-NM23-H1	Addgene
mCitrine (pOPIN)	Provided by Dortmund Protein Facility (DPF)
mCitrine-PHPT1 (pOPIN)	Provided by Dortmund Protein Facility (DPF)
pcDNA3.1 +	Invitrogen™ Life Technologies
pDONR223-NME2	Addgene
pmCherry-C1	Clonetech Laboratories Inc.
pmCherry-N1	Clonetech Laboratories Inc.

3.1.5 Kits and commercial solutions

Molecular biology

10x *Pfu* amplification buffer	Invitrogen™ Life Technologies
10x Accu Prime Pfx Reaction Mix	Thermo Fisher Scientific
2-log DNA ladder	New England Biolabs Inc.
5x reaction buffer (T4 DNA ligase)	Thermo Fisher Scientific
6x DNA gel loading buffer	Novagen
BigDye® Terminator v1.1 v3.1 5x Sequencing buffer	Thermo Fisher Scientific
BigDye® Terminator v3.1 cycle sequencing kit	Applied Biosystems

E. coli XL-10 Gold	StrataGen
Nucleobond® finalizer	Macherey-Nagel
NucleoBond® Xtra Maxi EF kit	Macherey-Nagel
NucleoSeq	Macherey-Nagel
RedSafe nucleic acid staining solution	iNtRON Biotechnology
Roti®-Prep Plasmid MINI kit	Carl Roth GmbH
Zymoclean™ Gel DNA recovery kit	Zymo Research

Cell culture

Dulbecco`s modified eagle`s medium (DMEM)	PAN™ Biotech GmbH
Dulbecco`s phosphate buffered salt solution (DPBS)	PAN™ Biotech GmbH
Fetal calf serum (FCS)	PAN™ Biotech GmbH
Fugene® 6 transfection reagent	Roche Applied Science
L-Glutamine	GIBCO®/Invitrogen™
Lipofectamine™ 2000	Invitrogen™
MCF-7 (Human mammary gland adenocarcinoma)	American tissue culture collection (ATCC)
Non-essential amino acids (NEAA)	PAN™ Biotech GmbH
Trypsin 0.25 %/EDTA 0.02 % in PBS	PAN™ Biotech GmbH

Biochemistry

30 % Acrylamide/Bis-solution	Bio-Rad Laboratories, Inc.
Bradford reagent	Sigma Aldrich®
NewBlot™ PVDF stripping buffer	LI-COR® Biosciences
Odyssey® Blocking Buffer (TBS)	LI-COR® Biosciences

3.1.6 Buffers and solutions

Molecular biology

1xTAE buffer	40 mM Tris/Acetate (pH7.5), 20 mM NaOAc, 1 mM EDTA
LB agar plate	15 g/L agar in LB medium, pour plates, add antibiotic at desired concentration
LB medium	10 g/L Bacto-trypton, 5 g/L bacto-yeast extract, 10 g/L

	NaCl, pH 7.4 and finally autoclave
TB medium	12 g/L trypton, 24 g/L yeast extract, 0.4 % glycerine, 2.31 g/L KH_2PO_4, 12.54 g/L K_2HPO_4 and autoclave

Cell culture

1xPBS buffer	135 mM NaCl, 2.7 mM KCl, 10 mM Na_2HPO_4, 2 mM KH_2PO_4, pH 7.4
Complete Growth Media	10 % FCS, 1 % L-Gln , 1 % NEAA in DMEM
Starvation Media	0.5 % FCS, 1 % L-Gln, 1 % NEAA in DMEM

Biochemistry

10 % APS	100 mg/mL APS in ddH_2O (freshly prepared)
10 % SDS	100 g/L SDS in ddH_2O
1xLysis buffer (Immunoprecipitation)	50 mM Tris pH 7.5, 150 mM NaCl, 1 mM EDTA, 1 mM EGTA, 10 % glycerol (optional: 0.25 % Na deoxycholate or 1 % IGEPAL)
1xRIPA lysis buffer	50 mM Tris pH 7.5, 150 mM NaCl, 1 mM EGTA, 1 mM EDTA, 0.25 % Na-deoxycholate, 1 % IGEPAL, 2.5 mM Na-pyrophosphate, 1 mM β-glycerophosphate in ddH_2O
1xRunning buffer	25 mM Tris-Base, 190 mM glycine, 0.1 % SDS
1xTBS buffer	50 mM Tris (pH 7.4), 150 mM NaCl
1xTBS-T	50 mM Tris (pH 7.4), 150 mM NaCl, 0.1 % Tween 20
1xTransfer buffer	25 mM Tris-Base, 190 mM
2xLaemmli buffer pH8.8	100 mM Tris-Base (pH 8.8), 20% glycerol, 4% SDS, 20 mM EDTA, 200 mM DTT, 0.008 % bromophenol blue
5xLaemmli buffer	60 mM Tris-HCl (pH 6.8), 25 % glycerol, 2 % SDS, 14.4 mM 2-mercapto-ethanol, 0.1 % bromophenol blue
TMD buffer	20 mM Tris-HCl pH 8.0, 5 mM $MgCl_2$, 1 mM DTT

3.1.7 Equipment

Centrifuges

Centrifuge 5417R (4°C)	Eppendorf
Centrifuge 5424 (RT)	Eppendorf
Centrifuge 5810R	Eppendorf
Concentrator Plus	Eppendorf

Sorvall™ RC 6+ Centrifuge	ThermoFisher Scientific

Molecular biology

Mastercycler® Pro	Eppendorf
Mini Electrophorese Unit	Carl Roth
Molecular Imager Gel Doc XR	Bio-Rad Laboratories
NanoDrop ND-1000 Spectrophotometer	Thermo Scientific
Power Pac™ 300	Bio-Rad Laboratories

Cell culture

TC-Plate 6 Well, Standard, F	Sarstedt
Nunc™ Lab-Tek™, 8 well, borosilicate coverglass	Thermo Fisher Scientific
Corning® 96 well plates (CLS3603)	Sigma-Aldrich
TC flask T75, Standard	Sarstedt
Vi-Cell™ XR cell counter	Beckman Coulter

Biochemistry

96 well microplates, black, F-bottom	Greiner Bio One
DU® 800 UV/Visible Spectrophotometer	Beckman Coulter
Heating Block QBD4	Grant Instruments
Immobilon-FL PVDF membrane	Merck Millipore
Microplate Reader SpectraMax M5	Molecular Devices
Mini Trans-Blot® Cell	Bio-Rad
Mini-Protean® Comb, 15-well, 1.5 mm	Bio-Rad
Mini-Protean® Tetra Cell System	Bio-Rad
Odyssey® CLx imaging system	LI-COR
PowerPac™ HC	Bio-Rad
Semi-micro cuvette, PS	Sarstedt
Sonicator Needle (MS 73)	Bandelin Electronic GmbH
Test tube rotator 34528	Snijders
Ultraschall HD 2200	Bandelin Electronic GmbH

Whatman filter paper	Thermo Fisher Scientific

Microscopes

Fiber coupling Uni	Picoquant GmbH
Leica TCS SP8	Leica
Olympus FluoView FV1000	Olympus
Sepia II controller	Picoquant GmbH

3.1.8 Software

Adobe Illustrator	Adobe Systems Inc.
DNASTAR Lasergene v12	DNASTAR Inc.
Fiji	Schindelin et al. Nat. Meth. (2012)[99]
FV10-ASW Fluoview Software	Olympus
GraphPad Prism 6	GraphPad Software Inc.
IgorPro v6.3	WaveMetrics
Leica Application Suite X	Leica Microsystems
MacPyMOL v1.8.2.2	Schrödinger
MS Office 2016	Microsoft Corporation
Python 2.7	Continuum Analytics
Sepia II software	PicoQuant GmbH
SymPhoTime v5.12	PicoQuant GmbH

3.2 Methods

3.2.1 Molecular biology

3.2.1.1 Transformation of chemically competent cells

To introduce foreign DNA into a cell, chemically competent *E. coli* XL-10 Gold cells (100 µL) were gently mixed with plasmid DNA (10 ng), Mutagenesis-PCR mix (7 µL) or ligation reaction (10 µL). The DNA/Cell mixture was incubated on ice for 15 min in the case of circular DNA, while linear DNA had to be incubated for 30 min. After heating for 90 s at 42 °C, the tubes were transferred to 4 °C for 2 min. LB medium

(800 µL) was added to the bacteria and incubated for 1 h at 37 °C and 200 rpm. For the transformation of circular DNA 20 µL were plated out on an antibiotic containing agar plate. In presence of linear DNA the cells were centrifuged for 1 min at 10.000 rpm and resuspended in a residual volume (100 µL). The cells were transferred to LB agar plates containing the appropriate antibiotic and incubated at 37 °C for 16 h.

3.2.1.2 Bacterial cultivation

The LB medium containing pre-cultures (5 mL) were inoculated with single *E. coli* XL-10 Gold colonies in presence of the appropriate amount of antibiotic. These bacterial cultures were incubated for 16h at 37 °C and 200 rpm before isolating the plasmid DNA via plasmid preparation.

3.2.1.3 Isolation of plasmid DNA by using Roti®-Prep MINI kit

The bacterial cultures (5 mL) were harvested at 13.000 rpm for 2 min and the supernatant discarded. The cell pellets were treated according to the manufacturers standard protocol to obtain purified plasmid DNA in elution buffer (30 µL).

3.2.1.4 Endotoxin-Free plasmid DNA purification using NucleoBond® Xtra Maxi EF kit

LB-medium cultures (100 mL) containing the appropriate antibiotic were inoculated with single *E. coli* XL-10 Gold colonies and incubated for 16 h at 37 °C and 200 rpm. To prove the cell growth, the optical density was determined at 600 nm (OD_{600} = 1.5-2.0). The Cells were harvested for 15 min at 4 °C and 4.000 rpm. After discarding the supernatant, the obtained pellets were treated as described in the user manual of the manufacturers and finally loaded to NucleoBond® finalizer to elute endotoxin free plasmid DNA once with 200 µL TE-EF and during a second elution step with 100 µL.

3.2.1.5 Amplification of DNA fragments via Polymerase Chain Reaction (PCR)

The polymerase chain reaction (PCR) was used to amplify a specific DNA sequence. Therefore, primers (forward and reverse) were designed complementary to the template DNA. The melting temperature T_m was calculated:

$$T_m = [2 \cdot (nA + nT) + 4 \cdot (nG + nC)]°C$$

The PCR reaction was catalysed by Accu Prime Pfx DNA polymerase under the following conditions.

Table 1: PCR reaction mixture using AccuPrime Pfx DNA polymerase

Component	Amount
DNA template	200 ng
Forward Primer (100 µM)	0.5 µL
Reverse Primer (100 µM)	0.5 µL
10xAccu Prime Pfx Reaction Mix	5.0 µL
Accu Prime Pfx DNA Polymerase (2.5 U/ µL)	0.4 µL
H_2O	add to 50 µL

Table 2: Temperature PCR protocol for insert amplification

Temperature	Time	Repeats
95 °C	2 min	
95 °C	15 s	
T_m - 5 °C	30 s	30x
68 °C	1 min/kbp	
68 °C	10 min	
8 °C	∞	

3.2.1.6 Site-directed mutagenesis via Quick Change Polymerase Chain Reaction (QC-PCR)

The Quick Change mutagenesis was performed to introduce site-directed mutagenesis in a plasmid, by substitution, insertion or deletion of single nucleotides. Therefore, complementary primers were designed containing 15bp before and after the desired mutation with a T_m of approx. 72 °C. The designed primers are listed in the supplementary material. The PCR was catalysed by *PfuTurbo* DNA Polymerase using the conditions represented in Table 3.

Table 3: Site-directed mutagenesis PCR reaction mixture using *PfuTurbo* DNA polymerase

Component	Amount
DNA template	100 ng
dNTPs (10 mM)	0.5 µL
DMSO (100%)	2.5 µL
Primer (10 µM)	1.0 µL
10x*Pfu* buffer	2.5 µL
PfuTurbo DNA Poymerase (2.5 U/µL)	1 µL
H_2O	add to 25 µL

Table 4: Site-directed mutagenesis PCR protocol

Temperature	Time	Repeats
95 °C	1 min	
94 °C	1 min	
55 °C	1 min	29x
65 °C	2 min/kbp	
65 °C	5 min	
4 °C	∞	

The parental methylated DNA was digested with the restriction enzyme DpnI (10 U/µL, 1 µL) at 37 °C for 1 h. The digested DNA (7 µL of digested solution) was transformed into chemically competent *E. coli* XL-10 Gold cells (100 µL) via heat shock.

3.2.1.7 DNA sequencing

The nucleotide sequence of template DNA was determined by Sanger sequencing method, which uses fluorescently labelled 2`,3`-dideoxy-nucleotides (ddNTPs) as chain terminators. The sequencing PCR reaction was performed using BigDye Terminator v 3.1 Cycle sequencing kit according to Table 5. The PCR reaction was purified by a NucleoSeq column and evaporated at 60 °C in a vacuum centrifuge. Capillary gel electrophoresis was used in our in-house facility Zentrale Einrichtung Biotechnologie to quantify the PCR reaction.

Table 5: BigDye Terminator PCR reaction

Component	Amount
DNA template	500 ng
BigDye Terminator mix	2 µL
5xSequencing buffer	4 µL
Primer (10 µM)	1 µL
ddH_2O	add to 20 µL

Table 6: Big Dye Terminator PCR protocol

Temperature	Time	Repeats
95 °C	5 min	
95 °C	30 sec	
50 °C	10 sec	26x
60 °C	4 min	
4 °C	∞	

3.2.1.8 Agarose gel electrophoresis of DNA

For DNA separation by size, agarose gel electrophoresis was performed. Agarose gels (0.9 % (w/v)) were prepared by dissolving low-melting point UltraPure agarose (4.5 g) in 1xTAE buffer (500 mL) by heating in a microwave for complete dissolution. After adding RedSafe nucleic acid staining solution (5 µL/100 mL), the agarose was poured into a gel tray and stayed at RT for solidification. The solid gel was placed into electrophoresis chamber and covered with 1xTAE buffer. The DNA samples were mixed with DNA loading buffer (6x), loaded into the wells next to the 2-log DNA ladder (1 µg) and separated at a constant voltage of 120 V for 30 to 60 min depending on the gel size. The DNA bound RedSafe has two excitation states (309 and 419 nm), which are used to visualize the DNA at the visible emission state (537 nm). To further proceed, the desired DNA fragment was excised from the agarose gel and purified using the Zymoclean Gel DNA Recovery Kit according to the manufacturers standard protocol. Finally, pure DNA was eluted with DNA elution buffer (6 µL).

3.2.1.9 Restriction digest and ligation of DNA fragments

Double strained DNA (2 µg) was digested with restriction enzymes (5 U/µL, 1 µL) in an appropriate reaction buffer (10x) and a final volume of 40 µL. The reaction was performed at 37 °C for 3 h and purified using agarose gel electrophoresis followed by the Zymoclean Gel DNA Recovery Kit according to the manufacturers protocol. After digestion and purification of the recipient plasmid and insert, both components were ligated using a three-fold molar excess of insert DNA. The required insert amount was calculated:

$$insert\ [ng] = vector\ [ng] \cdot \frac{insert\ [bp]}{vector\ [bp]} \cdot 3$$

The ligation reaction was catalysed by T4 DNA ligase (1 U/µL, 0.5 µL) in presence of 5xreaction buffer in a final volume of 20 µL and incubated at 37 °C for 3 h. The crude ligation reaction (10 µL) was used for transformation into chemically competent bacterial cells (100 µL) via heat shock.

3.2.2 Mammalian cell culture

3.2.2.1 Cultivation of mammalian cells

The passaging of adherent mammalian cells was exercised in a laminar flow hood under sterile conditions. The cells were grown in T75 flasks at 37 °C and 5% CO_2 in presence of complete growth media consisting of 10% fetal calf serum (FCS), 1% non-essential amino acids (NEAA) and 1% L-glutamine (Gln) in Dulbecco`s modified eagle`s medium (DMEM). For passaging cells with a confluency of 80-90% the media was removed from the culture flask and adherent cells were washed once with phosphate-buffered saline (PBS) buffer (2 mL per 10 cm^2 surface area). PBS supplemented with trypsin (0.25%) and EDTA (0.02%) were used to dissociate cells from the cell culture vessel (0.2 mL per 10 cm^2 surface area), where the incubation time depends on the cell line. Complete growth media was transferred to the flask (0.8 mL per 10 cm^2 surface area) and pipetted up and down. The single cell suspension was used to determine the total number of viable cells with the Vi-Cell™ XR cell counter from Beckman Coulter. The desired cell number was seeded into cell culture vessels and incubated at 37 °C and 5% CO_2.

3.2.2.2 Transfection with plasmid DNA

For ectopically protein expression, cells were transiently transfected with plasmid DNA showing 70-90% confluency on the day of transfection. The DNA-lipid complexes were prepared by diluting Lipofectamine™ 2000 DNA transfection reagent (4 µL) and plasmid DNA (1.6 µg) separately in serum free medium (100 µL). After incubation for 5 min at room temperature, the diluted DNA was combined with the diluted transfection reagent and again incubated for 20 min. The DNA-lipid complexes were added to the well (200 µL per 10 cm^2 surface area), containing cells and medium, and were incubated for 18 h at 37 °C and 5% CO_2. The medium was changed after 6 h to fresh complete growth media. While Lipofectamine™ 2000 was used to transfect cells for further lysate preparation and immunoblotting experiments, cells were transfected with Fugene® 6, showing lower cell toxicity effect, but less efficiency, to prepare samples for fluorescence microscopy. Therefore, Fugene® 6 transfection reagent (1.5 µL) was diluted in serum free medium (25 µL), mixed and incubated for 5 min at RT before

adding plasmid DNA (0.5 µg). After a second incubation step for 10 min at RT, the Fugene® 6/DNA mixture was transferred to the cells (25 µL per 0.8 cm^2), showing 50-80% confluency, and incubated for 18 h at 37 °C and 5% CO_2, while the media was changed after 6 h. The transfection efficiency was proved with a wide field fluorescence microscope.

3.2.3 Biochemistry

3.2.3.1 Cell lysate preparation

Transiently transfected cells were starved in presence of starvation medium containing 0.5% FCS, 1% NEAA and 1% L-Gln in DMEM for 4 h at 37 °C and 5% CO_2. The stimulation took place in presence of epidermal growth factor at various concentrations and for different time points. Whole cell lysates for immunoblots were prepared by placing the cell culture dishes on ice and washing with ice-cold 1xPBS before adding 1xRIPA buffer (100 µL per 10 cm^2 surface area). After incubation for 15 min, the adherent cells were scraped off the dish with a plastic cell-scraper and the cell suspension was transferred to pre-cooled Eppendorf tubes to sonicate the samples for 12 sec, 3 cycles, 30%. The obtained cell lysates were centrifuged at 13.000 rpm and 4 °C for 15 min and the supernatant transferred to fresh pre-cooled Eppendorf tubes. The whole cell lysates were stored at -80 °C after freezing in liquid nitrogen.

3.2.3.2 Bradford assay

The protein concentration of the obtained cell lysates was determined by Bradford Assay based on a protein-dye complex, which is formed between Coomassie Brilliant Blue G-250 and the basic amino acid residues of a protein under acidic conditions, which induces an absorbance shift. Serial dilution of bovine serum albumin (BSA) was prepared for a standard curve. Water (500 µL) was pipetted into a plastic cuvette and lysate (1 µL) or water (1 µL) or BSA (16, 8, 4, 2 and 1 µg/mL) was added. To form the protein-dye complex, Bradford reagent (500 µL) was added, mixed and incubated at RT for 5 min before measuring the OD at 595 nm with a spectrophotometer. Protein concentrations of the cell lysates were calculated based on the BSA standard curve.

3.2.3.3 Immunoprecipitation

Specific proteins were isolated from cell lysates by immunoprecipitation. Therefore, Protein-G-Sepharose® beads (500 µL), stored in 20% EtOH, were purified by washing with ice-cold 1xPBS (1 mL) and centrifugation at 850 rcf for 2 min at 4 °C. The washing step was performed four times until the supernatant was removed with a syringe to get rid of all liquid. 1xPBS (500 µL) was added to the beads to obtain a 50% Protein-G-Sepharose bead solution. The purified beads (20 µL) were incubated with cell lysate (0.5 mg) in a final volume of 500 µL at 4 °C for 2 h on a tube rotator to reduce unspecific binding. The unspecific bound fraction was pelleted at 850 rcf for 2 min at 4 °C and the supernatant used to incubate with the pull-down antibody (5 µL, 1:100) at 4 °C for 16 h. Freshly purified beads (30 µL) were transferred to the lysate and incubated at 4 °C for 2 h. The lysate-bead mixture was diluted with lysis buffer (500 µL), centrifuged at 850 rcf for 2 min at 4 °C and washed five times with 1xPBS. After the final washing step, buffer was removed with a syringe and protein were eluted from the beads in presence of 5x Laemmli buffer (5 µL) and lysis buffer (20 µL) at 95 °C for 5 min.

3.2.3.4 *In vitro* auto-phosphorylation of NME1 and PGAM1

The purified enzymes, NME1 and PGAM1, were diluted in TMD buffer (10 ng/µL) and incubated with substrate. NME1 was auto-phosphorylated in presence of ATP (1 mM) for 10 min at RT, while PGAM was incubated with 2,3-DPG (1 mM) for 10 min at 30 °C. The reaction was terminated by adding 2xLaemmli buffer pH 8.8 and control samples were heated at 95 °C for 10 min.

3.2.3.5 Sodium Dodecyl Sulfate-Polyacrylamide Gel Electrophoresis (SDS-PAGE)

Denaturing sodium dodecyl sulfate-polyacrylamide gel electrophoresis (SDS-PAGE) was performed using the Bio-Rad system. Therefore, gels consisting of a stacking and separating gel were prepared according to the protocol in Table 7 and

Table 8.

Table 7: Protocol for one stacking gel (1.5 mm).

Component	Volume [mL]
ddH_2O	1.72
Acrylamide/Bis (30%)	0.5
0.5 M Tris pH 6.8	0.76
10% SDS	0.03
10% APS	0.03
TEMED	0.003

Table 8: Protocol for one separating gel (1.5 mm).

Component	Volume [mL]		
	10%	**12%**	**15%**
ddH_2O	4.0	3.3	2.3
Acrylamide/Bis (30%)	3.3	4.0	5.0
1.5 M Tris pH 8.8	2.5	2.5	2.5
10% SDS	0.1	0.1	0.1
10% APS	0.1	0.1	0.1
TEMED	0.004	0.004	0.004

To define the pocket size a 15-well comb 1.5 mm was used. The formed pockets can be loaded with a sample volume up to 30 µL. The inner and outer buffer chambers of the electrophoresis cell were filled with 1xrunning buffer. For sample preparation, equal

amounts of protein (30 µg) were heated after adding 5xLaemmli buffer for 5 min at 95 °C, mixed and centrifuged for 1 min at 13.000 rpm. The samples and Chameleon duo pre-stained protein ladder (4 µL) were loaded on the gel. The electrophoresis was performed at 80 V for 10 min before increasing the voltage to 110 V for 90 min.

In order to run a SDS gel for further phosphohistidine detection, a modified stacking gel with a pH of 8.8 had to be prepared. The purified enzyme samples (250 ng) were diluted with 2xLaemmli buffer pH8.8. The heating step was omitted due to the temperature lability and the electrophoresis was performed at 100 V and 4 °C for 3 h.

3.2.3.6 Western blot

Proteins were eluted from gels and transferred to membranes using the electrophoretic transfer with a tank blotting Bio-Rad system. Therefore, the gel holder cassette, foam pads and Whatman filter paper were put into a tray filled with precooled 1xtransfer buffer. Polyvinylidene fluoride (PVDF) membrane was first activated in MeOH for 2 min and then equilibrated as well as the pre-cut SDS gel in 1xtransfer buffer for 5 min. The equilibrated gel was transferred to the filter paper, positioned on a foam pad, followed by the PVDF membrane and a second filter paper treated with a roller to avoid trapped air bubbles. The gel holder cassette, including the described membrane gel set up, was placed into the transfer tank, while the gel was facing the cathode. After adding an ice block and a magnetic stirrer, the tank was filled with precooled 1xtransfer buffer and the electrophoretic transfer was performed at 100 V for 90 min under continuous stirring. The protein containing membrane was blocked at RT for 1 h with Odyssey® Blocking Buffer (TBS) before primary antibody diluted in 1xTBS-T (dilution ratio varied between antibodies) was incubated over night at 4 °C under continuous shaking. Washing of the membrane was performed in presence of 1xTBS-T three times for 10 min. Antibodies labelled with different infrared dye fluorophores (1.5 µL) from LI-COR diluted in 1xTBS (10 mL) were used as secondary antibodies for multi-color detection. Therefore, the secondary antibodies were incubated at RT for 1 h in the dark. The stained membrane was rinsed three times with 1xTBS-T for 5 min and scanned with an Odyssey® CLx imaging system from LI-COR. For all western blots Tubulin served as an internal reference and loading control. For further re-probing, the membrane was stripped with NewBlot™ PVDF stripping buffer (1 mL) diluted with

ddH_2O (4 mL) for 20 min at RT. After rinsing with 1xPBS three times for 5 min, the membrane was scanned to ensure complete antibody removal and re-probed again with primary and secondary antibody described before.

3.2.3.7 Internalization assay

The internalization of EGF receptor was observed with an On-Cell Western Assay by monitoring the loss of receptor molecules on the cell surface. Therefore, Corning® 96 well plates in black and with clear flat bottom wells were coated with poly-L-lysine (5mg in 50 mL 1xPBS). The coating solution was incubated (50 µL per 0.3 cm^2 surface area) for 5 min at RT, removed and the wells were washed with sterile 1xPBS for 5 min at RT. The plates were allowed to dry over night or at least 2 h before seeding MCF7 cells ($1x10^4$ per 0.3 cm^2 surface area). The cells were transiently transfected after 24 h with EGFR_mCitrine (40 ng) and mCitrine empty vector or mCitrine_PHPT1 (20 ng) in presence of Fugene 6 (50 µL per 0.3 cm^2 surface area) described in chapter 3.2.2.2. After 6 h the medium was removed and replaced by fresh complete growth medium (200 µL per 0.3 cm^2 surface area). The cells were starved (90 µL per 0.3 cm^2 surface area) for 5 to 6 h with starvation medium containing 0.5% FCS after 16 to 18h and then stimulated with EGF (10 µL of 1000 ng/mL) at 37 °C for different time points. The old media was removed and Roti®-Histofix 4% (50 µL per 0.3 cm^2 surface area) was slowly added for 5 min at RT for cell fixation. The cells were washed three times with 1xTBS for 5 min (100 µL per 0.3 cm^2 surface area) and blocked with Odyssey® Blocking Buffer (TBS) (50 µL per 0.3 cm^2 surface area) for 30 min at RT without permeabilization. As primary antibody human EGFR/ErbB1 antibody (AF231) (1:200), a polyclonal goat IgG binding the extracellular protein domain of EGFR, was diluted in blocking buffer (50 µL per 0.3 cm^2 surface area) and incubated over night at 4 °C. Cells were washed three times with 1xTBS for 5 min before adding IRDye® 800 donkey anti-goat IgG (1:500) diluted with blocking buffer (50 µL per 0.3 cm^2 surface area) for 30 min at RT. Three final washing steps were performed in 1xTBS for 5 min and the plate was scanned with the Odyssey® CLx imaging system. The obtained signal was normalized to the cell number using Dil staining solution, a lipophilic membrane dye. Therefore, Dil staining solution (1:1000) was diluted with 1xPBS (50 µL per 0.3 cm^2 surface area) and transferred to the cells for 10 min at RT. The staining solution was

removed and the fixed cells were washed three times with 1xTBS for 5 min. The dye was excited at 549 nm and followed by detecting the emission maxima at 565 nm with the microplate reader SpectraMax M5.

3.2.3.8 Immunofluorescence

MCF7 cells were seeded ($2.5x10^4$ cells per 0.8 cm^2 surface area) into 8-well labteks and transiently transfected with EGFR_mCitrine (400 ng) and pcDNA3.1 or mCherry_PHPT1 (100 ng) in presence of Fugene 6 (25 µL per 0.8 cm^2 surface area) described in chapter 3.2.2.2. After 6 h the medium was removed and replaced by fresh complete growth medium (300 µL per 0.8 cm^2 surface area). The cells were starved (225 µL per 0.8 cm^2 surface area) for 5 to 6 h with starvation medium containing 0.5% FCS after 16 to 18 h and then stimulated with different EGF concentrations (25 µL per 0.8 cm^2 surface area) for 5 min at 37 °C. The old media was discarded and the cells were rinsed once with 1xPBS at RT before adding Roti®-Histofix 4% (250 µL per 0.8 cm^2 surface area) for 5 min at RT to fix the cells. The fixed samples were washed three times with 1xTBS (250 µL per 0.8 cm^2 surface area) for 5 min at RT and permeabilized in presence of 0.1 % Triton-X100 in 1xTBS (250 µL per 0.8 cm^2 surface area) for 5 min at RT. After three additional washing steps with 1xTBS for 5 min, unspecific binding was blocked with Odyssey® Blocking Buffer (TBS) (200 µL per 0.8 cm^2 surface area) at RT for 1 h. For EGFR phospho staining a mouse anti-EGF receptor pY845 and rabbit anti-EGF receptor pY1068 antibody were diluted (1:200) in blocking buffer (200 µL per 0.8 cm^2 surface area) and incubated over night at 4 °C. The samples were washed with 1xTBS three times for 5 min and incubated with secondary antibody Alexa Fluor® 647 donkey anti-mouse IgG or chicken anit-rabbit IgG diluted (1:200) in blocking buffer (200 µL per 0.8 cm^2 surface area) at RT for 1 h. 1xPBS was used three times to wash the cells for 5 min and Hoechst® 33342 dye to stain the nucleus. Therefore, the nucleic acid stain Hoechst® 33342 (10 mg/mL, 1:10.000) was diluted with 1xPBS (200 µL per 0.8 cm^2 surface area). The buffer was removed and the cells were covered with the staining solution for 5 min at RT. To get rid of the dye, the samples were washed three times with 1xPBS for 5 min and stored in 0.1% azide in 1xPBS at 4 °C for longer storage or only in 1xPBS at 4 °C for short storage.

3.2.4 Fluorescence microscopy

3.2.4.1 Laser Scanning Confocal Microscopy (LSCM)

Laser scanning confocal microscopy was performed to image fixed cells for immunofluorescence experiments using the Leica TCS SP8 and the Olympus FluoView FV1000 for additional FLIM measurements. The settings in Table 9 were used for the Leica TCS SP8 microscope.

Table 9: Excitation wavelength, source and emission filters used for Leica TCS SP8.

Fluorophore/Dye	Laser	Excitation	Emission band width	Detector
Hoechst® 33342	405 nm Diode	405 nm (15 %)	415-500 nm	PMT1
mCitrine	WLL	514 nm (10 %)	524-550 nm	HyD2 SMD1
mCherry	WLL	561 nm (5 %)	571-620 nm	HyD4 SMD2
Alexa647	WLL	633 nm (20 %)	643-768 nm	HyD 5

The samples were imaged sequentially as a frame average of two images and with a HC PL APO CS2 x 63/1.4 NA oil objective using the counting mode in a temperature controlled incubation chamber at 37 °C. For the Olympus Fluo View FV1000 confocal images of fixed cells were obtained using the following settings in Table 10.

Table 10: Excitation wavelength, source and emission filters used for Olympus Fluo View FV1000.

Fluorophore	Laser	Excitation	Emission band with	Beam splitter
mCitrine	argon	488 nm (10 %)	498-551 nm	SDM560
mCherry	DPSS	561 nm (5 %)	575-675 nm	

The UPLSAPO 60x/1.35 NA oil objective and excitation dichroic mirror DM405/488/561/633 were used to focus the excited light. The imaging was performed sequentially as a frame average of 2 images in an incubation chamber at 37 °C. The background of the obtained images was subtracted and single cell masks were generated to measure the mean fluorescence intensity for each channel with ImageJ (http://imagej.nih.gov/ij/). The relative phosphorylation level (pY/EGFR) were

calculated for each cell. To quantify the relative phosphorylation level of EGFR in space, the individual cells were split into ten segments with equal radius from the plasma membrane to the nucleus and the mean fluorescence intensity was measured for each segment.

3.2.4.2 Fluorescence Lifetime Imaging Microscopy (FLIM)

For FLIM measurements the Olympus Fluo View FV1000 laser scanning confocal microscope was set up with an external PicoQuant`s compact FLIM and FCS upgrade kit. The measurements were performed with a UPLSAPO 60x/1.35 NA oil objective. PicoHarp 300, a digitally modulatable driver, controlled the pulsed laser via Sepia II Software. The pulsed 40MHz laser was detected with an avalanche photodiode (APD) during an image integration time of 3 min and the signal was transferred to the PicoHarp 300 data acquisition unit. The 470 nm pulsed laser line (37 %) and the dichroic mirror DM470/532 were used to bring the fluorophore mCitrine in its excited state and the fluorescence was detected by an APD using a 525/15 bandpass filter. The acquired images were analysed according to the global analysis of time correlated FRET-FLIM data[100].

4 Results

4.1 Effect of PHPT1 on EGFR activation

An increased EGFR activity is linked to various types of cancer[101,102]. Due to the high clinical significance, identification of EGFR regulating factors is of utmost importance. Currently, several PTPs have been identified. Here, the effect of PHPT1 on EGFR activation was investigated. Accordingly, the relative phosphorylation level of the receptor, indicative for receptor activation, was detected in presence of PHPT1 for the spontaneous and ligand induced activation. As a readout, specific phosphorylation sites of EGFR with distinct functionalities were detected, pTyr1068 as signalling and pTyr845 as regulatory autocatalysis site.

4.1.1 Spontaneous activation of EGFR in presence of PHPT1

In absence of ligand, EGFR activation and further downstream phosphorylation occur at high receptor expression level due to thermal fluctuations. To investigate the effect of PHPT1 on the ligand independent EGFR activation mechanism, spontaneous activation was artificially induced by transfecting low and high EGFR cDNA amounts in presence of PHPT1 into MCF7 cells, containing low endogenous EGFR. The general Tyr phosphorylation (pY72) and the specific phospho sites pTyr1068 and pTyr845 were detected in absence and presence of PHPT1 in immunoblotting experiments (Figure 8). Since the location of the fluorescence protein, recombinantly expressed with PHPT1, showed no difference and with the knowledge that PHPT1 requires its flexible *C*-terminus for catalytic activity, the experiments were performed with an *N*-terminal tagged phosphatase. The results revealed an amplification of EGFR phosphorylation by PHPT1.

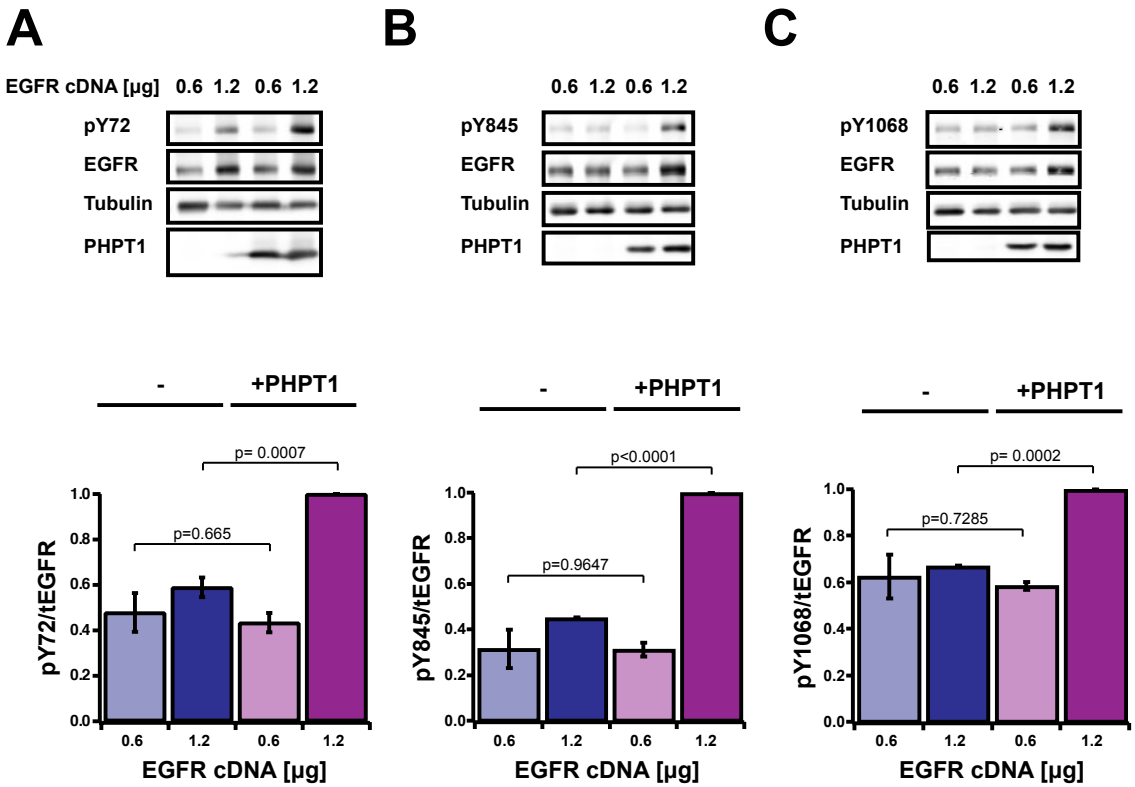

Figure 8: PHPT1 amplifies spontaneous EGFR activation. Immunoblotting experiments of unstimulated MCF7 cells transfected with increasing amounts of wt_EGFR_mCitrine cDNA (0.6 and 1.2 µg) and wt_PHPT1_mCitrine (0.3 µg). The cells were probed for general receptor phosphorylation (pY72) **(A)**, the autocatalysis (Tyr845) **(B)** and the signalling (Tyr1068) phospho site **(C)**. The relative phosphorylation level (pY over EGFR) was peak normalized and plotted for the indicated conditions. All blots are n=2-3 (mean ± SEM).

Densitometric analysis of the western blots displayed that PHPT1 increased the general Tyr phosphorylation level (pY72) of EGFR at high receptor expression level. The autocatalytic (pY845) as well as the signalling (pY1068) phospho-sites were involved in this effect, showing an amplified relative phosphorylation level in presence of PHPT1. To verifiy the cell population-based immunoblotting experiments, single cell immunofluorescence experiments were performed (Figure 9). Here, EGFR was ectopically co-expressed with PHPT1 in MCF7 cells. The receptor phosphorylation was detected in absence and presence of PHPT1. Since the receptor activation occurs at the plasma membrane, the cells were spatially segmented into 10 segments and the plasma membrane segment (segment 1) were considered for the analysis of the relative phosphorylation level. In addition, the phosphorlyation level was plotted for each segment to trace the signal regulation of cells in space going from the plasma membrane to the nucleus.

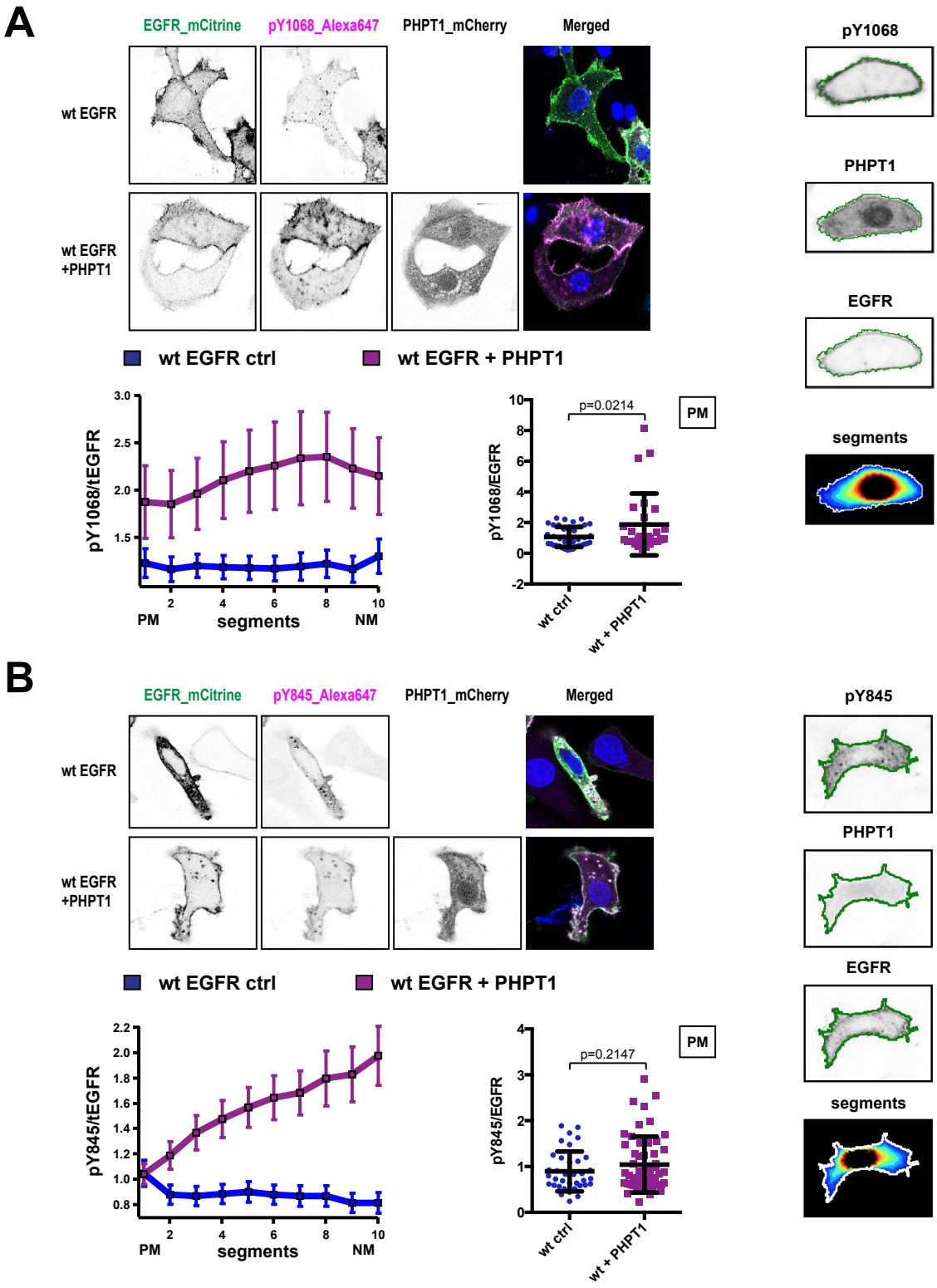

Figure 9: Enhanced spontaneous EGFR activation by PHPT1. Unstimulated MCF7 cells transfected with wt_EGFR_mCitrine (0.4 µg) and wt_PHPT1_mCherry (0.1 µg). Representative immunofluorescence images for the signalling phosphorylation site Tyr1068 **(A)** and autocatalysis site Tyr845 **(B)** (upper, left panels) and the segmentation exemplaric for one cell (upper, right panels). The cells were segmented into 10 spatial segments from the plasma membrane (PM) to the nuclear membrane (NM). The averaged relative phosphorylation level (pY over EGFR) was plotted for the different segments (lower, left panel) (Tyr1068: wt ctrl n=39, wt+P n=27; Tyr845: wt ctrl n=36, wt+P n=53)

(mean ± SEM). The relative phosphorylation level of EGFR located at the plasma membrane for single cells (lower, right panel) (mean ± STDEV).

Consistent with the immunoblot experiments, PHPT1 amplified the relative phosphorylation of the signalling site pTyr1068 as quantified by immunofluorescence. However, the phosphorylation of the autocatalysis site pTyr845 was significantly increased in the perinuclear area, unlike the plasma membrane segment.

4.1.2 Ligand induced EGFR activation in presence of PHPT1

In addition to the spontaneous activation, the receptor tyrosine kinase activation proceeds also in presence of ligand. The effect of PHPT1 on the ligand dependent receptor activation was monitored via immunoblot experiments (Figure 10). Here, EGFR was ectopically co-expressed in absence and presence of PHPT1 and the cells stimulated with increasing doses of EGF for 5 min. As observed in the western blots, PHPT1 reduced the phosphorylation level of EGFR and shifted the sigmoid dose response curves to the right, while the phosphorylation of the autocatalysis site pTyr845 showed only a slight shift (Figure 10A). In contrast to this, EGFR required a markedly increased amount of ligand to get phosphorylated at Tyr1068 residue and to induce further signalling (Figure 10B).

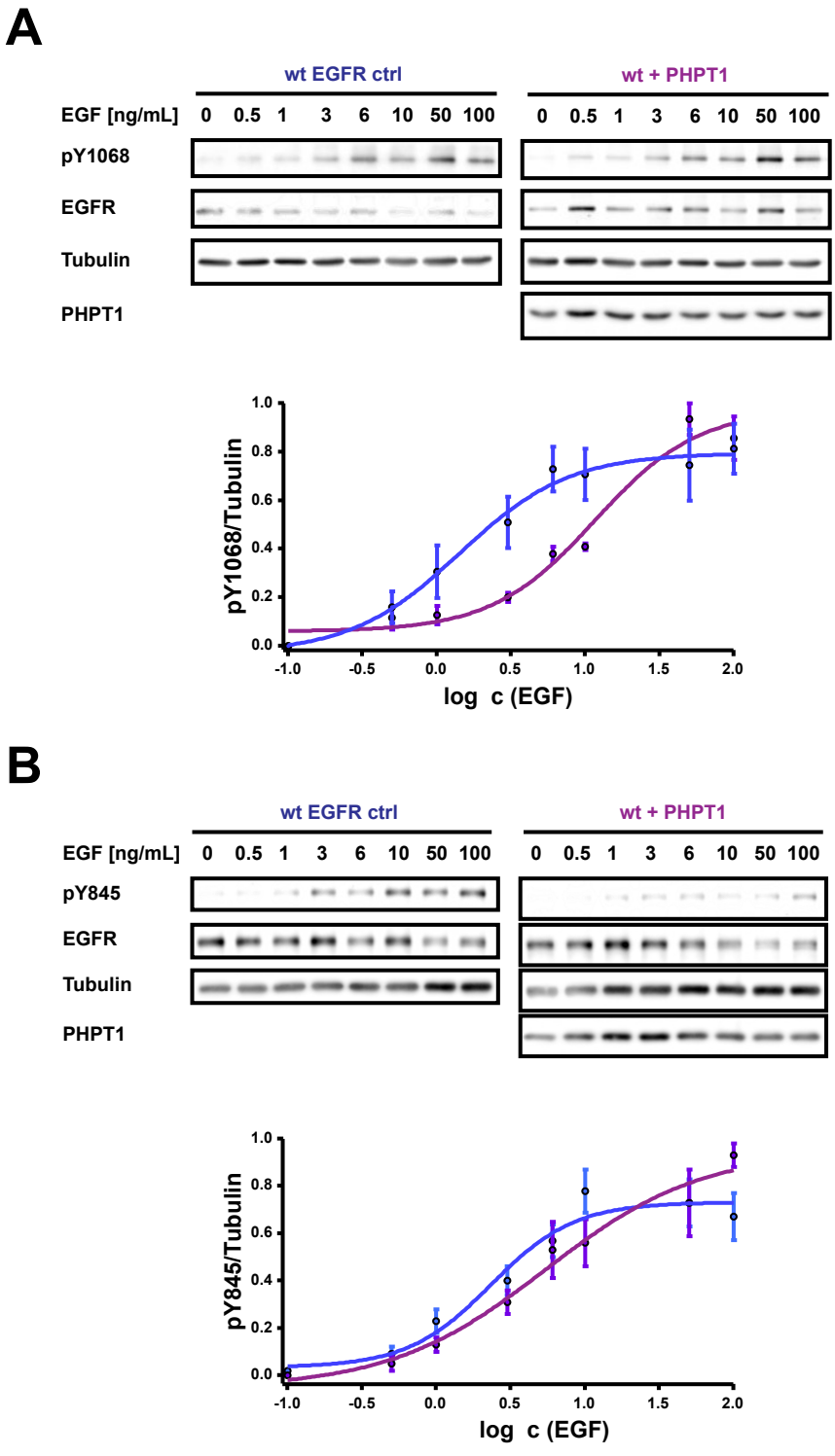

Figure 10: Regulation of ligand dependent EGFR activation by PHPT1. EGFR phosphorylation of signalling site Tyr1068 **(A)** and autocatalysis site Tyr845 **(B)** in a dose dependent manner. MCF7 cells were stimulated with different doses of EGF and total lysates were blotted (upper panels). Normalized phosphorylation level (pY over Tubulin) was plotted for the indicated logarithmic concentration (lower panel). All blots are n=3 (mean ± SEM).

Considering the results of the western blots, immunofluorescence experiments were performed to validate the inhibitory effect of PHPT1 on EGFR phosphorylation after ligand-induced activation (Figure 11). For this, EGFR was co-transfected with PHPT1 in MCF7 cells and stimulated with saturating EGF dose (c=100 ng/mL) for 5 min.

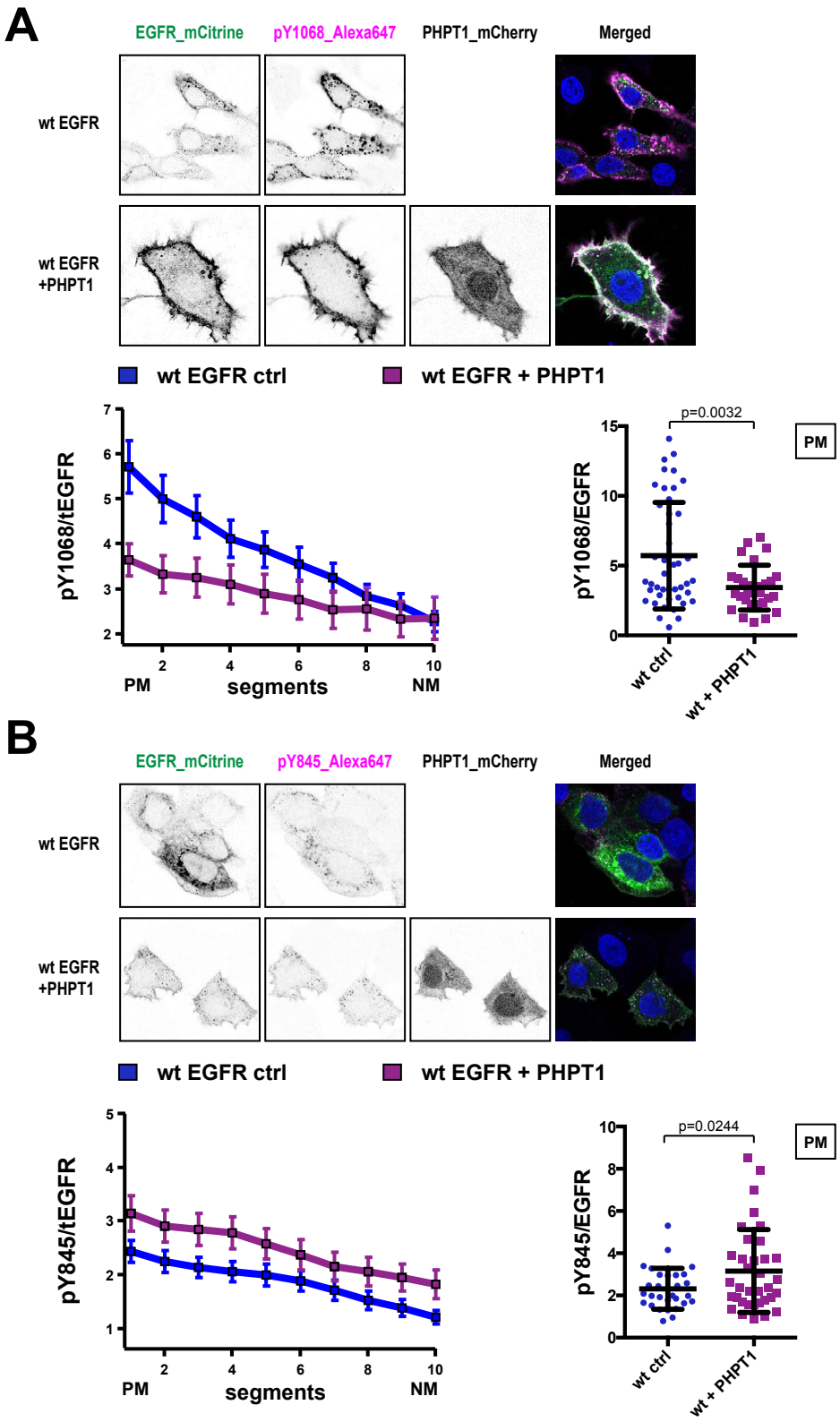

Figure 11: PHPT1 modulates ligand-dependent EGFR activation. EGFR phosphorylation of the signalling Tyr1068 **(A)** and the autocatalysis Tyr845 site **(B)**. Transiently transfected and fixed MCF7 cells were stimulated with EGF (100 ng/mL, t=5min). Representative fluorescence images for the indicated conditions (upper panels). Relative phosphorylation level (pY over EGFR) of EGFR was binned for 10 spatial segments from the plasma membrane (PM) to the nuclear membrane (NM) for individual

cells and plotted against the segments (lower, left panel) (Tyr1068: wt ctrl n=44, wt+P n=29; Tyr845: wt ctrl n=30, wt+P n=35) (mean ± SEM). Relative phosphorylation level of receptor, located at the PM, of single cells was plotted for the indicated conditions (lower, right panel) (mean ± STDEV).

The findings showed that PHPT1 also affected the ligand-induced EGFR phosphorylation (c=100 ng/mL) in immunofluorescence experiments. The signalling phospho-site Tyr1068 displayed a reduced phosphorylation at the plasma membrane consistent with the previous results, whereas phosphorylation of the regulatory autocatalysis residue Tyr845 was slightly increased globally in the cell, contrary to the western blots. However, the immunofluorescence data are in agreement with the time response experiments (Figure 12). Therefore, EGFR and PHPT1 were ectopically co-expressed in MCF7 cells and stimulated with EGF (100 ng/mL) for different time points. The plotted relative phosphorylation level revealed a decreased phosphorylation for the signalling Tyr1068 and a slight increased phosphorylation for the autocatalysis site Tyr845 at early time point (5min) (Figure 12).

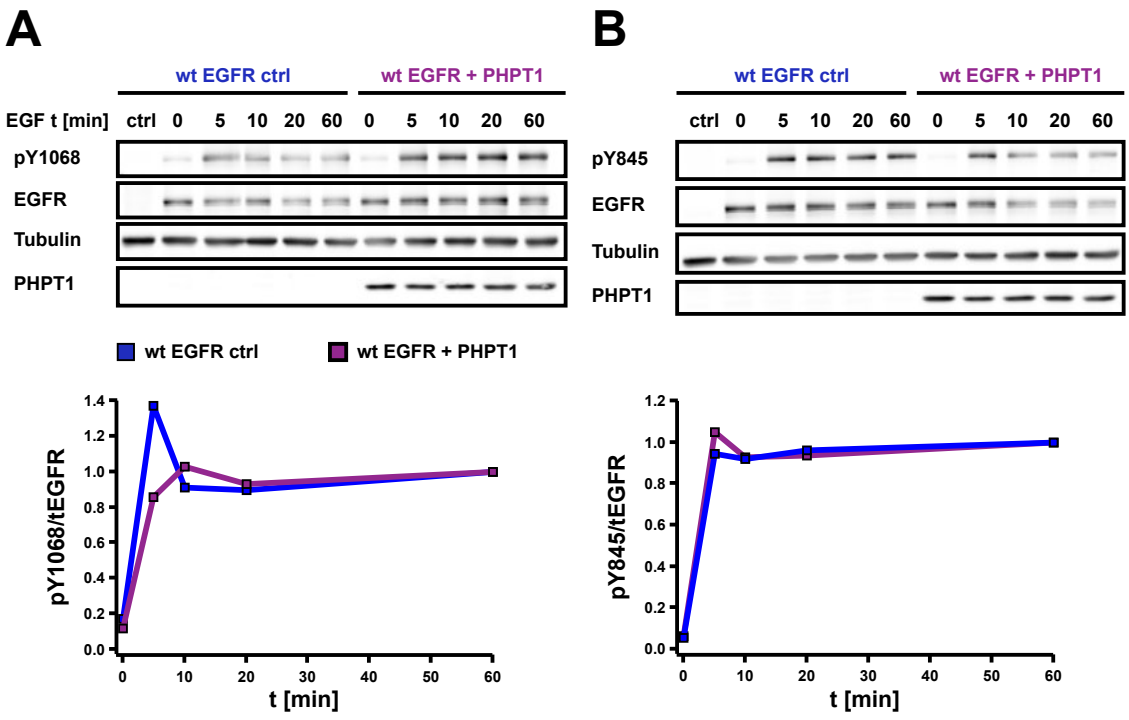

Figure 12: Temporal regulation of EGFR phosphorylation by PHPT1. EGFR phosphosphorylation of the signalling site Tyr1068 **(A)** and the autocatalysis site Tyr845 **(B)**. Transiently transfected MCF7 cells with wt_EGFR_mCitrine and wt_PHPT1_mCitrine were stimulated for different time points with EGF (100 ng/mL) and total lysates were analysed via immunoblotting (upper panels). Relative phosphorylation level (pY over EGFR) was plotted for the indicated time points (lower panel).

In order to explore the effect of PHPT1 on the switch-like behaviour of EGFR phosphorylation in response to ligand, EGFR was stimulated with different doses of

EGF in absence and presence of PHPT1 and stained against the specific phosphorylation sites in immunofluorescence experiments (Figure 13).

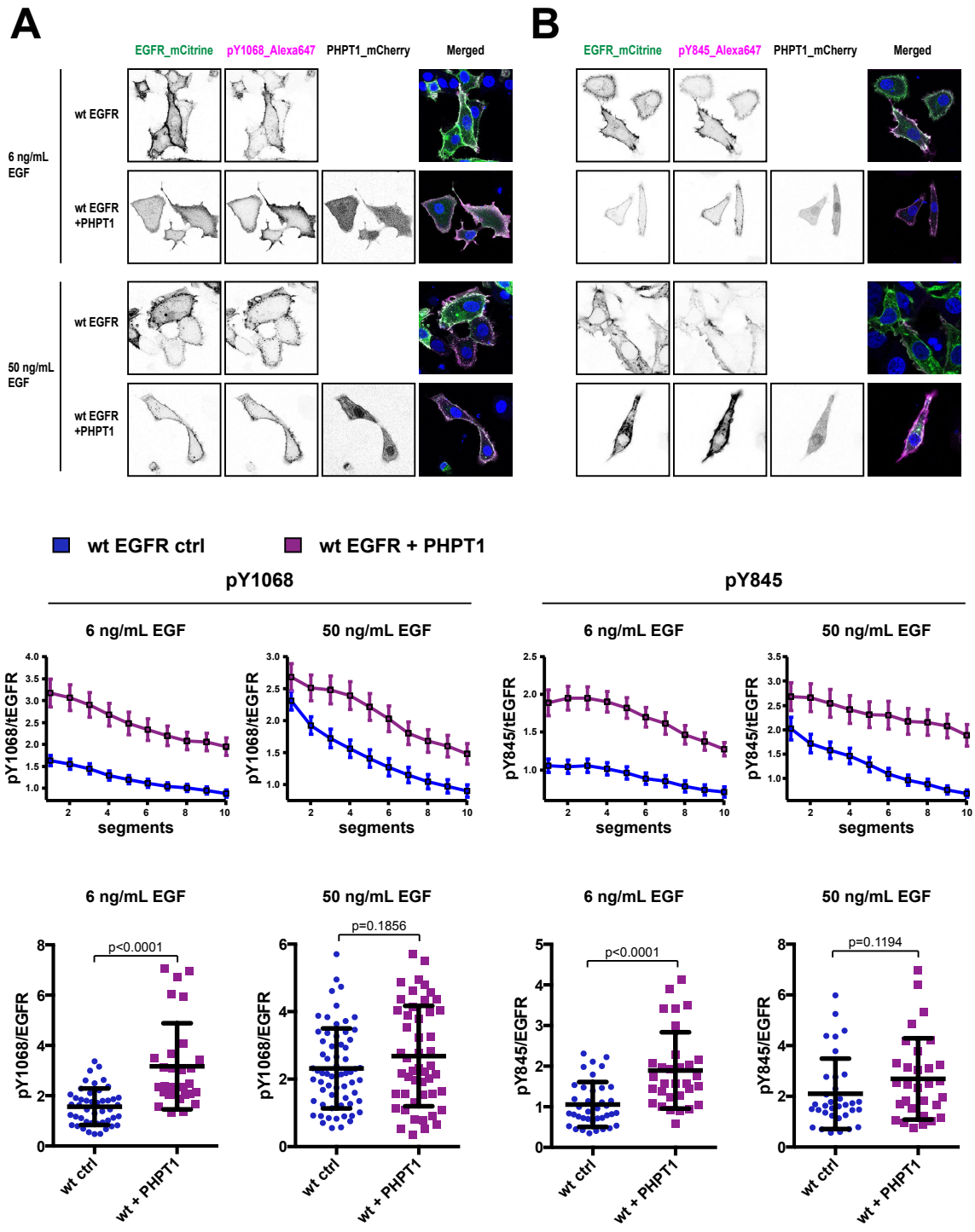

Figure 13: Effect of PHPT1 on EGFR phosphorylation after ligand stimulation with low and high doses of EGF. Wt_EGFR_mCitrine and wt_PHPT1_mCherry were ectopically expressed in MCF7. The cells were stimulated with different doses of EGF (6 and 50 ng/mL) and stained for the specific phospho sites pTyr1068 **(A)** and pTyr845 **(B)**. Representative fluorescence images for the indicated conditions (upper panels). The averaged relative phosphorylation level was plotted for the spatial segments (mean ± SEM) (middle panels), while the phosphorylation level of receptor, located at the plasma membrane, was

plotted for each single cell (lower panels) (Tyr1068: 6, 50 ng/mL EGF: wt ctrl n=46, 64; wt+PHPT1 n=29, 49) (Tyr845: 6, 50 ng/mL EGF: wt ctrl n=38, 34; wt+PHPT1 n=31, 31) (mean ± STDEV).

Furthermore, the obtained averaged phosphorylation levels of EGFR at the plasma membrane as well as in the perinuclear area were plotted for the indicated EGF doses (Figure 14).

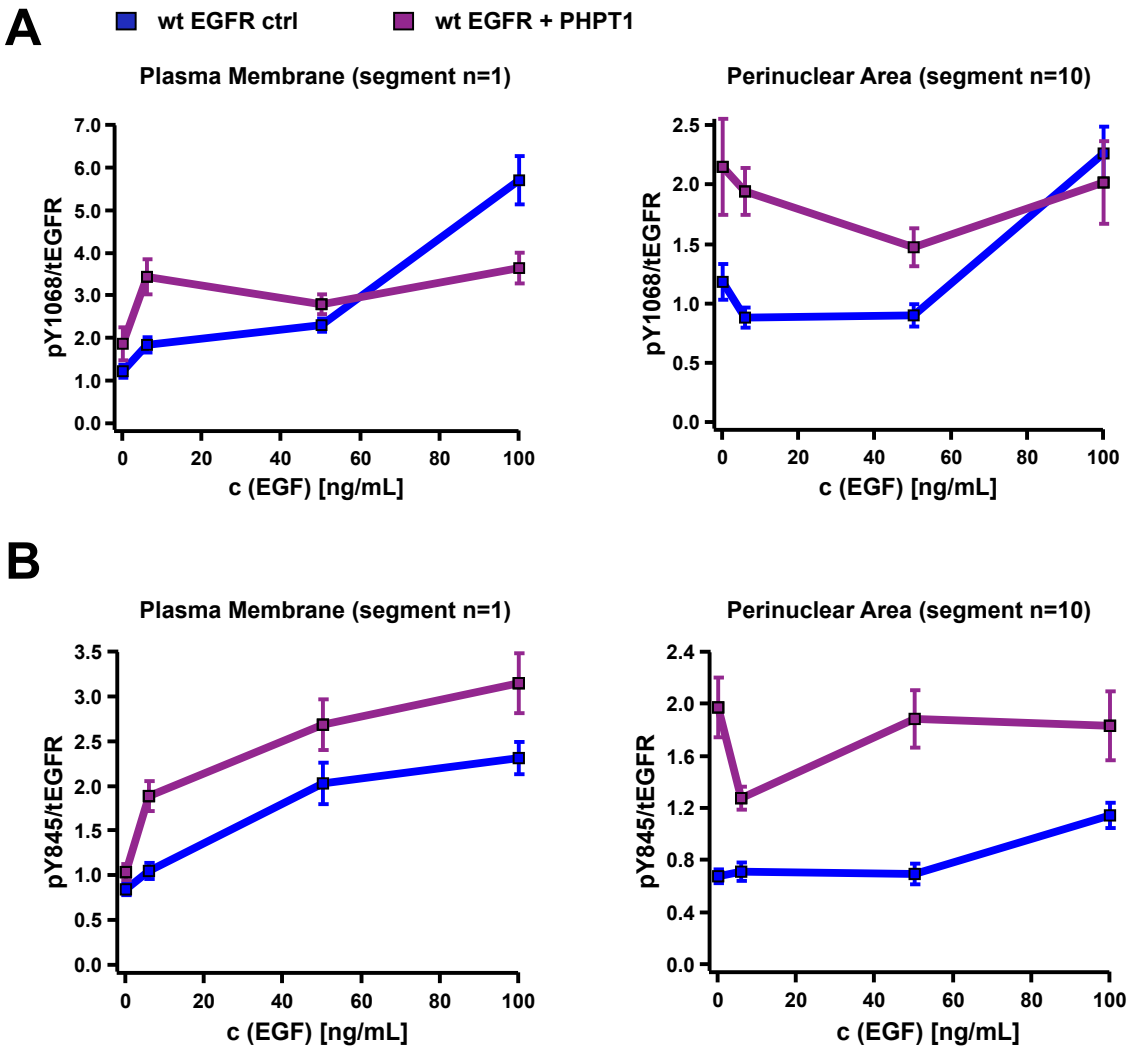

Figure 14: Regulation of EGFR phosphorylation at the plasma and nuclear membrane by PHPT1 in a dose dependent manner. The relative phosphorylation level was averaged for the specific spatial segments including the plasma membrane (left panel) and the nuclear membrane (right panel) for the signalling site Tyr1068 **(A)** and the autocatalysis site Tyr845 **(B)**. The averaged values were plotted against ligand concentration (mean ± SEM).

Regarding to the signalling site Tyr1068, EGFR phosphorylation at the plasma membrane and in the perinuclear area was amplified in absence of ligand and low doses, whereas PHPT1 led to phosphorylation suppression at high EGF concentration (50-100 ng/mL) (Figure 14A). At low EGF doses the autocatalysis site Tyr845 showed an

equal effect. However, PHPT1 further increased the receptor phosphorylation even at saturating amounts of ligand at the plasma and nuclear membrane (Figure 14B).

4.2 The role of His648 in JM for EGFR activation

In analogy to the potassium channel KCa3.1, the His648 residue located in the JM of EGFR, might act as a possible phosphorylation site. In the case of the ion channel, this phosphorylated residue is required for binding active calcium-CaM complex and further activation. In recent studies, it has been demonstrated that ligand-induced EGFR activation shows similar characteristics with the ion channel KCa3.1 activation, such as the CaM binding. This raised the question whether EGFR activation is regulated in a related mechanism. In order to answer this question, the importance of the His648 residue for receptor activation and the role of PHPT1 were investigated by analysing the phosphorylation of the JM (H648A) EGFR mutant in absence and presence of PHPT1. Therefore, the single His648 residue was mutated to an Ala, which is lacking the imidazole ring.

4.2.1 Spontaneous activation of H648A EGFR in presence of PHPT1

To investigate the role of the His648 residue on spontaneous EGFR activation, the EGFR mutant (H648A) was transfected with increasing amounts of cDNA to artificially induce receptor activation in absence of ligand and at high receptor expression level (Figure 15).

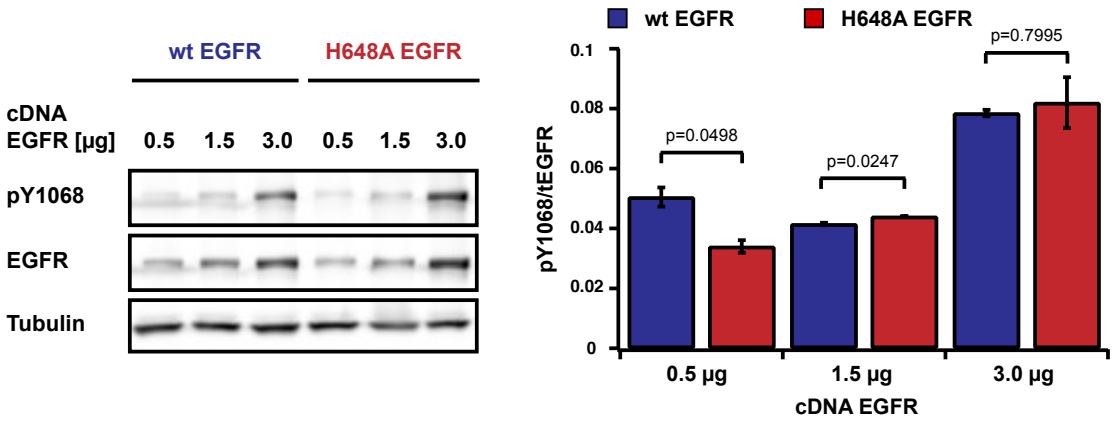

Figure 15: Phosphorylation of spontaneous activated JM (H648A) EGFR mutant. MCF7 cells were transiently transfected with increasing amounts of wt or H648A_EGFR_mCitrine cDNA (0.5, 1.5 and 3.0 µg). The total lysates of the unstimulated cells were analysed via immunoblotting experiments (left

panels) and the relative phosphorylation level (pY over EGFR) of the signalling site Tyr1068 was plotted for the determined conditions (right panel). The blots are n=2 (mean ± SEM).

Densitometric analysis of the western blots revealed that the H648A mutation does not affect the spontaneous activation according to the phosphorylation of the signalling site Tyr1068. Immunostainings were performed to validate the role of the His648 residue in spontaneous receptor activation, as well as if PHPT1 acts on this specific site (Figure 16).

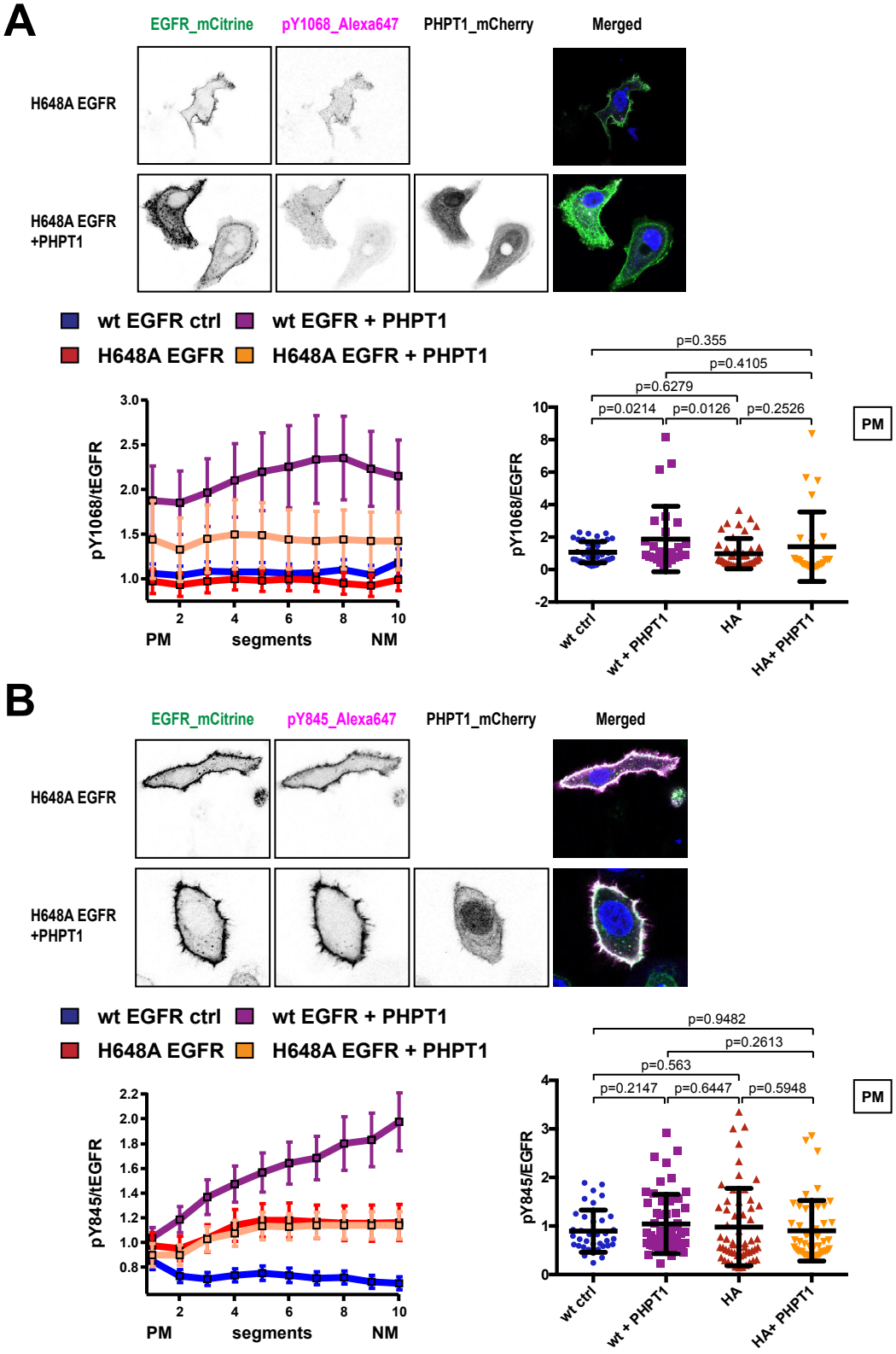

Figure 16: Regulation of spontaneous EGFR activation by PHPT1 and H648A mutation. EGFR phosphorylation without EGF treatment of transiently transfected and fixed MCF7 cells for the signalling site Tyr1068 **(A)** and the autocatalysis site Tyr845 **(B)**. Representative fluorescence images for H648A_EGFR_mCitrine in absence and presence of wt_PHPT1_mCherry (upper panels). Averaged phosphorylation level of segmented single cells plotted against segments (lower, left panel) (Tyr1068:

HA n=44, HA+PHPT1 n=26) (Tyr845: HA n=56, HA+PHPT1 n=47) (mean ± SEM). Relative phosphorylation level of receptor, located on the plasma membrane (PM), for single cells (lower, right panel) (mean ± STDEV).

As shown in the previous results, the H648A EGFR mutant had no significant effect on receptor phosphorylation, regarding to the signalling site Tyr1068 (Figure 16A). In contrast to this, the data demonstrated that autocatalysis of spontaneous activated receptor (pTyr845), located at the plasma membrane, was increased (Figure 16B). This effect was extended in the perinuclear area. PHPT1 amplified the relative wt EGFR phosphorylation level of the signalling site Tyr1068 as well as of the H648A EGFR mutant. However, the H648A receptor mutant revealed only a slight increase in presence of PHPT1, implying the idea that PHPT1 does not only act on the specific His648 residue. Whereas the autocatalysis (pTyr845) of H648A EGFR alone and in presence of PHPT1 showed the same slight increase raising evidence that PHPT1 requires an intact His648 residue and may act on this site.

4.2.2 Ligand dependent activation of H648A EGFR in presence of PHPT1

In addition to the spontaneous activation of EGFR, the well-studied ligand induced receptor activation was investigated. Therefore, MCF7 cells ectopically expressing wt or H648A EGFR, were stimulated with EGF (100 ng/mL, t=20min) (Figure 17A). After ligand stimulation, the H648A mutation increased general EGFR phosphorylation (pY72). Next, immunoblotting experiments were performed by staining for the specific phospho-sites in order to investigate the amplification effect (Figure 17B). Moreover, the cells were stimulated with different doses of EGF to prove the influence of phosphorylation in a dose dependent manner.

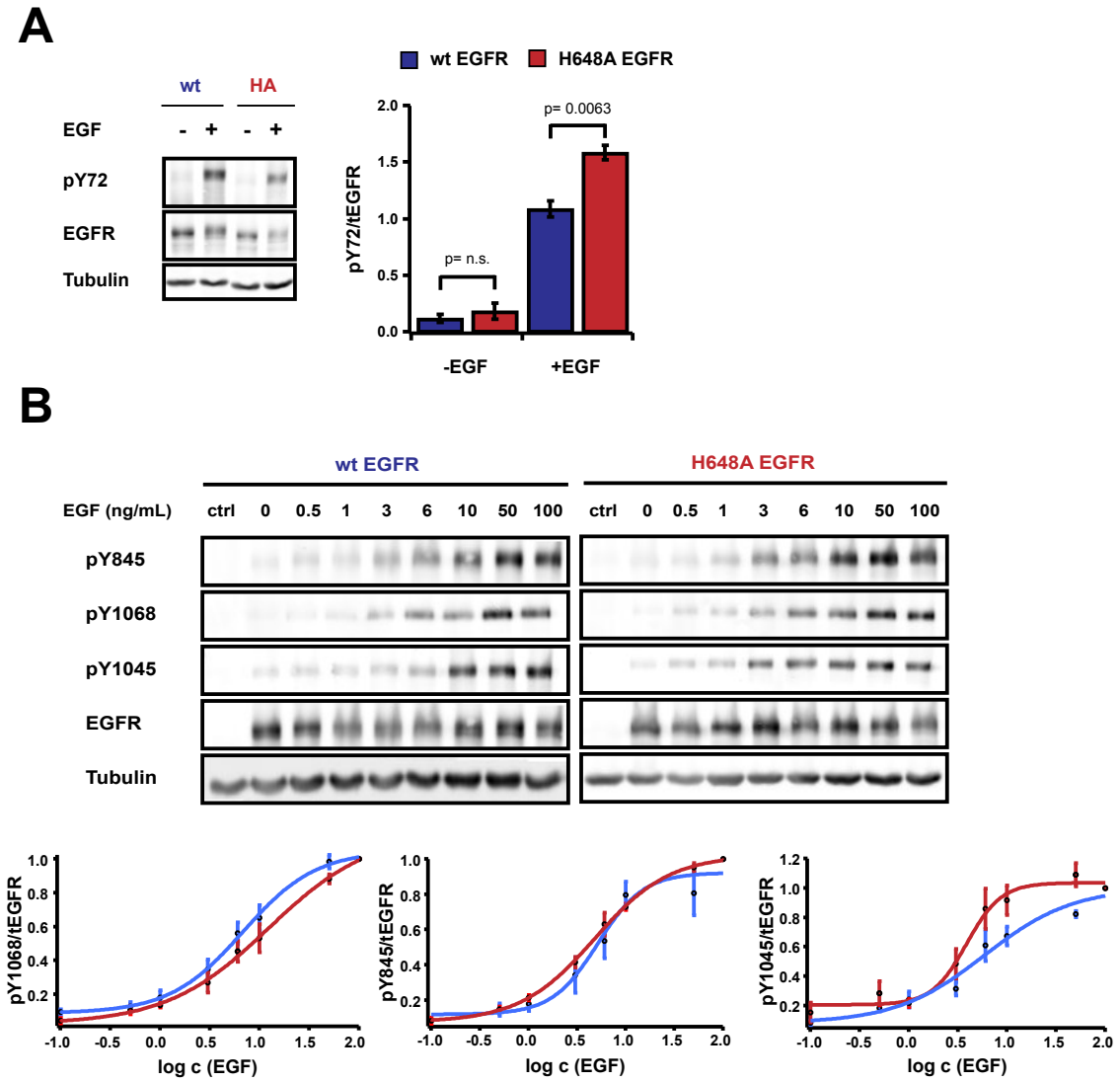

Figure 17: Effect of H648A mutation on ligand dependent EGFR phosphorylation. MCF7 cells were transiently transfected with wt or H648A_EGFR_mCitrine. The cells were stimulated with EGF (100 ng/mL, t=20min) and stained for general Tyr phosphorylation (pY72) (left panels) **(A)**. The relative phosphorylation level (pY over EGFR) of total lysates was quantified for the determined conditions (right panel). Transfected MCF7 cells were stimulated with various EGF doses (20min) and stained for the specific phospho sites pTyr1068, pTyr845 and pTyr1045 (upper panels) **(B)**. The relative phosphorylation level was peak normalized and plotted as a function of the logarithmic EGF concetration for each phospho site (lower panel). All blots are n=3 (mean ± SEM).

Although the phospho-sites Tyr1068 and Tyr845, which are directly connected to EGFR activation, showed no effect, the site involved in the amplified phosphorylation has been identified. As observed in the experiments, the trafficking phospho-site Tyr1045, which recruits c-Cbl after phosphorylation and therefore induces lysosomal receptor degradation, was responsible for the effect. Therefore, the sigmoid phosphorylation curve was shifted to the left at high EGF doses. Due to the rapid EGFR internalization rate, a large section of the receptor molecules was internalized via endocytosis and

degraded after 20 min post EGF stimulation. To avoid this degradation effect, EGFR phosphorylation was monitored at early stimulation time point (5min). According to this, transfected MCF7 cells were stimulated with different doses of EGF for 5min and the total lysates were analysed via immunoblotting experiments (Figure 18).

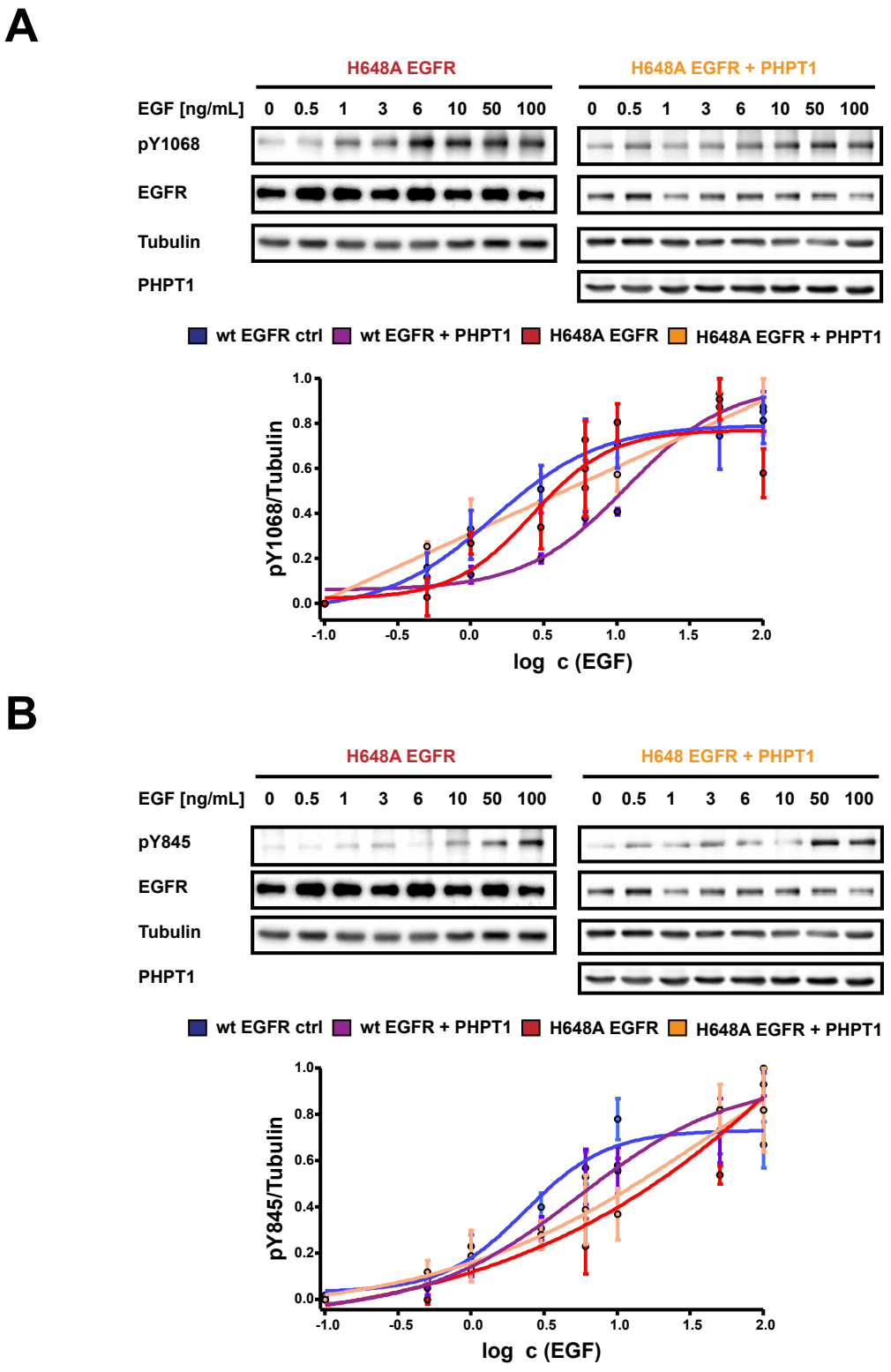

Figure 18: Regulation of EGFR phosphorylation in response to EGF by H648A mutation and PHPT1. EGFR phosphorylation in an EGF dose dependent manner for the signalling site Tyr1068 **(A)** and the autocatalysis site Tyr845 **(B)**. After EGF stimulation (5min) total lysates were probed (upper panels) and the phosphorylation level (pY over Tubulin) of wt and H648A_EGFR_mCitrine in absence

and presence of PHPT1 was base line and peak normalized and plotted against the EGF concentration (logarithmic) (lower panel). All blots are n=3-5 (mean ± SEM).

The plotted curves revealed an impaired auto-phosphorylation of the JM (H648A) EGFR mutant for the signalling site Tyr1068 in absence and presence of PHPT1 (Figure 18A) as well as for the autocatalysis site Tyr845 (Figure 18B). Both the H648A mutant in absence and presence of PHPT1 demonstrated an equal curve shift distinguishable from the phosphorylation of wt EGFR in presence of PHPT1. These findings indicated that PHPT1 required an intact His648 residue to influence ligand dependent EGFR activation. Moreover, the H648A mutant, mimicking the continuously dephosphorylated state, revealed an impaired phosphorylation, which is in agreement with the phosphorylation of wt EGFR in presence of PHPT1. In order to validate this inhibiting effect, single cell immunofluorescence experiments were performed (Figure 19).

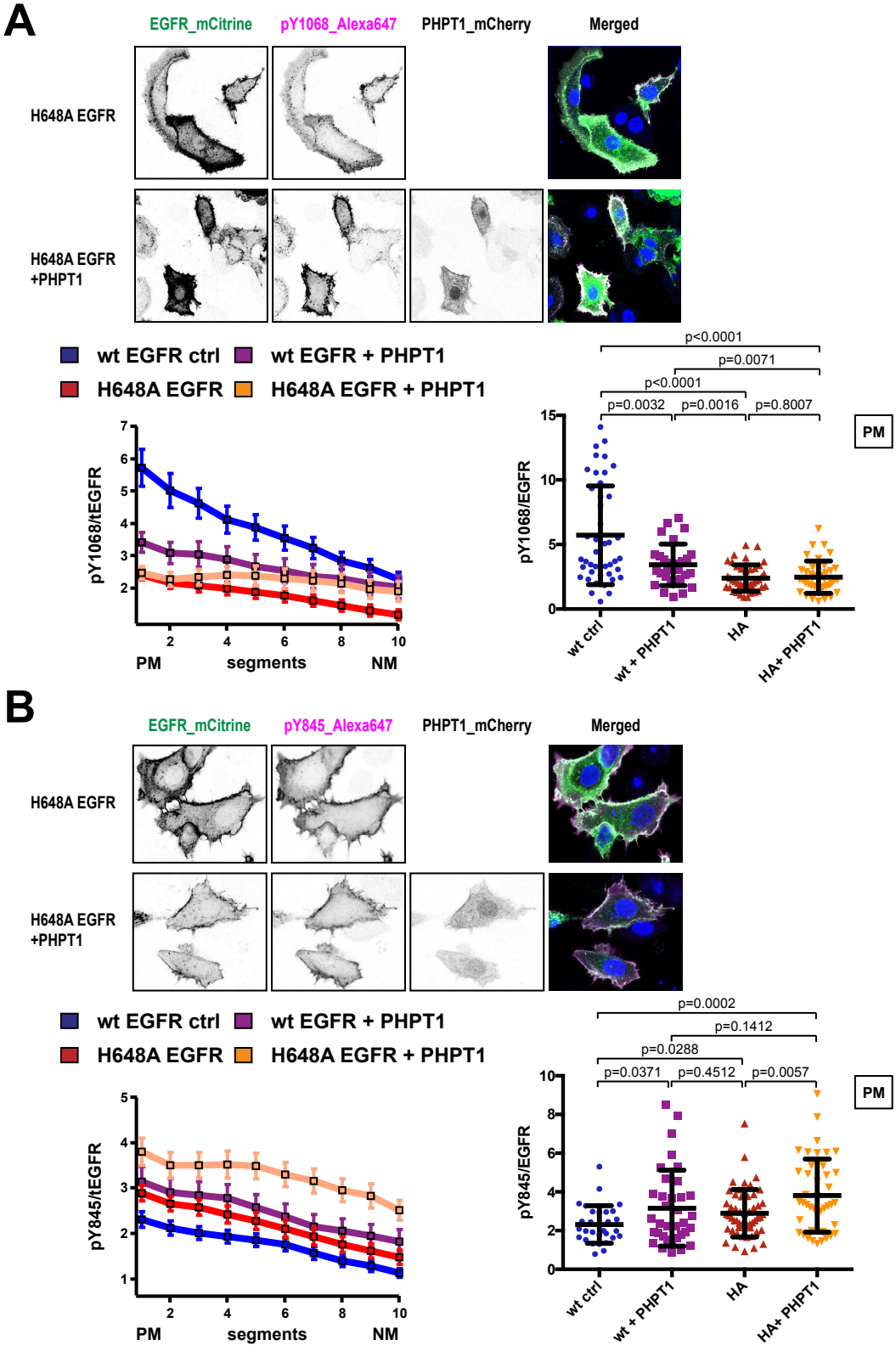

Figure 19: Regulation of ligand dependent EGFR phosphorylation by H648A mutation and PHPT1. MCF7 cells were transiently transfected, fixed and stained for the specific phospho sites pTyr1068 **(A)** and pTyr845 **(B)**. Representative fluorescence images of phosphorylated EGFR after EGF treatment (100 ng/mL, t=5min) (upper panels). Single cells were spatially segmented and the averaged phosphorylation level (pY over EGFR) plotted for the calculated segments (lower, left panel) (Tyr1068:

HA n=42, HA+PHPT1 n=39) (Tyr845: HA n=52, HA+PHPT1 n=42) (mean ± SEM). Relative phosphorylation level of EGFR in the plasma membrane segment for single cells (lower, right panel) (mean ± STDEV).

Indeed, the single cell immunofluorescence experiments showed that the H648A mutation in absence and presence of PHPT1 reduced the phosphorylation level of the signalling phospho-site Tyr1068 after EGF treatment (100 ng/mL, t=5min) mainly on the plasma membrane, consistent with the previous western blot results (Figure 19A). However, the ligand-induced autocatalysis of EGFR (pTyr845) was increased by PHPT1 and H648A mutation independent of the spatial distribution in the cell (Figure 19B). The results between immunoblotting and immunofluorescence experiments might vary, due to the more precise method based on single cell analysis compared to the cell population-based immunoblotting experiments taking all cells in account from low to high expression level. Therefore, additional immunofluorescence experiments were performed in order to verify the effect of the H648A mutation on EGFR activation in a dose dependent manner (Figure 20).

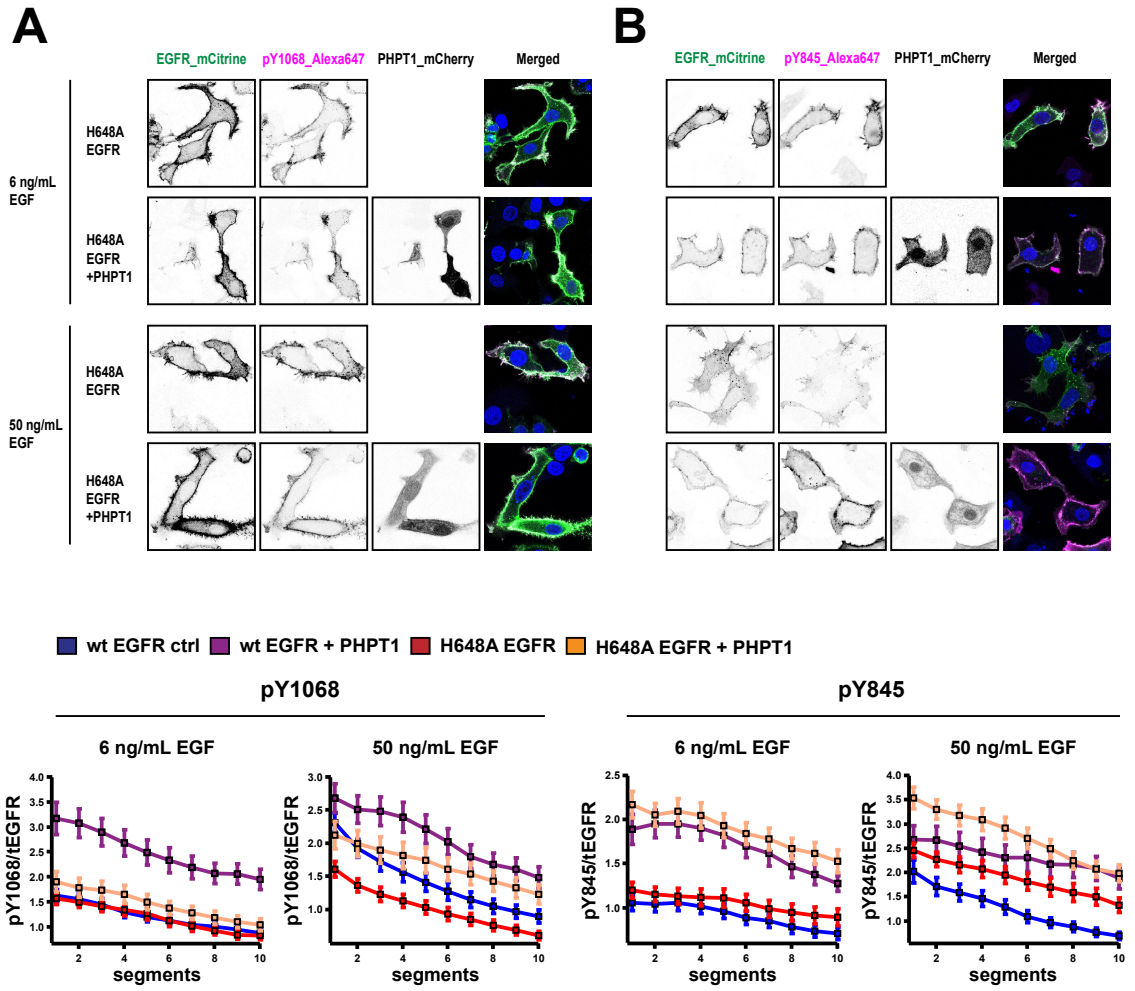

Figure 20: Regulation of EGFR phosphorylation in response to EGF by H648A mutation and PHPT1. Ligand induced EGFR phosphorylation of the signalling site Tyr1068 **(A)** and the autocatalysis site Tyr845 **(B)** at low and high EGF dose (6 and 50 ng/mL, 5min). Representative fluorescence images of phosphorylated EGFR for the indicated conditions (upper panels). The spatially binned realtive phosphorylation level was plotted for each segment (6, 50 ng/mL EGF: Tyr1068: HA n=40, 52, HA+PHPT1 n=44, 47) (6, 50 ng/mL EGF: Tyr845: HA n=60, 51, HA+PHPT1 n=47, 54) (mean ± SEM) (lower panels).

Additionally, the relative phosphorylation levels of single cells were plotted for the determined conditions (Figure 21). In order to validate the regulation of EGFR phosphorylation in space and in response to ligand, the binned phosphorylation level was displayed as a function of EGF concentration for the plasma and nuclear membrane segment (Figure 22).

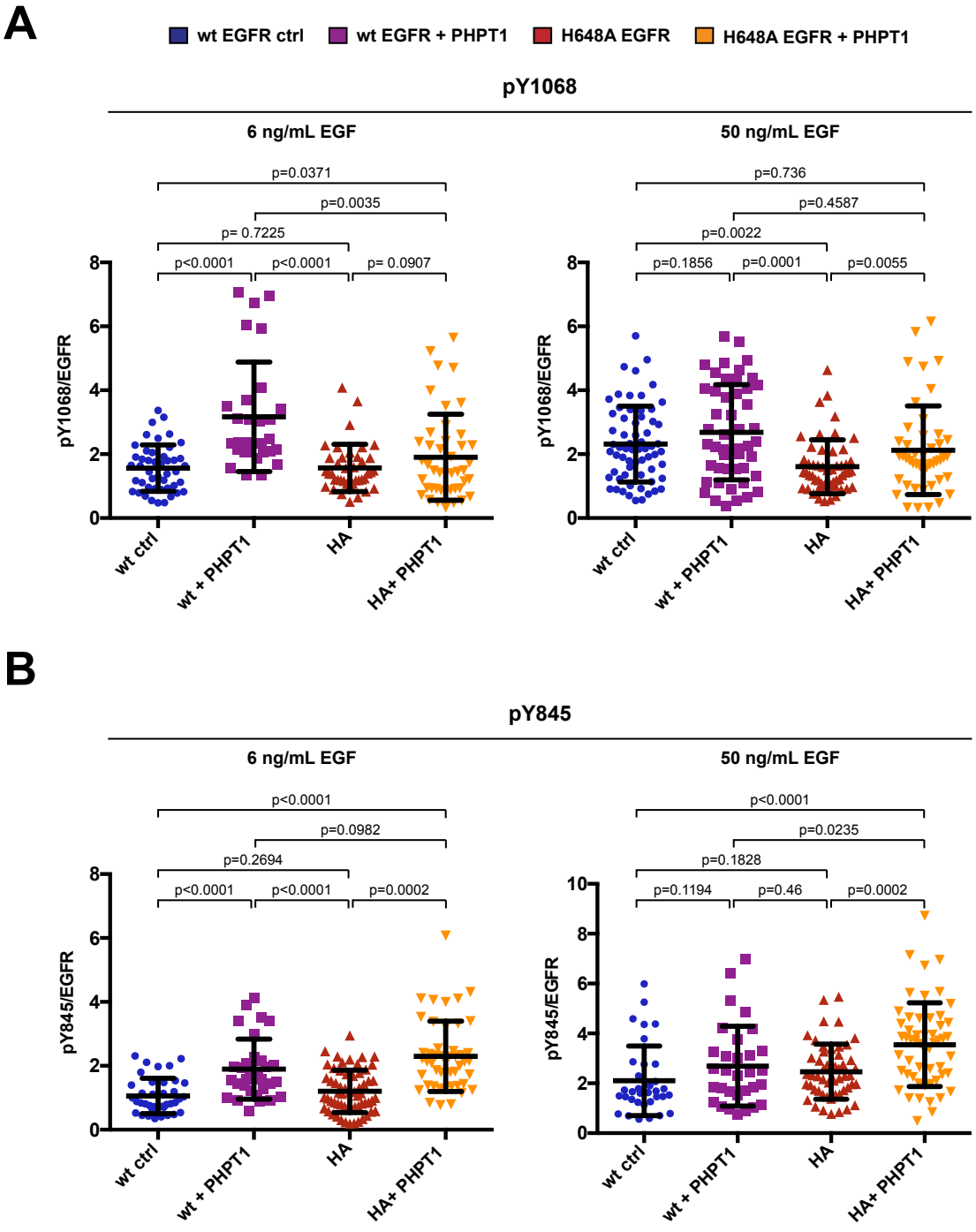

Figure 21: Single cell phosphorylation level of EGFR affected by PHPT1 and H648A mutation. Relative phosphorylation level of EGFR located at the plasma membrane of the signalling phospho site Tyr1068 **(A)** and the autocatalysis site Tyr845 **(B)** at low (6 ng/mL) (left panels) and high (50 ng/mL) (right panels) EGF dose (mean ± STDEV).

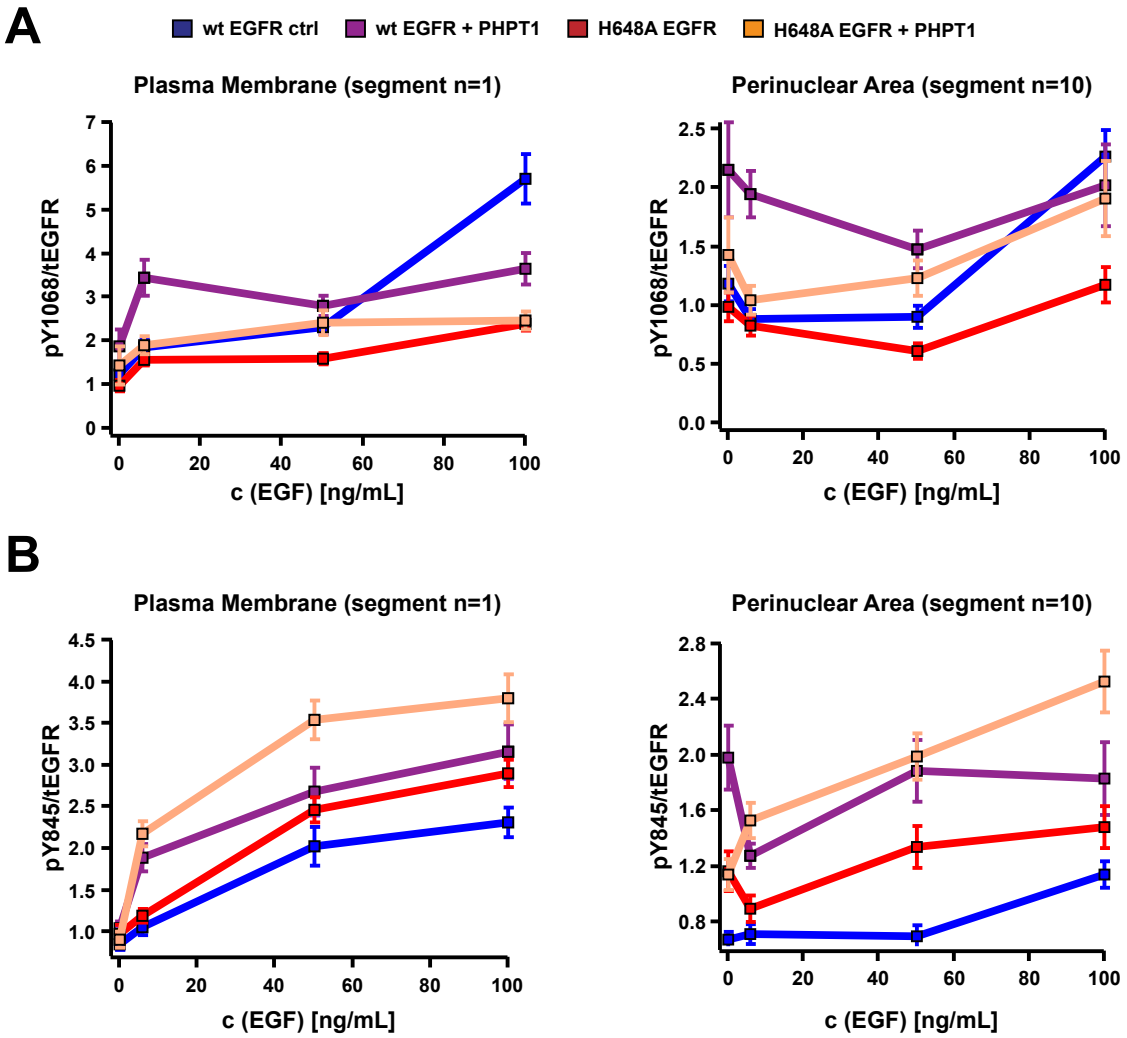

Figure 22: Effect of H648A mutation and PHT1 on EGFR phosphorylation at the plasma and nuclear membrane in a EGF-dose dependent manner. The relative phosphorylation level of the plasma membrane (left panels) and the nuclear membrane segment (right panels) was averaged for the different EGF doses and plotted for the specific phosphorylation sites Tyr1068 **(A)** and Tyr845 **(B)** (mean ± SEM).

The plots illustrated that PHPT1 increased the ligand-induced auto-phosphorylation of Tyr1068 at low EGF concentration (6 ng/mL), at which the receptor mainly becomes activated via spontaneous activation (Figure 22A). Therefore, these results are in agreement with the increased phosphorylation level of spontaneous activated receptor in absence of ligand (Figure 16). In presence of the H648A mutation PHPT1 showed only a modest increase; raising the possibility that the His648 residue plays a crucial role to regulate the spontaneous EGFR activation by PHPT1 and that PHPT1 might act on this position. Moreover, the phosphorylation at saturating dose (100 ng/mL) was reduced by both conditions, the H648A mutation and PHPT1 overexpression. This regulation was

observed at the plasma membrane (Figure 22A, left panels) as well as in the perinuclear area (Figure 22A, right panels). A markedly amplification of phosphorylation was found for the autocatalysis site Tyr845 at low and high doses of EGF for both the plasma membrane (Figure 22B, left panel) and the perinuclear segment located receptor (Figure 22B, right panel). However, a combination of both conditions, H648A_EGFR in presence of PHPT1, showed an additive effect.

In order to perform control experiments, a catalytic incompetent PHPT1 (H53A) mutant was generated and ectopically co-expressed with wt EGFR (Figure 23)[103]. The EGFR phosphorylation was detected via immunofluorescence experiments. Therefore, the spontaneous and ligand induced EGFR activation was affected directly by PHPT1 and depends on its catalytic activity (Figure 23). Moreover, except for the autocatalysis of ligand induced EGFR activation, the H53A PHPT1 mutant showed the opposite effect indicative for a trapped complex, which hampered the general regulation of EGFR phosphorylation. These findings supported the idea that PHPT1 affects spontaneous and ligand induced EGFR activation in a direct mechanism.

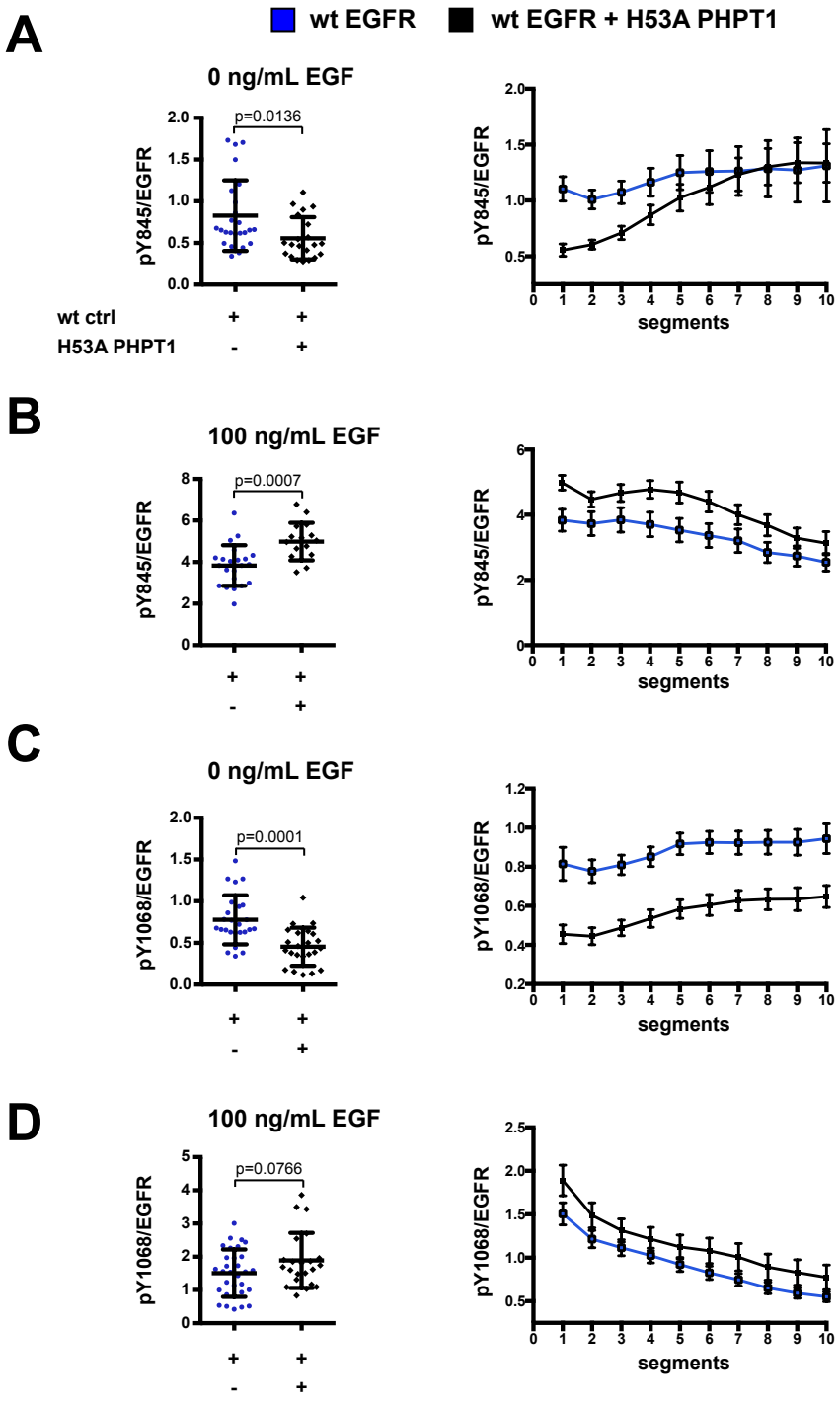

Figure 23: EGFR phosphorylation in presence of the catalytic incompetent PHPT1 mutant (H53A) in absence and presence of ligand. The relative phosphorylation level of EGFR located at the plasma membrane was plotted for single cells (left panels) (mean ± STDEV) as well as the spatially binned and averaged values from the plasma to the nuclear membrane (right panels) (mean ± SEM) (0, 100 ng/mL EGF: Tyr845: wt n=25, 22; wt+H53A PHPT1 n= 23, 16) (0, 100 ng/mL EGF: Tyr1068: wt n= 26, 31; wt+H53A PHPT1 n= 27, 22).

4.2.3 EGFR activation in presence of the phosphohistidine kinases NME1/2

The identified phosphatase/kinase system of histidine phosphorylation in vertebrates consists of PHPT1, acting as a specific phosphohistidine phosphatase, and the kinases, NME1 and NME2, which phosphorylate the targets of PHPT1. In the case that PHPT1 regulates EGFR activation by dephosphorylating phosphohistidine in a direct or indirect manner, the kinases NME1 and NME2 might counteract. To validate the effect of NME1 and NME2 on EGFR activation, immunofluorescence experiments were performed (Figure 24).

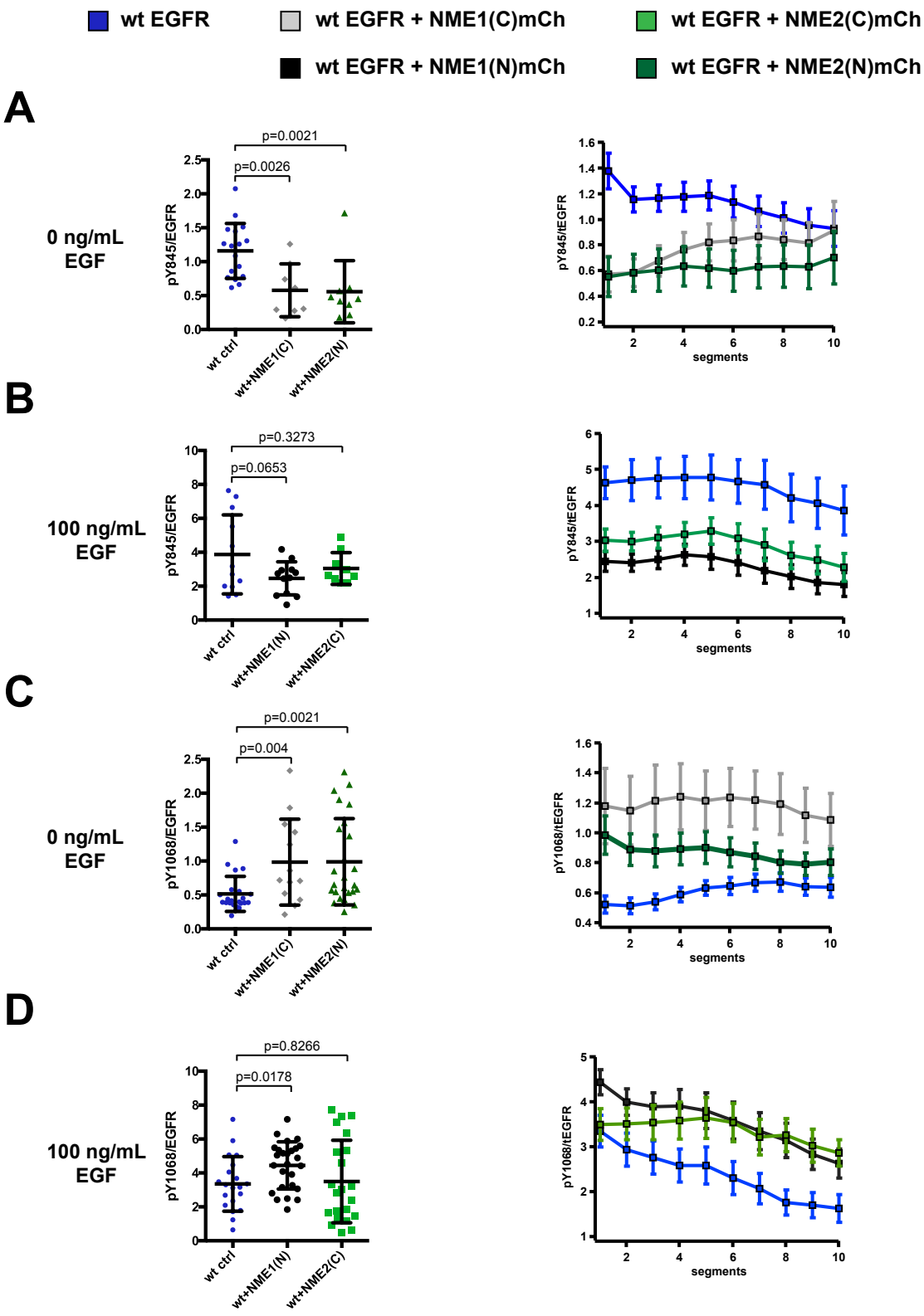

Figure 24: Regulation of EGFR phosphorylation by NME1 and NME2. The relative phosphorylation level (pY over EGFR) of wt_EGFR_mCit in presence and absence of each kinase (N- or C-terminal mCherry) was plotted for spatial segmented single cells for the plasma membrane segment (left panels) (mean ± STDEV) and binned for the different segments to show the spatial distribution from the plasma membrane to the perinuclear area in the cell (right panels) (mean ± SEM). The phosphorylation of the

autocatalysis site Tyr845 **(A,B)** and the signalling site Tyr1068 **(C,D)** was detected (0, 100 ng/mL EGF: Tyr845: wt n=17, 12; NME1 n= 8, 12; NME2 n= 9, 9) (0, 100 ng/mL EGF: Tyr1068: wt n= 11, 20; NME1 n= 14, 26; NME2 n= 25, 22).

The regulation of spontaneous and ligand induced EGFR activation by different tagged kinases (N- or C-terminal) were tested, while only the tagged kinases, affecting EGFR activation, were shown here. In agreement with the amplified phosphorylation of the autocatalysis site Tyr845 in presence of PHPT1, the phosphorylation was reduced by NME1 and NME2 in both cases, the spontaneous and the ligand induced (100 ng/mL, 5min) EGFR activation (Figure 24A, B). The same consistency was observed for the phosphorylation of the signalling site Tyr1068 after EGF dependent receptor activation (Figure 24D). The kinase NME1 enhanced EGFR auto-phosphorylation, whereas NME2 showed a significant increase only in the cytosolic and perinuclear area. However, NME1 and NME2 increased EGFR signalling of spontaneous activated receptor such as PHPT1 (Figure 24C). Furthermore, the tagged versions of NME1 and NME2, showing an effect for ligand dependent activation, does not influence the spontaneous activation. This observation supports the idea that there are two distinct regulation mechanisms of EGFR activation in absence and presence of ligand.

4.3 Effect of PHPT1 and His648 mutation on receptor internalization

EGFR internalization terminates receptor enrichment on the plasma membrane, thus preventing receptor hyperactivation. Spontaneous activated EGFR is internalized and recycled back to the plasma membrane via recycling endosomes, whereas ligand-induced activation leads to internalized receptor, which is degraded via the lysosomal pathway. Previous studies showed that the kinases NME1 and NME2 facilitate the dynamin-dependent endocytosis[104,105]. To confirm the effect of PHPT1 and the JM (H648A) mutation on receptor internalization, an on-cell western assay based on immunofluorescence experiments, and western blot analyses were performed (Figure 25).

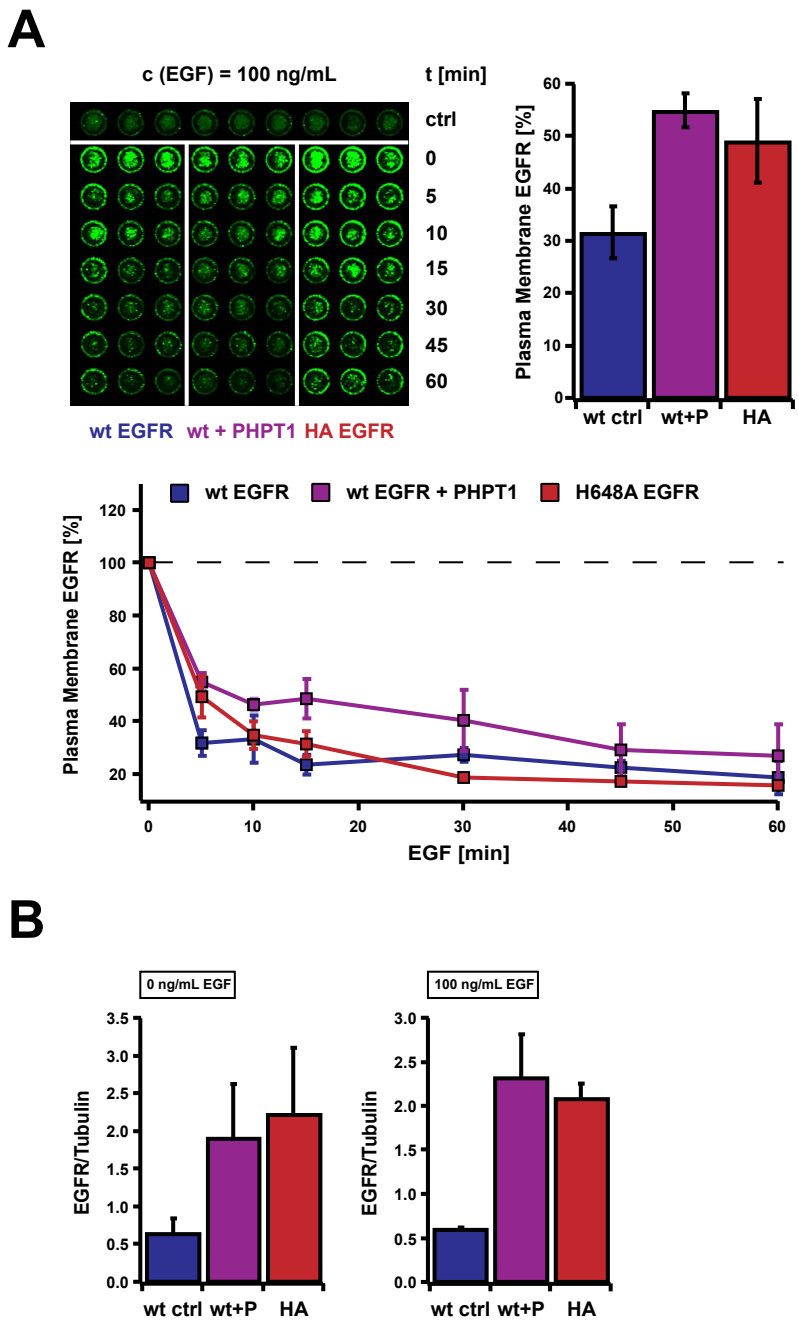

Figure 25: PHPT1 and H648A mutation reduces EGFR internalization rate. MCF7 cells were transfected with EGFR in absence and presence of PHPT1 in 96 well plates and stimulated with EGF (100 ng/mL) for different time points. The fixed, but unpermeabilized cells were stained with EGFR antibody (epitope: extracellular part) **(A)**. A representative fluorescence image (upper, left panel) and the percentage of receptor sitting on the plasma membrane after EGF stimulation (5min) (upper, right panel) and as a function of time (lower panel). The assay was performed as n=2 (mean ± SEM). The normalized EGFR expression level (EGFR/Tubulin) was quantified for wt EGFR in absence and presence of PHPT1 as well as for the H648A EGFR mutant in immunoblotting experiments **(B)**. All blots are n=2 (mean ± SEM).

The data showed that PHPT1 increased the amount of plasma membrane located receptor after EGF stimulation (100 ng/mL). Additionally, the JM (H648A) mutation

revealed an equal effect at early time point (5min), indicative for a reduced internalization rate (Figure 25A). Furthermore, the JM (H648A) mutant increased the internalization at late time point (t >15min), which was consistent with a higher degradation rate of mutated receptor after EGF stimulation (100 ng/mL, 20min) and an increased phosphorylation level of the trafficking phospho-site Tyr1045 in previous western blots (Figure 17). To validate this effect, the EGFR expression level of wt and H648A EGFR of unstimulated and stimulated (100 ng/mL, 5min) cells was determined via western blot analysis (Figure 25B). In agreement with the internalization assay, the amount of receptor in unstimulated and stimulated cells was enhanced for wt EGFR in presence of PHPT1 and for H648A EGFR, suggesting that receptor internalization is reduced by PHPT1 and JM (H648A) mutation.

4.4 Detection of phosphohistidine in immunoblotting experiments

To identify the histidine phosphorylation as a new posttranslational modification of EGFR, immunoblotting experiments were performed using monoclonal antibodies against both isoforms, 1-pHis and 3-pHis[106]. Although the specific isoforms of *in vitro* auto-phosphorylated enzymes, NME1 and PGAM1 (Figure 26)[107,108], have been detected in this study, EGFR His phosphorylation could not be identified for overexpressed as well as for endogenous receptor in presence of high kinase expression level, NME1 and NME2. Due to the unstable phosphoramidate bond and the lack of phosphohistidine phosphatase inhibitors, the detection of this modification is demanding[108].

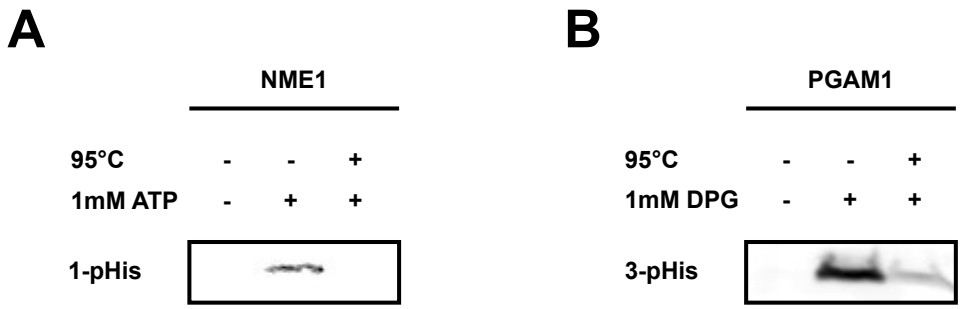

Figure 26: Detection of the phosphohistidine isoforms 1-pHis and 3-pHis. Histidine phosphorylation of purified and auto-phosphorylated enzymes. NME1 was incubated in absence (-/-) and presence (-/+) of adenosine triphosphate (ATP) (1 mM) at RT for 10min **(A)** and PGAM1 with 2,3-diphosphoglycerate (2,3-DPG) (1 mM) at 30°C for 10min **(B)**. The dephosphorylation of the temperature-sensitive phosphohistidine was induced at 95°C for 10min (+/+).

4.5 Protein interaction between EGFR and PHPT1

In order to clarify whether the regulation of EGFR activation by PHPT1 undergoes an indirect or direct mechanism, co-immunoprecipitation experiments were performed. After the optimization procedure, the substrate-trapping mutant of the phosphatase (H53A PHPT1) was not eluted in presence of EGFR as well as in the opposite case (data not shown). Due to the method, excluding transient interactions, the binding between EGFR and PHPT1 may proceed in a short-lived interaction. Therefore, the co-immunoprecipitation might not be the optimal tool. To further elucidate the protein interaction, the more sensitive microscopy method fluorescence lifetime imaging-fluorescence resonance energy transfer (FLIM-FRET) was performed (Figure 27).

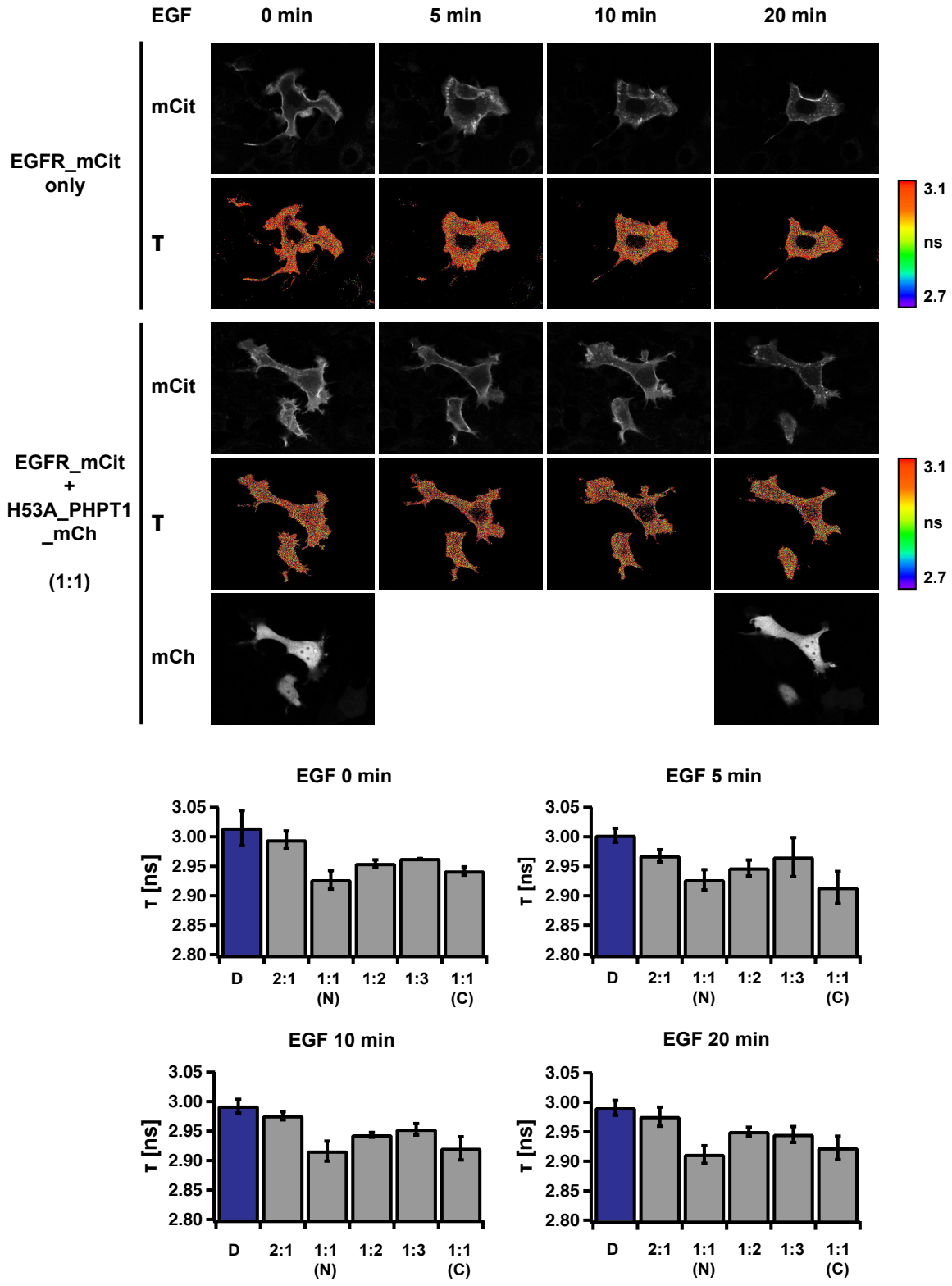

Figure 27: Analysis of protein interaction between EGFR and PHPT1 via FLIM-FRET. MCF7 cells were transfected with wt_EGFR_mCitrine (donor) and H53A_PHPT1_mCherry (acceptor) (N-terminal mCherry (N), C-terminal mCherry (C)) in different ratios (D:A) and stimulated with EGF (100 ng/mL) for different time points. The living cells were analysed via FLIM-FRET. Representative fluorescence

images and the calculated lifetime (τ in ns) (upper panel). The averaged lifetime was plotted for the indicated conditions (lower panel). The measurements were performed as n=3-6 (mean ± STDEV).

The FLIM-FRET experiments, based on an energy transfer between two fluorophores, revealed a slight FRET shift between 70 and 80 ps (1:1, (N) and (C)), indicative for a transient protein-protein interaction between EGFR and PHPT1.

5 Discussion

An increased EGFR activation and amplified signalling is linked to various types of cancer[28]. Therefore, the identification of key players regulating receptor activation plays a crucial role. Recent studies have shown that receptor phosphorylation of Tyr as well as Ser and Thr residues affect EGFR function in its activity, its endocytosis and further signalling[38,109]. Although these studies provide important insights into EGFR regulation, the role of His phosphorylation remains unknown. It has been demonstrated that His phosphorylation affects ion channel and G-protein signalling, whereas the receptor tyrosine kinase signalling has been overlooked until now[91,92,110]. To address this issue, we investigated the effect of the mammalian phosphohistidine phosphatase and kinase cycle, consisting of PHPT1, NME1 and NME2, on EGFR activation. Moreover, we elucidated the role of the specific His648 residue, which is located in the polybasic JM directly next to the plasma membrane and may act as a possible regulatory phosphorylation site. We monitored the EGFR activity by detecting specific receptor phosphorylation sites, the signalling site Tyr1068 and the regulatory autocatalysis site Tyr845. For the first time, we show the regulation of EGFR activation by PHPT1 and the kinases NME1, NME2. The data reveal that the regulation of ligand-induced and spontaneous receptor activation might occur in two distinct mechanisms.

5.1 PHPT1 and JM (H648A) mutation affect spontaneous EGFR activation

In absence of ligand and at high expression level, EGFR undergoes spontaneous activation, which requires no stimulus and plays a crucial role in cancerogenesis[98,111]. To investigate the effect of PHPT1 and the JM (H648A) mutation on spontaneous EGFR activation, immunoblotting and immunofluorescence experiments of MCF7 cells, ectopically co-expressing EGFR and PHPT1, were performed. The obtained results show that PHPT1 amplifies the signalling (pTyr1068) as well as the autocatalysis (pTyr845) of spontaneous activated wt EGFR (Figure 8 and Figure 9). In a model in which EGFR activation is regulated in a related mechanism as the ion channel KCa3.1, the His648 residue gets phosphorylated, while PHPT1 catalyses the dephosphorylation. Subsequently, the embedded state would be favoured due to a hampered release of the intracellular part. EGFR may be trapped in the plasma

membrane causing an increased density of receptor molecules. Since the spontaneous EGFR activation depends on the amount of plasma membrane bound receptor, an increased density enhances the possibility of two monomers coming in contact via thermal fluctuation and therefore enhances the spontaneous activation.

In contrast to PHPT1, the JM (H648A) mutation of EGFR shows no effect on EGFR signalling (pTyr1068) in absence of ligand (Figure 15 and Figure 16), whereas the autocatalysis (pTyr845) is slightly increased (Figure 16). There is probably a safeguard mechanism, preventing a propagation of this amplifying effect to downstream signalling.

To ascertain if the specific His648 residue serves as a substrate site for PHPT1, the effect of the phosphatase on the H648A EGFR mutant was analysed. The immunofluorescence experiments reveal the same autocatalysis level (pTyr845) for the H648A EGFR mutant alone as well as in presence of PHPT1, while the signalling is slightly increased (Figure 16). In both cases, autocatalysis and signalling, the relative phosphorylation level is distinguishable from wt EGFR phosphorylation in presence of PHPT1. This suggests the idea that PHPT1 requires an intact His648 residue in the JM of EGFR to affect spontaneous receptor activation. It also indicates that PHPT1 may act directly on this residue. For EGFR signalling (pTyr1068) the H648A mutation hampers the amplification by PHPT1, but not completely. Therefore, it is tempting to speculate that PHPT1 acts on further His residues or that the enzyme increases EGFR signalling of spontaneous activated receptor not only via His dephosphorylation. The phosphatase may serve additionally as an allosteric regulator or as a binding partner, stabilizing a protein complex crucial for spontaneous receptor signalling. The amplified signalling (pTyr1068) as well as the autocatalysis (pTyr845) depend on the catalytic activity of PHPT1 (Figure 23). The catalytic inactive PHPT1 mutant (H53A) does not only act as a catalytically incompetent mutant, but also as a substrate trapping mutant[79,20]. As a substrate trapping mutant, PHPT1 H53A would bind EGFR and traps it into a complex caused by its incapacity to catalyse the dephosphorylation of the receptor. Therefore, wt EGFR activation and further phosphorylation would be impaired, which could be observed in the previous experiments.

The regulation of EGFR phosphorylation in the cell shows a high complexity. Therefore, the phosphorylation is not only modulated in a temporal and a ligand dose

dependent manner, but also by endocytosis in a spatial manner. Using the single cell segmented immunofluorescence data, the regulation of EGFR phosphorylation has been quantified in space, showing an altered spatial regulation between the signalling (pTyr1068) and the autocatalysis (Tyr845) phosphorylation (Figure 16). The phosphorylation of the signalling site (Tyr1068) has been amplified all over the cell, while the autocatalysis site (Tyr845) shows the strongest amplification in the perinuclear area. The autocatalysis site is located in the activation loop, which may lose its accessibility to become phosphorylated in the embedded state by facing the plasma membrane, while the signalling site is located in the accessible flexible C-terminus. During endocytosis, the stabilization of the embedded receptor state, containing a non-accessible Tyr845 site, might be decreased, which would enhance the possibility of Tyr845 phosphorylation of EGFR in the cytosol.

5.2 Regulation of ligand induced EGFR activation by PHPT1 and JM (H648A) mutation

In addition to the spontaneous activation, EGFR gets also activated in presence of ligand. Therefore, ligand binding generates an asymmetric dimer conformation, which activates the receptor tyrosine kinase and induces trans-phosphorylation. To uncover the effect of PHPT1 on the ligand induced EGFR activation, EGF dose response experiments were performed (Figure 10). The results reveal a significant right shift of the signalling phosphorylation (pTyr1068) in presence of PHPT1, indicative for a changed threshold, which means that EGFR requires an increased amount of EGF to get activated. Only a slight right shift has been observed for the phosphorylation of the autocatalysis site (pTyr845). To further validate this effect, immunofluorescence experiments were performed, showing consistently a decrease of phosphorylation for EGFR signalling at high EGF concentration (Figure 14). In contrast to the western blots, the immunofluorescence experiments show an amplified phosphorylation of the autocatalysis site (pTyr845). This might be due to the more precise single cell method, whereas the western blot is based on a cell population based assay taking all cells with low and high EGFR and PHPT1 expression level into account, which might falsify the results of only weak effects.

EGFR recycles back to the plasma membrane via the clathrin dependent pathway at low EGF doses, whereas high doses induce lysosomal EGFR degradation via the clathrin independent pathway[112]. This change in trafficking may be caused by a shift from the monomeric spontaneous activation to the dimeric ligand induced activation and may explain the obtained results. At low doses (0-50ng/mL) EGFR signalling (pTyr1068) is amplified consistent with the data of spontaneous activated receptor in absence of ligand (Figure 9 and Figure 14), while PHPT1 suppresses the phosphorylation increase at high doses (>50 ng/mL). Previous studies have reported that CaM facilitates ligand dependent activation by releasing the intracellular part of EGFR from the plasma membrane, thus enables the dimerization. However, the role of CaM for the spontaneous activation of EGFR in absence of ligand has not been defined[113]. If the CaM dependent activation requires the phosphohistidine (pHis648), the dephosphorylation by PHPT1 would hamper the dimerization by a continuously embedded inactive state causing a decreased phosphorylation at high EGF doses. Furthermore, phosphorylation of Thr654 and Thr669, located in the JM region of EGFR, shifts the monomer-dimer equilibrium of ligand bound receptor towards the monomeric state, while Thr669 phosphorylation inhibits CaM binding and therefore further ligand induced EGFR activation[114,65]. This raises evidence that PHPT1 may modulate the monomer-dimer equilibrium of EGFR by affecting CaM binding.

In general, EGFR phosphorylation is coupled to PTP inhibition by reactive oxygen species (ROS), like H_2O_2. Therefore, ligand-induced EGFR activation produces an increased amount of ROS at the plasma membrane via sequential activation of PI3K and Rac1, which binds and activates specific NADPH oxidases (NOX) located in the plasma membrane[115]. Since ROS oxidizes the catalytic cysteine residue of PTPs, the inactive phosphatases are not able to dephosphorylate EGFR[116]. This coupling causes a double negative feedback, which leads to an increased amount of phosphorylated receptor in presence of high EGF doses at the plasma membrane[45]. In contrast to the PTPs, PHPT1 gets oxidized at Met95 in presence of H_2O_2. This residue is located in the substrate binding site, but does not impair the functionality of PHPT1[117]. Therefore, PHPT1 is able to affect ligand induced EGFR signalling even at high EGF doses by suppressing the switch-like receptor response. In contrast to the signalling (pTyr1068), the autocatalysis (pTyr845) is still amplified at high doses of EGF. Recent studies have been demonstrated that ROS activates the Src kinase in MCF7 cells.[118] Hence, the Src

kinase also phosphorylates the autocatalysis site (Tyr845), an increased kinase activity may overcome the suppressing effect of PHPT1. This is confirmed by a sustained increased EGFR autocatalysis in presence of ligand by the catalytic incompetent PHPT1 mutant (Figure 23).

The immunofluorescence experiments show that not only PHPT1 overexpression, but also H648A JM mutation reduce the ligand induced EGFR signalling at high EGF doses (Figure 22), consistent with recent reports in which mutations in the CaM binding domain decreases EGFR phosphorylation in presence of ligand[61]. Therefore, the H648A JM mutation, mimicking a continuously dephosphorylated state located in the CaM binding domain of EGFR[64], might prevent CaM binding, which requires His phosphorylation in the case of the ion channel KCa3.1. If EGFR is regulated in analogous to KCa3.1, this would impede the ligand dependent receptor activation and lead to a reduced phosphorylation and attenuated signalling, which has been shown in the experiments. The H648A JM mutant has the same effect in presence of PHPT1, which raises the possibility that PHPT1 acts on the His648 residue. Moreover, the catalytically incompetent PHPT1 mutant (H53A) shows the opposite effect of ligand induced EGFR phosphorylation at high EGF dose (Figure 23).

Controversially, the autocatalysis (pTyr845), which is directly connected to the signalling, is increased for the JM H648A mutation and in presence of PHPT1. This effect is amplified for H648A EGFR in presence of PHPT1. In previous studies, it has been demonstrated that PHPT1 inhibits certain targets such as KCa3.1 and ACL, which impair the Src kinase activity[119,120]. An inhibition of these targets would increase Src activation which causes an amplified phosphorylation of the autocatalysis site. Since the autocatalysis site Tyr845 becomes not only auto-phosphorylated, but also external phosphorylated by the Src kinase[40], PHPT1 overexpression may lead to an amplified Src activity causing an increased phosphorylation of the autocatalysis site Tyr845. This may prevent the inhibitory effect of PHPT1 at high EGF doses.

5.3 Regulation of EGFR activation by phosphohistidine kinases NME1 and NME2

The kinases NME1 and NME2 catalyse the phosphorylation of His residues. While PHPT1 has been identified as an oncogene, NME1 and NME2 are known as metastasis

suppressor genes. In the performed immunofluorescence experiments, the kinases showed the opposite effect compared to PHPT1 (Figure 24). Thus, the data reveals a decreased autocatalysis of EGFR (pTyr845) of spontaneous and ligand induced activated receptor as well as an increase of ligand dependent EGFR signalling (pTyr1068) raising evidence that the kinases counteract PHPT1. However, NME1 and NME2 enhanced EGFR signalling in absence of ligand equal to PHPT1. Since EGFR downstream signalling varies between spontaneous and ligand dependent receptor activation[46], NME might regulate the downstream signalling of spontaneous activated EGFR in a different way, which remains unknown at this state. Therefore, further experiments have to be performed. Moreover, the functionality of NME1 and NME2 is affected by the localization of the tagged fluorophore. Indeed, different tagged versions regulate spontaneous and ligand induced receptor activation, which indicates that both activation mechanisms are regulated by NME1 and NME2 in two distinct mechanisms. Finally, both kinases may act as metastasis suppressor genes caused by an impaired EGFR activity.

5.4 PHPT1 and JM (H648A) mutation attenuate EGFR internalization

EGFR activity on the plasma membrane is also regulated by endocytosis, where receptor molecules get internalized after activation. Upon stimulus, the receptor becomes internalized and degraded through lysosomes, whereas spontaneous activated receptors (non-ligand dependent) are recycled back to the plasma membrane through the recycling endosomes[47,46]. Moreover, previous studies have shown that NME1 and NME2 facilitate dynamin-mediated endocytosis by interacting with and providing GTP to dynamins[105,121]. Since active dynamin is required for EGFR endocytosis, an internalization assay has been performed to validate the effect of PHPT1 and the H648A JM mutation of EGFR on receptor internalization rate (Figure 25A). The assay reveals an increased amount of EGFR on the plasma membrane after EGF stimulation in presence of PHPT1, indicative for a decreased internalization rate. The same effect has been observed for the JM H648A EGFR mutant at early time point (5min) and could be confirmed via immunoblotting experiments (Figure 25B). The reduced internalization rate is consistent with the previous results, where the spontaneous activation, inducing recycling, has been amplified, while the ligand dependent activation, inducing receptor degradation, is reduced. Additionally, an increased density of receptor molecules on the

plasma membrane amplifies the spontaneous EGFR activation by increasing the possibility of receptor molecules encounter each other and forming a short-lived dimer for activation. It is possible that PHPT1 does not only regulate EGFR activation in a direct manner; it may also play a crucial role in an indirect mechanism by affecting the endocytosis rate. While the effect on endocytosis has been discussed as a crucial factor involved in the tumour suppressor activity of NMEs, with respect to PHPT1 it may cause its oncogenic potential[104].

5.5 Phosphohistidine detection with immunoblotting experiments

The phosphorylation of His occurs on two possible positions, forming two isoforms 1-pHis and 3-pHis containing an unstable phosphoramidate. This high-energy bond is less stable against hydrolysis compared to the general phosphohydroxyamino acids such as pTyr, pSer or pThr. Due to its acid and temperature sensitivity, the detection turns out to be demanding. During this work the His phosphorylation of *in vitro* auto-phosphorylated enzymes (NME1 and PGAM1) was detected, while EGFR phosphohistidine remained undetected (Figure 26). Reasons for this may be the dephosphorylation during lysis procedure caused by the lack of phosphohistidine phosphatase inhibitors. Therefore, previous studies have shown that unspecific phosphohistidine phosphatases such as PP1, PP2A and PP2C exist, which might be able to dephosphorylate EGFR. Even if cell lines with low PHPT1 endogenous level have been chosen, these phosphatases may falsify the results. The detection of total lysates containing ectopically overexpressed EGFR as well as concentrated receptor samples after immunoprecipitation of endogenous receptor was unsuccessful. EGFR may form a transient phosphohistidine intermediate, which transfers its phosphate directly after phosphorylation. This would also circumvent the detection of phosphorylated histidine.

5.6 Protein interaction between EGFR and PHPT1

In order to identify the direct interaction between PHPT1 and EGFR, co-immunoprecipitation experiments were performed. Therefore, a substrate trapping PHPT1 mutant (H53A) was generated and ectopically co-expressed with EGFR in MCF7 cells. Since the method includes only strong protein-protein interactions and the binding may proceed in a transient short-lived interaction, co-immunoprecipitation is probably not the optimal tool and could not be used to detect a direct interaction

between EGFR and PHPT1. Therefore, a more sensitive and precise fluorescence microscopy method, FLIM-FRET, was performed (Figure 27). FRET is based on a non-radiative energy transfer between a donor and an acceptor molecule. This transfer induces a reduced life time (τ) of the donor fluorophore, which is detected by FLIM. The FRET efficiency depends on a correct dipole-dipole coupling based on the distance and the orientation between the dipole moments of the donor and acceptor molecule[122]. In the performed FLIM-FRET experiments of wt EGFR, *C*-terminally tagged with mCitrine, and H53A PHPT1, *N*-terminal tagged with mCherry, a shift in life time of 70 to 80 ps was observed. Although this change is low, it raises evidence that PHPT1 probably interact with EGFR. Increased distances between the two fluorophores may cause a decreased FRET efficiency. PHPT1 might bind EGFR through a secondary binding partner. By forming a sterically hindered protein complex, the dipole-dipole coupling might be impaired. If the resulting protein complex is too labile, the detection of protein interaction between EGFR and PHPT1 would be also unsuccessful via co-immunoprecipitation. Additionally, the fluorescence protein mCherry, which is linked to PHPT1, has a molecular weight of 27 kDa, while the small phosphatase PHPT1 has only a molecular weight of 14 kDa. According to this, the size of the recombinant protein used for the studies is three-fold higher as the phosphatase. This increase in size might also hamper PHPT1 binding, due to sterically hindrance, in FLIM-FRET as well as co-immunoprecipitation experiments.

5.7 A proposed model of EGFR activation regulated by phosphohistidine phosphatase/kinase cycle

Despite the open questions concerning the His phosphorylation of EGFR and the direct interaction between EGFR and PHPT1, this study has identified the first phosphohistidine phosphatase regulated EGFR activation mechanism. This pioneering work goes one step further and shows that EGFR autocatalysis and signalling of spontaneous as well as ligand induced receptor activation are regulated by the phosphohistidine phosphatase/kinase cycle. Accordingly, not only GPCR and calcium signalling are regulated by His phosphorylation, but also RTK signalling.

Based on the assumption that PHPT1 regulates EGFR in a direct manner, a mechanistic model is proposed (Figure 28).

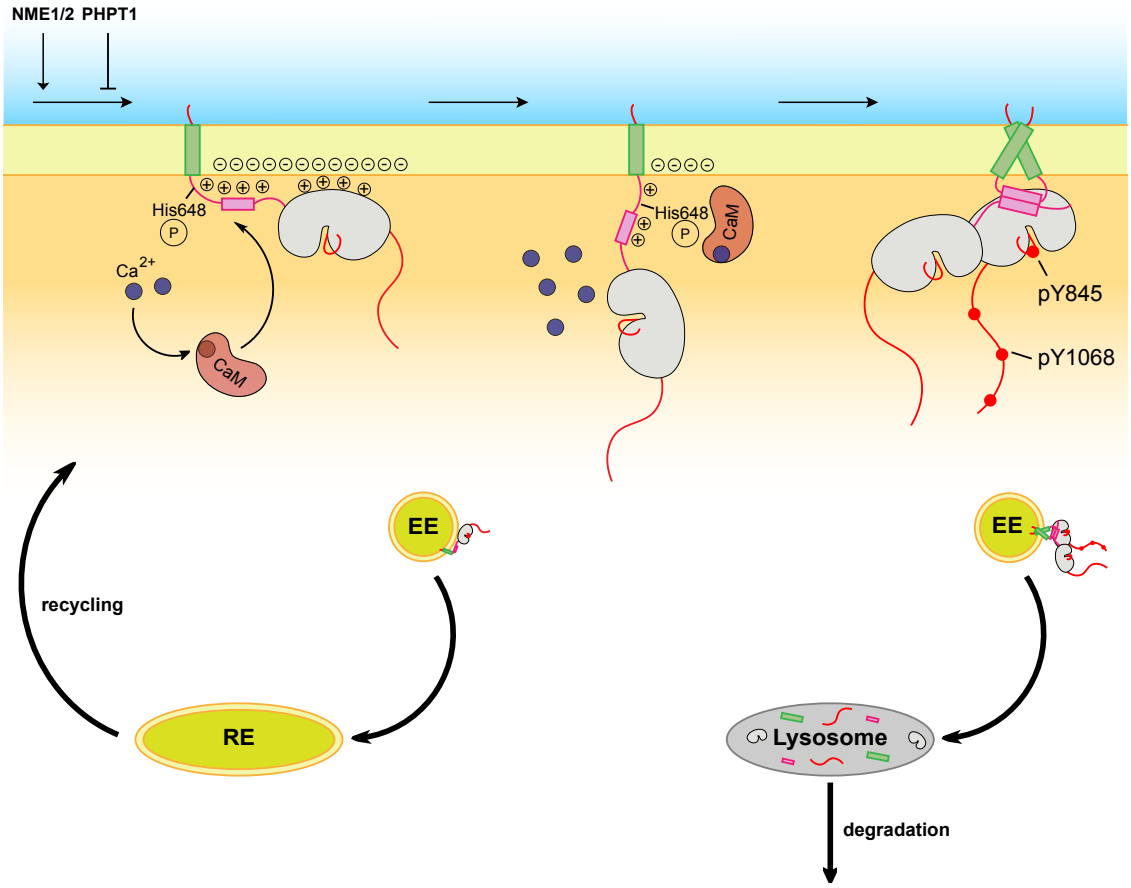

Figure 28: Model of EGFR activation regulated by phosphohistidine phosphatase/kinase cycle. Vesicular trafficking (thick arrows) of EGFR from plasma membrane via early endosomes (EE). Monomers are recycled back to the plasma membrane via recycling endosomes (RE), while formed dimers are degraded by lysosomes. Extracellular part is excluded for simplification. Horizontal arrows: conversion. Vertical arrows: causality.

In this model, EGFR becomes His phosphorylated (His648) in its polybasic JM by NME1/2, which is required for binding active calcium-CaM complex. The negatively charged CaM repeals the embedded intracellular part from the plasma membrane and facilitates dimerization by increasing the flexibility of the receptor. This causes an increased EGFR signalling of ligand induced receptor activation in presence of NME1/2. As opposed to this, PHPT1 dephosphorylates the phosphohistidine (pHis648) to hamper the ligand dependent dimerization by favouring the inactive embedded state of EGFR, which induces a decreased EGFR signalling (Figure 29A). Subsequently, EGFR is trapped in the plasma membrane leading to an increased density of plasma membrane bound receptor. Previous studies have shown that spontaneous EGFR activation depends on its expression level[98]. Therefore, an increased amount of receptor

on plasma membrane enhances the probability of two molecules coming together and forming a short-lived dimer for further receptor activation. As the experiments have shown, the receptor internalization is decreased in presence of PHPT1 as well as for the JM H648A mutation. The signalling and autocatalysis of spontaneous receptor activation might be amplified by modulating the endocytosis of EGFR. While the ligand induced EGFR signalling is reduced by PHPT1, the autocatalysis, which is directly connected to the signalling, shows an amplification (Figure 29B). This amplified effect might be caused by an increased Src kinase activity, which might amplify the phosphorylation of the autocatalysis site Tyr845 and therefore suppresses the inhibitory effect of PHPT1.

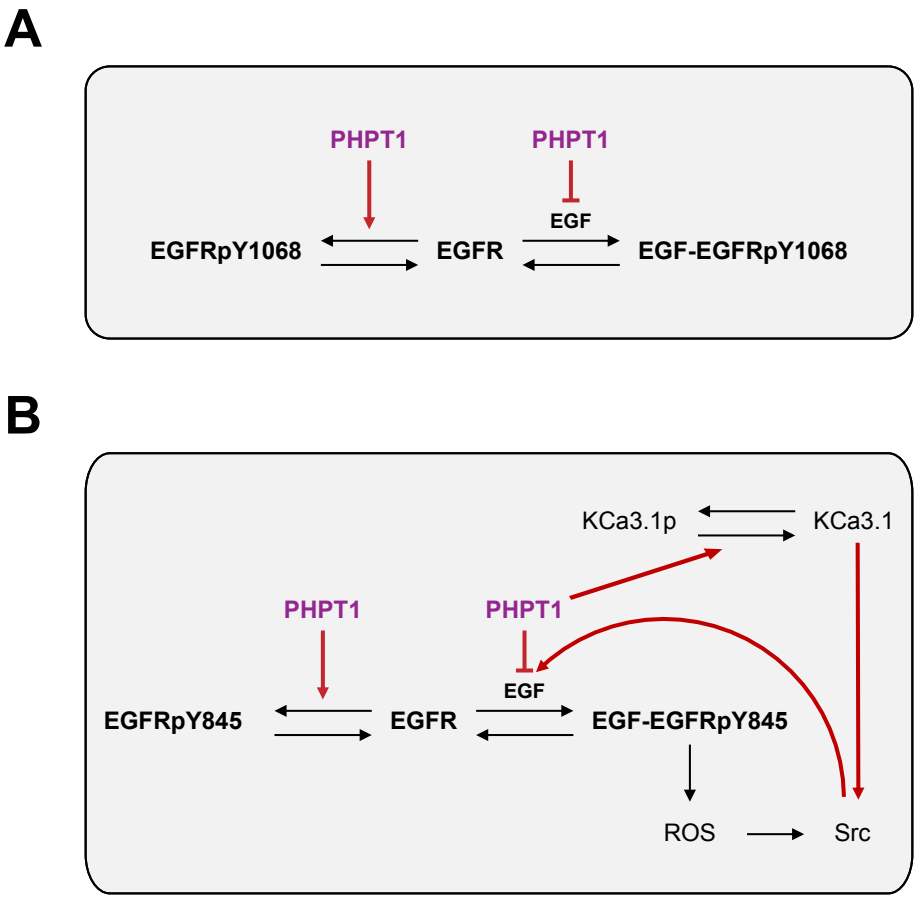

Figure 29: Scheme for EGFR activity regulation by PHPT1. (A) PHPT1 amplifies EGFR signalling (pTyr1068) of spontaneous acitvated recepor, while the ligand induced activation is de00creased. **(B)** Autocatalysis of spontanoues activated EGFR (pTyr845) is increased by PHPT1 in a direct mechanism, while the ligand induced activation might be amplified through an indirect mechanism.

While PHPT1 might reduce the ligand dependent activation by suppressing the formation of the active asymmetric dimer state via pHis648 dephosphorylation, an

impaired EGFR endocytosis process might amplify the spontaneous activation. This implies two distinct regulation mechanisms between the ligand independent and dependent EGFR activation by PHPT1.

In addition to EGFR, the other members of the ErbB family (ErbB2, ErbB3 and ErbB4) might reveal a related regulation mechanism. Instead of the His residue in EGFR, ErbB2 contains a Gln, ErbB3 an arginine (Arg) and ErbB4 a Ser residue. Therefore, the Arg and Ser might also become phosphorylated, affecting the activation of ErbB2 and ErbB4.

PHPT1 has been identified as an oncogene. This raises the question if its oncogenic potential originates from the amplified spontaneous EGFR activation. Both oncogenes, PHPT1 and EGFR, are involved in the tumour invasion and migration in lung cancer cell lines[29,76,77]. Moreover, EGFR is involved in the malignancy of glioblastoma cells, which shows a high expression level of PHPT1[78,123]. By connecting these two oncogenes, PHPT1 itself might become a potential drug target.

6 Future Directions

During this study PHPT1 has been identified as a new key player in regulating EGFR activation for the first time. This work shows that EGFR autocatalysis and signalling of spontaneous- as well as ligand-induced receptor activation events are regulated by the phosphohistidine phosphatase/kinase cycle.

As mentioned before, only a piece of the puzzle has been discovered. To solve this puzzle, further experiments have to be performed in the near future. First of all, the His phosphorylation of EGFR has to be detected. Since the staining with monoclonal antibodies in immunoblotting experiments was unsuccessful, the next step would be to use mass spectrometry to monitor the phosphohistidine at the specific His648 residue[106].

In order to further validate the proposed model, the effect of PHPT1 on the interaction between EGFR and CaM has to be elucidated. One possibility to test this hypothesis is the FLIM-FRET approach. By measuring FRET between EGFR mCitrine and CaM mCherry in presence of PHPT1 and the H648A JM mutation, the hypothesis that PHPT1 activity hampers CaM binding and thus impede receptor dimerization and further activation can be tested.

Another piece of the puzzle is formed by the conformational fluctuation of the receptor. If EGFR is regulated as described in the model, dephosphorylation catalysed by PHPT1 would hamper the release of the intracellular part of EGFR generating a less flexible receptor, which is stuck to the plasma membrane. Therefore, the increased rigidity can be detected by fluorescence anisotropy. This method uses the change of fluorescence polarization caused by an altered molecular orientation of the receptor[124].

To finalize the overall picture, the influence on the endocytosis divided into recycling and lysosomal degradation has to be validated in detail. There are several techniques to visualize EGFR endocytosis. One of these is the imaging in living cells by fluorescence microscopy. To validate if the kinases NME1 and NME2 reduce EGFR phosphorylation by increasing the internalization rate, a dynamin inhibitor can be used. Additionally, fluorescently labelled EGF is used to detect the ligand bound EGFR complex during endocytosis. A second approach could be the use of an ubiquitination assay based on the detection of ubiquitin bound to immunoprecipitated EGFR by western blotting[125].

Finally, the obtained results in this study are generated by an artificial system in which EGFR and PHPT1 are ectopically overexpressed in MCF7 cells. To further confirm the regulation of EGFR activation by PHPT1, the receptor phosphorylation has to be validated at endogenous level. Therefore, knock down of protein expression level with small interfering ribonucleic acid (siRNA) or the clustered regulatory interspaced short palindromic repeats/Cas (CRISPR/Cas) method could be performed.

7 References

1. Kim, S. H., Turnbull, J. & Guimond, S. Extracellular matrix and cell signalling: The dynamic cooperation of integrin, proteoglycan and growth factor receptor. *J. Endocrinol.* **209,** 139–151 (2011).
2. Leventis, P. A. & Grinstein, S. The Distribution and Function of Phosphatidylserine in Cellular Membranes. *Annu. Rev. Biophys.* **39,** 407–427 (2010).
3. Di Paolo, G. & De Camilli, P. Phosphoinositides in cell regulation and membrane dynamics. *Nature* **443,** 651–657 (2006).
4. Li, L., Shi, X., Guo, X., Li, H. & Xu, C. Ionic protein–lipid interaction at the plasma membrane: what can the charge do? *Trends Biochem. Sci.* **39,** 130–140 (2014).
5. Heo, W. Do *et al.* PI(3,4,5)P3 and PI(4,5)P2 Lipids Target Proteins with Polybasic Clusters to the Plasma Membrane. *Science* **314,** 1458–1461 (2006).
6. McLaughlin, S. & Murray, D. Plasma membrane phosphoinositide organization by protein electrostatics. *Nature* **438,** 605–611 (2005).
7. Xu, C. *et al.* Regulation of T Cell Receptor Activation by Dynamic Membrane Binding of the CD3 Cytoplasmic Tyrosine-Based Motif. *Cell* **135,** 702–713 (2008).
8. Aivazian, D. & Stern, L. J. Phosphorylation of T Cell Receptor ζ is Regulated by a Lipid Dependeny Folding Transition. *Nat. Struct. Biol.* **7,** 1023–1026 (2000).
9. Suh, B.-C. & Hille, B. PIP2 is a necessary cofactor for ion channel function: how and why? *Annu. Rev. Biophys.* **37,** 175–95 (2008).
10. Hansen, S. B., Tao, X. & MacKinnon, R. Structural basis of PIP2 activation of the classical inward rectifier K+ channel Kir2.2. *Nature* **477,** 495–499 (2011).
11. Shi, X. *et al.* Ca2+ regulates T-cell receptor activation by modulating the charge property of lipids. *Nature* **493,** 111–115 (2013).
12. Kadamur, G. & Ross, E. M. Mammalian phospholipase C. *Annu. Rev. Physiol.* **75,** 127–154 (2013).
13. Meador, W., Means, A. & Quiocho, F. Modulation of Calmodulin Plasticity in Molecular Recognition on the Basis of X-ray Structures. *Science* **262,** 1718–1721 (1993).
14. Swulius, M. T. & Waxham, M. N. Ca2+ /Calmodulin-dependent Protein Kinases. *Cell. Mol. Life Sci.* **65,** 2637–2657 (2008).
15. Clapham, D. E. Calcium Signaling. *Cell* **131,** 1047–1058 (2007).
16. Adelman, J. P., Maylie, J. & Sah, P. Small-Conductance Ca 2+ -Activated K + Channels: Form and Function. *Annu. Rev. Physiol.* **74,** 245–269 (2012).
17. Morales, P. *et al.* Contribution of the KCa3.1 channel-calmodulin interactions to the regulation of the KCa3.1 gating process. *J. Gen. Physiol.* **142,** 37–60 (2013).
18. Srivastava, Shekhar, Papiya Choudhury, Zhai Li, GongXin Liu Nadkarni, V. & Kyung Ko, William A. Coetzee, E. Y. S. Phosphatidylinositol 3-Phosphate

Indirectly Activates KCa3.1 via 14 Amino Acids in the Carboxy Terminus of KCa3.1. *Mol. Biol. Cell* **17,** 146–154 (2005).

19. Di, L. *et al.* Nucleoside diphosphate kinase B knock-out mice have impaired activation of the K+ channel KCa3.1, resulting in defective T cell activation. *J. Biol. Chem.* **285,** 38765–38771 (2010).
20. Srivastava, S. *et al.* Protein histidine phosphatase 1 negatively regulates CD4 T cells by inhibiting the K+ channel KCa3.1. *Proc. Natl. Acad. Sci.* **105,** 14442–14446 (2008).
21. Schmidt, D., Jiang, Q. & Mackinnon, R. Phospholipids and the origin of cationic gating charges in voltage sensors. *Nature* **444,** 775–779 (2006).
22. Ramu, Y., Xu, Y. & Lu, Z. Enzymatic activation of voltage-gated potassium channels. *Nature* **442,** 696–699 (2006).
23. Escribá, P. V, Wedegaertner, P. B., Goñi, F. M. & Vögler, O. Lipid – protein interactions in GPCR-associated signaling. *Biochim. Biophys. Acta* **1768,** 836–852 (2007).
24. Saliba, A., Vonkova, I. & Gavin, A. The systematic analysis of protein–lipid interactions comes of age. *Nature* **16,** 753–761 (2015).
25. Abd Halim, K. B., Koldsø, H. & Sansom, M. S. P. Interactions of the EGFR juxtamembrane domain with PIP2-containing lipid bilayers: Insights from multiscale molecular dynamics simulations. *Biochim. Biophys. Acta - Gen. Subj.* **1850,** 1017–1025 (2015).
26. Yewale, C., Baradia, D., Vhora, I., Patil, S. & Misra, A. Epidermal growth factor receptor targeting in cancer: A review of trends and strategies. *Biomaterials* **34,** 8690–8707 (2013).
27. Riese, D. J., Gallo, R. M. & Settleman, J. Mutational activation of ErbB family receptor tyrosine kinases: Insights into mechanisms of signal transduction and tumorigenesis. *BioEssays* **29,** 558–565 (2007).
28. Normanno, N. *et al.* Epidermal growth factor receptor (EGFR) signaling in cancer. *Gene* **366,** 2–16 (2006).
29. Sharma, S. V, Bell, D. W., Settleman, J. E. & Haber, D. A. Epidermal growth factor receptor mutations in lung cancer. *Nat. Rev. Cancer* **7,** 169–181 (2007).
30. Westphal, M., Meima, L., Szonyi, E., Lofgren, J., Meissner, H., Hamel, W., Nikolics, K., Sliwkowski, M. Heregulins and the ErbB-2/3/4 receptors in gliomas. *J. Neurooncology* **3,** 335–346 (1997).
31. Harari, D. & Yarden, Y. Molecular mechanisms underlying ErbB2/HER2 action in breast cancer. *Oncogene* **19,** 6102–6114 (2000).
32. Endres, N. F., Engel, K., Das, R., Kovacs, E. & Kuriyan, J. Regulation of the catalytic activity of the EGF receptor. *Curr. Opin. Struct. Biol.* **21,** 777–784 (2011).
33. Lemmon, M. A. *et al.* The EGFR Family : Not So Prototypical Receptor Tyrosine Kinases. *Cold Sprin Harb. Perspect. Biol.* **6,** 1–18 (2014).
34. Kovacs, E., Zorn, J. A., Huang, Y., Barros, T. & Kuriyan, J. A Structural

Perspective on the Regulation of the Epidermal Growth Factor Receptor. *Annu. Rev. Biochem.* **84,** 739–764 (2015).

35. Ferguson, K. M. *et al.* EGF activates its receptor by removing interactions that autoinhibit ectodomain dimerization. *Mol. Cell* **11,** 507–517 (2003).

36. Mendrola, J. M., Berger, M. B., King, M. C. & Lemmon, M. A. The single transmembrane domains of ErbB receptors self-associate in cell membranes. *J. Biol. Chem.* **277,** 4704–4712 (2002).

37. Jura, N. *et al.* Mechanism for Activation of the EGF Receptor Catalytic Domain by the Juxtamembrane Segment. *Cell* **137,** 1293–1307 (2009).

38. Zhang, X., Gureasko, J., Shen, K., Cole, P. A. & Kuriyan, J. An Allosteric Mechanism for Activation of the Kinase Domain of Epidermal Growth Factor Receptor. *Cell* **125,** 1137–1149 (2006).

39. Shan, Y. *et al.* Oncogenic mutations counteract intrinsic disorder in the EGFR kinase and promote receptor dimerization. *Cell* **149,** 860–870 (2012).

40. Sato, K. ichi. Cellular functions regulated by phosphorylation of EGFR on TYR845. *Int. J. Mol. Sci.* **14,** 10761–10790 (2013).

41. Okabayashisg, Y. *et al.* Grb2/Ash Binds Directly to Tyrosines 1068 and 1086 and Indirectly to Tyrosine 1148 of Activated Human Epidermal Growth Factor Receptors in Intact Cells. *J. Biol. Chem.* **269,** 31310–31314 (1994).

42. Gao, J. *et al.* Mechanistic insights into EGFR membrane clustering revealed by super-resolution imaging. *Nanoscale* **7,** 2511–2519 (2015).

43. Lemmon, M. A. & Schlessinger, J. Cell signaling by receptor tyrosine kinases. *Cell* **141,** 1117–1134 (2010).

44. Nagy, P., Claus, J., Jovin, T. M. & Arndt-Jovin, D. J. Distribution of resting and ligand-bound ErbB1 and ErbB2 receptor tyrosine kinases in living cells using number and brightness analysis. *Proc. Natl. Acad. Sci.* **107,** 16524–16529 (2010).

45. Reynolds, A. R., Tischer, C., Verveer, P. J., Rocks, O. & Bastiaens, P. I. H. EGFR activation coupled to inhibition of tyrosine phosphatases causes lateral signal propagation. *Nat Cell Biol* **5,** 447–453 (2003).

46. Baumdick, M. *et al.* EGF-dependent re-routing of vesicular recycling switches spontaneous phosphorylation suppression to EGFR signaling. *Elife* **4,** 1-28 (2016).

47. Levkowitz, G. *et al.* c-Cbl/Sli-1 regulates endocytic sorting and ubiquitination o the epidermal growth factor receptor. *Genes Dev.* **12,** 3663–3674 (1998).

48. Goh, L. K. & Sorkin, A. Endocytosis of Receptor Tyrosine Kinases. *Cold Spring Harb. Perspect. Biol.* **5,** 1–17 (2013).

49. Vanlandingham, P. A. & Ceresa, B. P. Rab7 regulates late endocytic trafficking downstream of multivesicular body biogenesis and cargo sequestration. *J. Biol. Chem.* **284,** 12110–12124 (2009).

50. Endres, N. F. *et al.* Conformational Coupling across the Plasma Membrane in Activation of the EGF Receptor. *Cell* **152,** 543–556 (2013).

51. Arkhipov, A. *et al.* Architecture and Membrane Interactions of the EGF

Receptor. *Cell* **152,** 557–569 (2013).

52. Thiel, K. W. & Carpenter, G. Epidermal growth factor receptor juxtamembrane region regulates allosteric tyrosine kinase activation. *PNAS* **104,** 19238–19243 (2007).

53. Red Brewer, M. *et al.* The Juxtamembrane Region of the EGF Receptor Functions as an Activation Domain. *Mol. Cell* **34,** 641–651 (2009).

54. Hubbard, S. R. The Juxtamembrane Region of EGFR Takes Center Stage. *Cell* **137,** 1181–1183 (2009).

55. Choowongkomon, K., Carlin, C. R. & Sönnichsen, F. D. A Structural Model for the Membrane-bound Form of the Juxtamembrane Domain of the Epidermal Growth Factor Receptor. *J. Biol. Chem.* **280,** 24043–24052 (2005).

56. Endres, N. F., Barros, T., Cantor, A. J. & Kuriyan, J. Emerging concepts in the regulation of the EGF receptor and other receptor tyrosine kinases. *Trends Biochem. Sci.* **39,** 437–446 (2014).

57. Wang, Y. *et al.* Regulation of EGFR nanocluster formation by ionic protein-lipid interaction. *Cell Res.* **24,** 959–76 (2014).

58. T. Hunter, N. Ling, J. A. C. Protein kinase C phosphorylation of the EGF receptor at a threonine residue close to the cytoplasmic face of the plasma membrane. *Nature* **311,** 480–483 (1984).

59. Li, X., Huang, Y., Jiang, J. & Frank, S. J. ERK-dependent threonine phosphorylation of EGF receptor modulates receptor downregulation and signaling. *Cell. Signal.* **20,** 2145–2155 (2008).

60. Stateva, S. R. *et al.* The Activating Role of Phospho-(Tyr)-Calmodulin on the Epidermal Growth Factor Receptor. *Biochem. J.* **472,** 195-204 (2015).

61. Li, H. *et al.* Regulation of the Ligand-dependent Activation of the Epidermal Growth Factor Receptor by Calmodulin. *J. Biol. Chem.* **287,** 3273–3281 (2012).

62. Cheyette, T. E. & Gross, D. J. Epidermal Growth Factor-Stimulated Calcium-Ion Transients in Individual a431 Cells - Initiation Kinetics and Ligand Concentration-Dependence. *Cell Regul.* **2,** 827–840 (1991).

63. Sengupta, P. *et al.* EGFR Juxtamembrane Domain, Membranes, and Calmodulin: Kinetics of Their Interaction. *Biophys. J.* **96,** 4887–4895 (2009).

64. McLaughlin, S., Smith, S. O., Hayman, M. J. & Murray, D. An Electrostatic Engine Model for Autoinhibition and Activation of the Epidermal Growth Factor Receptor (EGFR/ErbB) Family. *J. Gen. Physiol.* **126,** 41–53 (2005).

65. Aifa, S. *et al.* Phosphorylation of Thr654 but not Thr669 within the juxtamembrane domain of the EGF receptor inhibits calmodulin binding. *Biochem. Biophys. Res. Commun.* **347,** 381–387 (2006).

66. Karin, M. & Hunter, T. Transcriptional control by protein phosphorylation: signal transmission from the cell surface to the nucleus. *Curr. Biol.* **5,** 747–757 (1995).

67. S. Klumpp, J. K. Reversible Phosphorylation of Histidine Residues in Proteins from Vertebrates. *Sci. Signal.* **2,** 13 (2009).

68. Wieland, T. & Attwood, P. V. Alterations in reversible protein histidine phosphorylation as intracellular signals in cardiovascular disease. *Front. Pharmacol.* **6,** 173 (2015).

69. Steeg, P. S., Palmieri, D., Ouatas, T. & Salerno, M. Histidine kinases and histidine phosphorylated proteins in mammalian cell biology, signal transduction and cancer. *Cancer Lett.* **190,** 1–12 (2003).

70. Kee, J.-M. & Muir, T. W. Chasing Phosphohistidine, an Elusive Sibling in the Phosphoamino Acid Family. *ACS Chem. Biol.* **7,** 44–51 (2012).

71. Kim, Y., Huang, J., Cohen, P. & Matthews, H. R. Protein Phosphatases 1,2A, and 2C Are Protein Histidine Phosphatase. *Am. Soc. Biochem. Mol. Biol.* **268,** 18513–18518 (1993).

72. Panda, S. *et al.* Identification of PGAM5 as a Mammalian Protein Histidine Phosphatase that Plays a Central Role to Negatively Regulate CD4+ T Cells. *Mol. Cell* **63,** 457–469 (2016).

73. Yokoi, F., Hiraishi, H. & Izuhara, K. Molecular cloning of a cDNA for the human phospholysine phosphohistidine inorganic pyrophosphate phosphatase. *J. Biochem.* **133,** 607–614 (2003).

74. Koike, E. *et al.* Expression of new human inorganic pyrophosphatase in thyroid diseases: Its intimate association with hyperthyroidism. *Biochem. Biophys. Res. Commun.* **341,** 691–696 (2006).

75. Ek, P. *et al.* Identification and characterization of a mammalian 14-kDa phosphohistidine phosphatase. *Eur. J. Biochem.* **269,** 5016–5023 (2002).

76. Xu, A. *et al.* 14-kDa phosphohistidine phosphatase and its role in human lung cancer cell migration and invasion. *Lung Cancer* **67,** 48–56 (2010).

77. Xu An-jian, Xia Xiang-hou, Du Song-tao & Gu Jun-chao. Clinical significance of PHPT1 protein expression in lung cancer. *Chin. Med. J. (Engl).* **123,** 3247–3251 (2010).

78. Zhang, X.-Q., Sundh, U. B., Jansson, L., Zetterqvist, Ö. & Ek, P. Immunohistochemical localization of phosphohistidine phosphatase PHPT1 in mouse and human tissues. *Ups. J. Med. Sci.* **114,** 65–72 (2009).

79. Seeger, A. *et al.* Influence of protein histidine phosphatase overexpression and down-regulation on human umbilical-vein endothelial cell viability. *Cell Biol. Int.* **36,** 245–249 (2012).

80. Shen, H., Yang, P., Liu, Q. & Tian, Y. Nuclear expression and clinical significance of phosphohistidine phosphatase 1 in clear-cell renal cell carcinoma. *J. Int. Med. Res.* **43,** 747–757 (2015).

81. R. D. Busam A. Flores, M. Hammarström, C. Persson, B. M. Hallberg, A.-G. T. First Structure of a Eukaryotic Phosphohistidine Phosphatase. *J. Biol. Chem.* **281,** 33830–33834 (2006).

82. Ma, R. *et al.* Mutational study of human phosphohistidine phosphatase: Effect on enzymatic activity. *Biochem. Biophys. Res. Commun.* **337,** 887–891 (2005).

83. Klumpp, S., Ma, N. T., B??umer, N., Bechmann, G. & Krieglstein, J. Relevance of glycine and cysteine residues as well as N- and C-terminals for the activity of

protein histidine phosphatase. *Biochim. Biophys. Acta - Proteins Proteomics* **1804,** 206–211 (2010).

84. Wagner, P. D. & Vu, N. D. Phosphorylation of ATP-citrate lyase by nucleoside diphosphate kinase. *J. Biol. Chem.* **270,** 21758–21764 (1995).

85. Hippe, H. *et al.* Activation of Heterotrimeric G Proteins by a High Energy Phosphate Transfer via Nucleoside Diphosphate Kinase (NDPK) B and G $^{N}_{L}$ Subunits. *J. Biol. Chem.* **278,** 7227–7233 (2003).

86. Chen, Y. *et al.* Nucleotide binding to nucleoside diphosphate kinases: X-ray structure of human NDPK-A in complex with ADP and comparison to protein kinases. *J. Mol. Biol.* **332,** 915–926 (2003).

87. Lapek, J. D., Tombline, G. & Friedman, A. E. Mass Spectrometry Detection of Histidine Phosphorylation on NM23-H1. *J. Proteome Res.* **10,** 751–755 (2011).

88. Mitchell, K. A. P., Szabo, G. & de S. Otero, A. Direct binding of cytosolic NDP kinases to membrane lipids is regulated by nucleotides. *Biochim. Biophys. Acta - Mol. Cell Res.* **1793,** 469–476 (2009).

89. Takács-Vellai, K. The metastasis suppressor Nm23 as a modulator of Ras/ERK signaling. *Journal of molecular signaling* **9,** 4 (2014).

90. Klumpp, S., Bechmann, G., Mäurer, A., Selke, D. & Krieglstein, J. ATP-citrate lyase as a substrate of protein histidine phosphatase in vertebrates. *Biochem. Biophys. Res. Commun.* **306,** 110–115 (2003).

91. Mäurer, A. *et al.* The β-subunit of G proteins is a substrate of protein histidine phosphatase. *Biochem. Biophys. Res. Commun.* **334,** 1115–1120 (2005).

92. Cai, X., Srivastava, S., Surindran, S., Li, Z. & Skolnik, E. Y. Regulation of the epithelial Ca2+ channel TRPV5 by reversible histidine phosphorylation mediated by NDPK-B and PHPT1. *Mol. Biol. Cell* **25,** 1244–1250 (2014).

93. Beckman-Sundh, U., Ek, B., Zetterqvist, Ö. & Ek, P. A screening method for phosphohistidine phosphatase 1 activity. *Ups. J. Med. Sci.* **116,** 161–168 (2011).

94. Krieglstein, J. *et al.* Reduced viability of neuronal cells after overexpression of protein histidine phosphatase. *Neurochem. Int.* **53,** 132–136 (2008).

95. Klumpp, S., Faber, D., Fischer, D., Litterscheid, S. & Krieglstein, J. Role of protein histidine phosphatase for viability of neuronal cells. *Brain Res.* **1264,** 7–12 (2009).

96. Hippe, H.-J. *et al.* Regulation of Cardiac cAMP Synthesis and Contractility by Nucleoside Diphosphate Kinase B/G Protein βγ Dimer Complexes. *Circ. Res.* **100,** 1191–1199 (2007).

97. Kowluru, A., Klumpp, S. & Krieglstein, J. Protein histidine [de]phosphorylation in insulin secretion: Abnormalities in models of impaired insulin secretion. *Naunyn. Schmiedebergs. Arch. Pharmacol.* **384,** 383–390 (2011).

98. Guo, G. *et al.* Ligand-independent EGFR signaling. *Cancer Res.* **75,** 3436–3441 (2015).

99. Schindelin, J. *et al.* Fiji: an open-source platform for biological-image analysis. *Nat Meth* **9,** 676–682 (2012).

100. Grecco, H. E., Roda-Navarro, P. & Verveer, P. J. Global analysis of time correlated single photon counting FRET-FLIM data. *Opt. Express* **17,** 6493–6508 (2009).

101. Seshacharyulu, P. *et al.* Targeting the EGFR signaling pathway in cancer therapy. *Expert Opin. Ther. Targets* **16,** 15–31 (2012).

102. Weihua, Z. *et al.* Survival of Cancer Cells is maintained by EGFR independent of its Kinase Activity. *Cancer Cell* **13,** 385–393 (2008).

103. Gong, W. *et al.* Solution structure and catalytic mechanism of human protein histidine phosphatase 1. *Biochem. J.* **418,** 337–44 (2009).

104. Krishnan, K. S. *et al.* Nucleoside Diphosphate Kinase, a Source of GTP, Is Required for Dynamin-Dependent Synaptic Vesicle Recycling. *Neuron* **30,** 197–210 (2001).

105. Boissan, M. *et al.* Nucleoside diphosphate kinases fuel dynamin superfamily proteins with GTP for membrane remodeling. *Science* **344,** 1510–1515 (2014).

106. Fuhs, S. R. *et al.* Monoclonal 1- and 3-Phosphohistidine Antibodies: New Tools to Study Histidine Phosphorylation. *Cell* **162,** 198–210 (2015).

107. Lapek, J. D., Tombline, G. & Friedman, A. E. Mass Spectrometry Detection of Histidine Phosphorylation on NM23 H1. *J. Proteome Res.* **10,** 751–755 (2011).

108. Kee, J. M. & Muir, T. W. Chasing phosphohistidine, an elusive sibling in the phosphoamino acid family. *ACS Chem. Biol.* **7,** 44–51 (2012).

109. Tong, J., Taylor, P., Peterman, S. M., Prakash, A. & Moran, M. F. Epidermal growth factor receptor phosphorylation sites Ser991 and Tyr998 are implicated in the regulation of receptor endocytosis and phosphorylations at Ser1039 and Thr1041. *Mol. Cell. Proteomics* **8,** 2131–2144 (2009).

110. Matthews, H. R. Protein kinases and phosphatases that act on histidine, lysine, or arginine residues in eukaryotic proteins: A possible regulator of the mitogen-activated protein kinase cascade. *Pharmacol. Ther.* **67,** 323–350 (1995).

111. Choi, S. H., Mendrola, J. M. & Lemmon, M. A. EGF-independent activation of cell-surface EGF receptors harboring mutations found in gefitinib-sensitive lung cancer. *Oncogene* **26,** 1567–1576 (2007).

112. Sigismund, S. *et al.* Clathrin-independent endocytosis of ubiquitinated cargos. *Proc. Natl. Acad. Sci. U. S. A.* **102,** 2760–5 (2005).

113. Sánchez-González, P., Jellali, K. & Villalobo, A. Calmodulin-mediated regulation of the epidermal growth factor receptor. *FEBS J.* **277,** 327–42 (2010).

114. Kluba, M., Engelborghs, Y., Hofkens, J. & Mizuno, H. Inhibition of receptor dimerization as a novel negative feedback mechanism of EGFR signaling. *PLoS One* **10,** 1–21 (2015).

115. Park, H. S. *et al.* Sequential Activation of Phosphatidylinositol 3-Kinase, βPix, Rac1, and Nox1 in Growth Factor-Induced Production of H2O2. *Society* **24,** 4384–4394 (2004).

116. Heppner, D. E. & van der Vliet, A. Redox-dependent regulation of epidermal growth factor receptor signaling. *Redox Biol.* **8,** 24–27 (2016).

117. Martin, D. R., Dutta, P., Mahajan, S., Varma, S. & Stevens, S. M. Structural and activity characterization of human PHPT1 after oxidative modification. *Sci. Rep.* **6,** 23658 (2016).

118. Zibara, K. *et al.* ROS mediates interferon gamma induced phosphorylation of Src, through the Raf/ERK pathway, in MCF-7 human breast cancer cell line. *J. Cell Commun. Signal.* **11,** 57–67 (2017).

119. Sevelsted Møller, L. *et al.* The calcium-activated potassium channel KCa3.1 is an important modulator of hepatic injury. *Sci. Rep.* **6,** 28770 (2016).

120. Hanai, J.-I., Doro, N., Seth, P. & Sukhatme, V. P. ATP citrate lyase knockdown impacts cancer stem cells in vitro. *Cell Death Dis.* **4,** e696 (2013).

121. Palacios, F., Schweitzer, J. K., Boshans, R. L. & D'Souza-Schorey, C. ARF6-GTP recruits Nm23-H1 to facilitate dynamin-mediated endocytosis during adherens junctions disassembly. *Nat Cell Biol* **4,** 929–936 (2002).

122. Grecco, H. E. & Bastiaens, P. I. H. Quantifying cellular dynamics by fluorescence resonance energy transfer (FRET) microscopy. *Curr. Protoc. Neurosci.* 5.22.1-5.22.14 (2013).

123. Taylor, T. E., Furnari, F. B. & Cavenee, W. K. Targeting EGFR for Treatment of Glioblastoma: Molecular Basis to Overcome Resistance. *Curr Cancer Drug Targets* **12,** 197–209 (2012).

124. Rusinova, E., Tretyachenko-Ladokhina, V., Vele, O. E., Senear, D. F. & Alexander Ross, J. B. Alexa and Oregon Green dyes as fluorescence anisotropy probes for measuring protein-protein and protein-nucleic acid interactions. *Anal. Biochem.* **308,** 18–25 (2002).

125. Pinilla-Macua, I. & Sorkin, A. Methods to study endocytic trafficking of the EGF receptor. *Biophys. Methods Cell Biol.* **130,** 347–367 (2015).

8 Supplementary Material

Table 11: Primer sequences for cloning and quick change PCR.

Gene	Vector	Primer	Sequence
PHPT1	pmCherry-C1	Forward	CAAGCTTCGATGGCAGTGGCGGACCTC
PHPT1	pmCherry-C1	Reverse	CGCGGTACCTTAGTAGCCGTCGTTAGCCCAGG
PHPT1	pmCherry-N1	Forward	CTCAAGCTTATGGCAGTGGCGGACCTC
PHPT1	pmCherry-N1	Reverse	CGCGGTACCGTGTAGCCGTCGTTAGCCCAGGTGAC CTCG
PHPT1_H53A	-	QC	AAGTGGGCTGAGTACGCGGCGGACATCTACGAC
NME1	pmCherry-C1	Forward	ATCTCGAGCTCAAGCTTCGATGGCCAACTGTGAGC GTAC
NME1	pmCherry-C1	Reverse	GTACCGTCGACTGCAGAATTTCATTCATAGATCCAG TTCTGAGCACAG
NME1	pmCherry-N1	Forward	CGAATTCTGCAGTCGACGGTACATGGCCAACTGTG AGCGAC
NME1	pmCherry-N1	Reverse	GGATCCCGGGCCCGCGGTACCGTTTCATAGATCCA GTTCTGAGCACAGC
NME2	pmCherry-C1	Forward	GATCTCGAGCTCAAGCTTCGATGGCCAACCTGGAG CGCAC
NME2	pmCherry-C1	Reverse	GTACCGTCGACTGCAGAATTTCATTCATAGACCCA GTCATAGCACAAG
NME2	pmCherry-N1	Forward	GAATTCTGCAGTCGACGGTACATGGCCAACCTGGA GCG
NME2	pmCherry-N1	Reverse	CGGTGGATCCCGGGCCCGCGGTACCGTTTCATAGA CCCAGTCATGAGCACAAG

9 Acknowledgement

First of all, I have to thank Prof. Dr. Philippe Bastiaens for taking care of us, me and my exciting research project based on the challenging histidine phosphorylation, for the last two and a half years. Not only for taking care, but also for his supervision and discussions during this period.

A special thank goes to Prof. Dr. Christian Hedberg for introducing me into the fascinating research field of histidine phosphorylation, but also for his continuous support and discussions even when I had moved from his lab to Philippe`s lab.

I would also like to thank Ola Sabet for taking me under her wings, as well as for showing me, as a biochemist, the diverse world of the systemic cell biology and last but not least for keeping me always smiling.

During my PhD I had the opportunity to participate in great courses, seminars, symposia and retreats to further improve my scientific as well as my personal skills. Therefore, I would like to thank the International Max Planck Research School in Chemical and Molecular Biology (IMPRS-CMB), especially the coordinators Christa Hornemann and Lucia Sironi, who had always an open ear for me.

I have to thank Stephen Fuhs for providing me with purified enzymes, NME1 and PGAM1, used as control samples for phosphohistidine detection.

When I thank people for their support, the technical assistants have to be listed here. Hendrike Schütz, the guardian of our lab, who does not only organize the common stocks, but made my life easier in several ways. Jutta Luig, who helped me by cloning experiments. Manuela Grygier, who performed plasmid preparations and finally, the heart of the cell culture, Michael Reichl.

I would also like to thank Astrid Krämer and Tanja Forck for the organizational part.

My thanks to the people who I have met and taken to my heart do not only go to the people of department 2, but also to department 4, where I started my journey, especially Kirsten Tschapalda, Lea Kremer, Janine Schulte-Zweckel and Melanie Schwalfenberg for the nice time during BBQ evenings, PhD heat preparation and for one or the other running event, which we managed together. During the move from the chemistry to the systemic cell biology department I passed Ingrid Vetter`s research group in the

department of mechanistic cell biology and I am really not sure how this trip would have ended, if I had not met these people. There, my thanks go to Kathrin Estel, Arthur Porfetye and Stefan Baumeister for the funny evenings and breakfast sessions, which would never start without mett. I would also like to thank my running group, especially Anika Altenfeld and Carolin Körner, who always remind me that sport can overcome a day full of non-working experiments, which is not so unusual for a biologist. Last but not least, I have to thank Patricia Stege for her relentless humour and for being not only a nice colleague, but also for getting a really good friend. Finally, my journey ended up in the department for system cell biology, where the people have welcomed me with open arms. I would like to thank Ola Sabet, Martin Baumdick, Yannick Brüggemann, Amit Mhamane, Rabea Stockert, Jana Mallah, Lisaweta Roßmannek and all the other amazing guys for their support, discussions and the hilarious evenings not only during the retreats.

In this period of my life my friends and family never stopped supporting me even during unsocial phases caused by a tough schedule. On days on which I was not able to build myself up, they did it for me. I would like to thank for this and I will never forget it.

This brings me to the end of my acknowledgement, where I have to thank my lovely husband Sebastian, who never stopped giving me the feeling that everything is feasible in good times as well as bad and at least for showing me the bright side of life.